FUNCTIONAL AND MORPHOLOGICAL EVALUATION OF *DROSOPHILA* CMT MODELS

by

Elif Begüm Gökerküçük

B.S., in Molecular Biology and Genetics, Bilkent University, 2012

Submitted to the Institute for Graduate Studies in
Science and Engineering in partial fulfillment of
the requirements for the degree of
Master of Science

Graduate Program in Molecular Biology and Genetics
Boğaziçi University

2015

To my family and friends…

ACKNOWLEDGEMENTS

I would like to express my sincere thanks to my thesis supervisor Prof. Esra Battaloğlu for her great supervision, guidance and encouragement during my graduate studies. I consider myself lucky to have a chance to work with her throughout this project.

I would like to express my gratitude to my co-advisor Assoc. Prof. Arzu Çelik for helping me throughout my project, leading my way with her knowledge, kindly encouraging me to learn from my mistakes.

I am very grateful to my committee members, Prof. Kuyaş Buğra, Assoc. Prof. Uygar Tazebay and Assist. Prof. İbrahim Yaman for accepting to read and review my thesis. It is an honor to receive feedback from them about my work.

I also would like to thank Prof. Patrick Verstreken for hosting me in his laboratory to learn the techniques used in this study and conduct some of the experiments together with his post-doc students Valerie Uyyterhoeven and Sven Vilain.

I would like to thank Cansu Küey, who as a precious friends, my research would not have been possible without her helps. I would like to express my sincere thanks to my friends and lab mates Burçak, Kaya, Kerem, Merve, Burcu, Burak, and Çağlayan for their moral support and invaluable friendship. I also wish to thank Lab 204 and Fly Lab members.

Above all, I would like to express my deepest thanks to my family members for their endless love, support and trust at all stages of my life.

Lastly, I would like to acknowledge Science and Technological Research Council of Turkey (TÜBİTAK) and Science Research Projects (BAP) for supporting me and this project (112T275 and 7563P).

ABSTRACT

FUNCTIONAL AND MORPHOLOGICAL EVALUATION OF *DROSOPHILA* CMT MODELS

Charcot-Marie-Tooth (CMT) disease is the most frequent inherited peripheral neuropathy in humans with a prevalence of 1 in 2500. It comprises a large group of genetically heterogeneous hereditary motor and sensory neuropathies with mutations identified in 40 causative genes. It is clinically characterized with progressive distal muscle weakness and atrophy, foot deformities, distal sensory loss and depressed tendon reflexes. Mutations in the *GDAP1* gene are associated with demyelinating, axonal or mixed forms of the disease with recessive or dominant modes of inheritance. Additionally, GDAP1 is a mitochondrial fission factor with glutathione S-transferase activity and involved in mitochondrial dynamics. MTMR2, on the other hand, is a phosphatase that is suggested to regulate vesicular trafficking in nervous system. Loss of function mutations in *MTMR2* gene are linked with autosomal recessive demyelinating CMT type 4B1 neuropathy with myelin outfoldings. Both *GDAP1* and *MTMR2* genes are good candidates to model CMT disease in terms of their involvement in CMT pathogenesis. In this study, our aim was to generate *Drosophila* models for CMT disease, specifically for its subtype CMT4, by altering the expression levels of *GDAP1* and *MTMR2* genes. We have up-or-down regulated *Drosophila* homologs of *GDAP1* and *MTMR2*, which are *CG4623* and *mtm* in order. In the first part of the study, a CG4623 antibody was generated allowing us to investigate expression pattern of the protein using Western blot and immunohistochemistry assays. With these experiments, ubiquitous expression of CG4623 was shown to be more prominent in the brain, neurons and imaginal discs. Later, we performed synaptic electrophysiology to elucidate functional roles of CG4623 and mtm at the synapses. Our results implicated that both proteins had an effect on synaptic transmission and neurotransmitter release. Lastly, we have investigated changes in neuromuscular junction (NMJ) morphology, bouton structure and mitochondrial dynamics. Since we did not observe any drastic change in the morphology of the mentioned structures in the third instar larvae, we attributed this phenomenon to progressive characteristics of CMT. With this study, we showed that the generated CMT models and the newly developed CG4623 antibody can be further used to illuminate the CMT pathogenesis.

ÖZET

DROSOPHILA CMT MODELLERİNİN İŞLEVSEL VE MORFOLOJİK DEĞERLENDİRMESİ

Charcot-Marie-Tooth (CMT) hastalığı, her 2500 kişiden birinde görülen ve genel nüfus içerisinde en sık rastlanılan kalıtsal periferik nöropati grubudur. Motor ve duysal sinir sistemlerini etkileyen ve genetik açıdan bu güne kadar 40 faklı gende görülen mutasyonlarla ilişkilendirilmiş olan CMT heterojen bir hastalıktır. Hastalık semptomları, ilerleyen yaşla artan distal kaslarda zaaf ve atrofi, motor bozukluklar, duyu kaybı, ve iskelet bozukluklarını içerir. *GDAP1* genindeki mutasyonlar, çekinik veya baskın kalıtılır, ve demiyelizan, aksonal ya da ara tiplere neden olabilir. Ayrıca, GDAP1 glutatyon S-transferaz aktivitesine sahip bir mitokondriyal fizyon faktörü olup, mitokondriyal dinamikleri etkilemektedir. Buna karşılık MTMR2 veziküler trafiği düzenleyen bir fosfatazdır. Bu genin mutasyonları otozomal çekinik demiyelizan CMT alt tipi CMT4B1'e sebep olurken, miyelinin aşırı katlanmasına neden olmaktadır. *GDAP1* ve *MTMR2* genleri CMT patogenezine farklı mekanizmalar ile katkıda bulunmaları dolayısıyla hastalığın modellenmesi açısından önemli adaylardır. Bu çalışma, *GDAP1* ve *MTMR2* genlerinin anlatım seviyelerinin değiştirilmesiyle CMT hastalığının alt tipi olan CMT4 için *Drosophila* modeli üretmeyi amaçlamaktadır. *GDAP1* ve *MTMR2'*nin *Drosophila* homoloğu olan *CG4623* ve *mtm* genleri yüksek veya düşük anlatılarak CMT hastalığı modellenmiştir. Araştırmanın ilk kısmında, CG4623 proteinine karşı üretilen antikor ile gerçekleştirilen immunohistokimya deneylerinde CG4623 proteininin beyinde, nöronlarda ve imgesel disklerde daha yoğun olmakla birlikte tüm vücutta anlatımı olduğu gösterilmiştir. Üçüncü evre larvalarda gerçekleştirilen sinaptik elektrofizyoloji deneyleriyle ise CG4623 ve mtm proteinlerinin sinaptik transmisyon ve nörotransmiter salınımında etkisi olduğu belirlenmiştir. Yine üçüncü evre larvalarda immünohistokimyasal boyamalar ile gerçekleştirilen deneylerde nöromüsküler bağlarda, buton yapılarında ve mitokondrilerde morfolojik değişimlere rastlanmamıştır. Bu bulgular, CMT hastalığının ilerleyen yaşla artan karakteristiği ile ilişkilendirilmektedir. Bu çalışma ile, geliştirilen CMT modellerinin ve yeni üretilen CG4623 antikorunun CMT patogenezinin aydınlatılması amacıyla daha sonraki projelerde kullanılabileceği gösterilmiştir.

TABLE OF CONTENTS

LIST OF FIGURES

LIST OF TABLES

LIST OF ACRONYMS/ABBREVIATIONS

AD	Autosomal Dominant
APS	Ammonium peroxodisulfate
AR	Autosomal Recessive
attB	Attachment site B
attP	Attachment site P
BLAST	Basic Local Alignment Search Tool
bp	basepair
BSA	Bovine Serum Albumin
CNS	Central Nervous System
CMT	Charcot-Marie-Tooth disease
dH_2O	distilled H2O
DNA	Deoxyribonucleic Acid
Drp1	Dynamin-related protein 1
EDTA	Ethylenediaminetetraacetic acid
EJP	Excitatory Junction Potential
ELISA	Enzyme-Linked ImmunoSorbent Assay
Fis1	Fission 1
GDAP1	Ganglioside-induced differentiation-associated protein 1
GDAP1L1	Ganglioside-induced differentiation-associated protein 1 like 1
GSH	Glutathione
GST	Glutathione S-transferase
GFP	Green Fluorescent Protein
GRAM	Glucosyltransferase, Rab-like GTPase activators and myotubularins
GTP	Guanosine Triphosphate
HD	Hydrophobic Domain
HEPES	4-(2-hydroxyethyl)-1-piperazineethanesulfonic acid

HMSN	Hereditary Motor and Sensory Neuropathy
HRP	Horse Raddish Peroxidase
IP3	Inositol Trisphosphate
IPTG	Isopropyl β-D-1-thiogalactopyranoside
kb	kilobase
KCl	Potassium Chloride
kDa	Kilodalton
KH_2PO_4	Potassium Phosphate
KOAc	Potassium Acetate
LB	Luria Bertani
Marf	Mitochondrial assembly regulatory factor
MFN1	Mitofusin 1
MFN2	Mitofusin 2
$MgCl_2$	Magnesium Chloride
MTM	Myotubularin
MTMR2	Myorubularin-related protein 2
MTMR5	Myorubularin-related protein 5
MTMR13	Myorubularin-related protein 13
MOM	Mitochondrial Outer Membrane
NaCl	Sodium Chloride
$NaHCO_3$	Sodium Bicarbonate
NaH_2PO_4	Monosodium phosphate
NaOAc	Sodium Acetate
NCV	Nerve conduction velocity
NMJ	Neuromuscular Junction
OE	Overexpression
O/N	Overnight
OPA1	Optic Atrophy Protein 1
PH GRAM	Pleckstrin Homology Glucosyltransferases, Rab-like GTPase Activators and Myotubularin
PI	Phosphatidyl Inositol

PI3P	Phosphoinositol 3-Phosphate
$PI3,5P_2$	Phosphoinositol 3,5-Biphosphate
PMP-22	Peripheral Myelin Protein 22
PNS	Peripheral Nervous System
qRT-PCR	Quantitative Reverse Transcription-PCR
ROS	Reactive Oxygen Species
RNA	Ribonucleic Acid
RNAi	Ribonucleic Acid Interference
SDS	Dodecylsulfate Sodium Salt
SEM	Standart Error of Mean
siRNA	Small Interfering RNA
TCA	Trichloroacetic acid
TEMED	N,N,N′,N′-Tetramethylethylenediamine
TM	Transmembrane Domain
UAS	Upstream Activating Sequence
VDRC	Vienna Drosophila Resource Center

1. INTRODUCTION

Charcot-Marie-Tooth (CMT) disease, also called 'Hereditary Motor and Sensory Neuropathy' (HMSN), is the most common inherited neuromuscular disorder, with clinical phenotypes of progressive distal muscle weakness and atrophy, foot deformities, distal sensory loss, and depressed tendon reflexes (Harding & Thomas, 1980). Its prevalence is estimated to be 1/2500 though it changes according to geographical location (Braathen *et al.,* 2011). In 60% of CMT cases, symptoms may appear in the first decade, however, late diagnosis is also observed in mild CMT neuropathies (Vallat *et al.,* 2013). Until now, no effective treatment or medications have been found for CMT however; clinical trials for drugs are ongoing.

Classically, CMT can be classified in two major groups, autosomal dominant demyelinating CMT1 and axonal CMT2. This classification of CMT is based on nerve conduction velocity (NCV), which is a very important clinical tool to facilitate the genetic diagnosis. NCV values of the CMT1 patients are less than 38 m/s in the upper extremities and they show demyelination and onion bulb formation in their nerve biopsies. Typical CMT2 patients show evidence of axonal loss in their biopsies and their NCV values are above the cutoff of 38 m/s with reduced amplitude. While CMT1 and CMT2 show autosomal dominant inheritance, CMT4 includes all forms of autosomal recessive CMT with either demyelinating or axonal NCV values. Intermediate conduction velocities of 25-45 m/s are often found in male patients with X-linked CMT1X (Siskind *et al.,* 2013). Both the demyelinating and the axonal type patients show similar phenotypes with an age of onset in the second decade. Severity of the disease is variable even in between the family members with the same mutation implicating that the progression of the disease may depend on the patients' genetic makeup (Parman & Battaloğlu, 2013).

After 30 years of genetic research since the first CMT locus was mapped in 1982, 40 CMT disease-causing genes have been identified until now (Bird *et al.,* 1982; Timmerman *et al.,* 2014). Mutations in more than 20 genes are related to the demyelination of Schwann cells. The most common gene related with demyelinating type of CMT is

PMP22. It is important to note that 20-64% of all CMT patients carry the *peripheral myelin protein 22 (PMP22)* duplication, known as CMT1A duplication (Van Paassen *et al*., 2014). Two genes among several, whose mutations cause alterations in axonal functions, are *NEFL* and *GAN*. The remaining mutations are mostly related with the intermediate CMT that is either demyelinating or axonal type. Protein products of CMT disease-causing genes can be localized in different cellular compartments of the myelinating Schwann cells or axons (Timmerman *et al*., 2014). They may function in the nucleus as a transcription factor, involved in intracellular trafficking, or related with the Golgi, endoplasmic reticulum or mitochondria functioning (Figure 1.1). However, for most of these genes, it is still unknown how their mutation causes neurodegeneration specifically in the peripheral nerves.

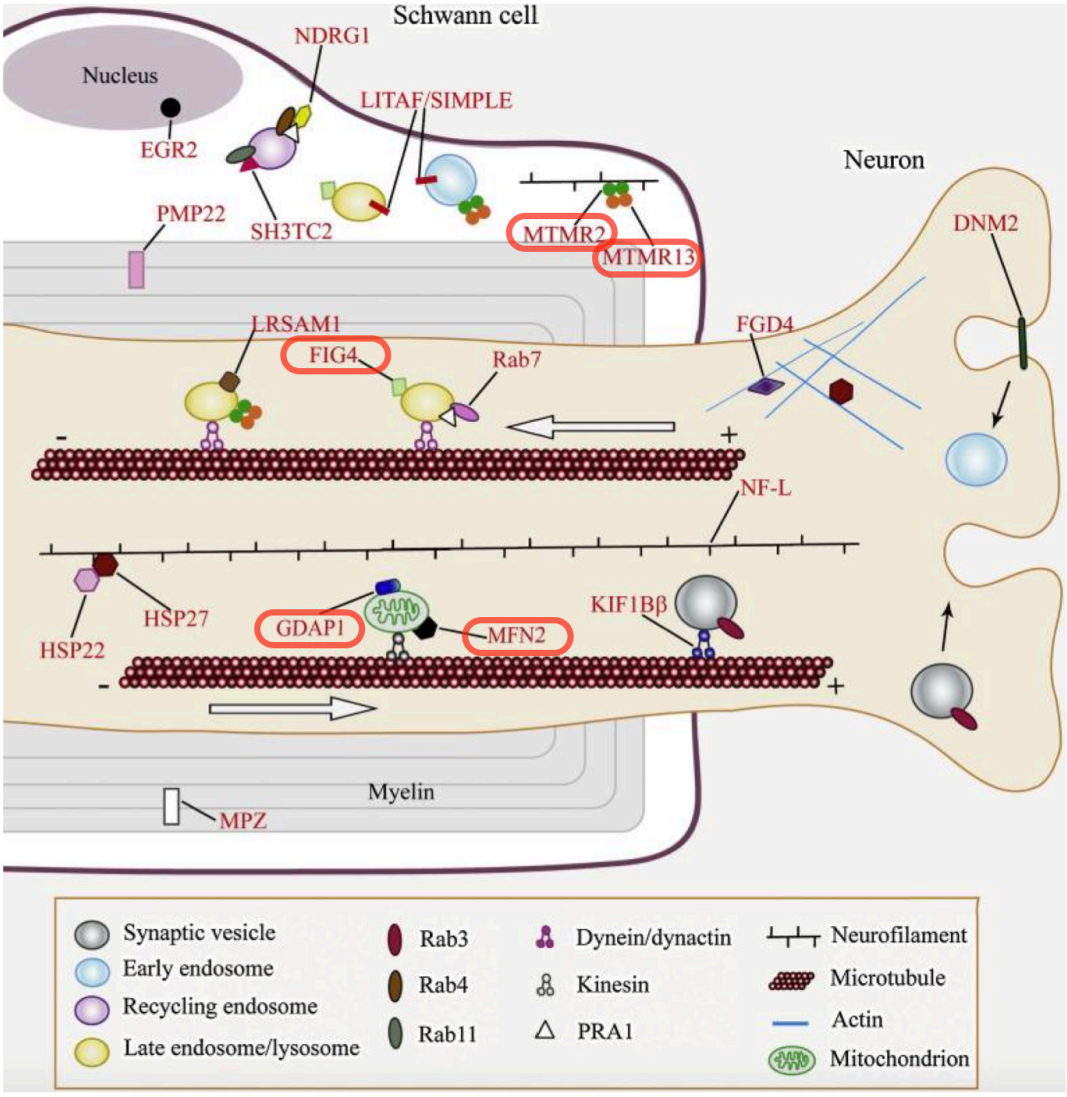

Figure 1.1. Cellular localization of proteins that are involved in CMT neuropathy. Proteins that are mentioned in the text were circularized (adapted from Bucci *et al*., 2012).

For many years, CMT disease-causing genes have been studied *in vitro*. However, animal models have also been developed to understand the complex pathogenesis of demyelination and axonal defects. Mouse models available for several subtypes of CMT1, CMT1X and CMT4B together with fly and zebrafish models can be highly instrumental for development of therapies for CMT disease.

1.1. *GDAP1*

Among the CMT disease-causing genes, mutations in *ganglioside-induced differentiation associated protein 1* (*GDAP1)* gene can be linked to demyelinating, axonal, or mixed forms of the disease with recessive or dominant modes of inheritance. Patients with *GDAP1* mutations show various clinical phenotypes of mild to very severe disease progression with late and early onset (Cassereau *et al.,* 2011). Additionally, *GDAP1* is a mitochondrial fission factor and involved in mitochondrial dynamics, which is a very essential pathway to maintain in peripheral nerves (Niemann *et al.,* 2005, 2009, 2014; Pedrola *et al.,* 2005; Lopez Del Amo *et al.*, 2014). These distinct forms of *GDAP1* mutations together with its involvement in mitochondrial dynamics make this gene promising to study and understand the underlying pathogenesis in CMT disease.

GDAP1 gene spans 13.9 kb of genomic DNA and it has six exons. It gives rise to a 4.1 kb transcript that encodes for a 358 amino acid long protein (Cuesta *et al.,* 2002). Ubiquitous expression of *GDAP1* has been shown in several human tissues, though its predominant expression is in the nervous system (Cuesta *et al.,* 2002). It has been shown that in the myelinated peripheral nerves, both Schwann cells and neurons express *GDAP1* (Niemann *et al.*, 2005; Pedrola *et al.*, 2005, 2008). The amino acid sequence of GDAP1 is similar to that of glutathione S-transferases (GSTs). In fact, secondary structure analysis showed that GDAP1 has two GST domains (GST-N and GST-C). GSTs are the regulators of the detoxification and reduction events of reactive oxygen species (ROS). The carboxyl-terminal sequence of GDAP1 has a hydrophobic domain (HD) and a transmembrane domain (TM) (Figure 1.2). Mitochondrial targeting and the fission function of GDAP1 are thought to be regulated by its TM domain, whereas its HD domain seems to be essential for mitochondrial fission (Wagner *et al.,* 2009). Like other GSTs, GDAP1 has a dimeric

and insoluble structure due to its TM domain (Cuesta *et al*., 2002; Shield *et al*., 2006). GDAP1 has also two helices, α4–α5 loop, in between the amino acids at position 152 to 195 (Cassereau *et al*., 2011).

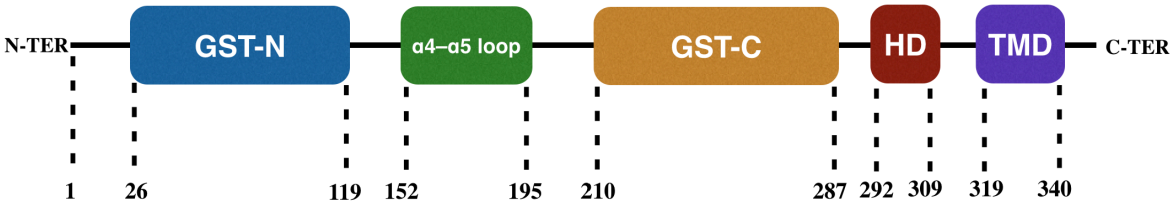

Figure 1.2. Schematic representation of the GDAP1 protein and its domains. Numbers represent the aminoacid numbers.

Mutation analyses of the *GDAP1* gene showed that mutations leading to CMT disease are in sequences coding for its key domains (Cassereau *et al*., 2011). Depending on the type of mutations, *GDAP1*-related CMT cases can be broadly categorized into two groups. First group is the CMT cases with rare dominant mutations of *GDAP1* that are less aggressive with the late age of onset and known as CMT2K subtype (Zimon *et al*. 2011). Second group is the CMT cases with the recessive mutations that are in the mitochondrial targeting domain or cause premature stop of translation. This group of mutations are much more severe with the early age of onset compared to the dominant ones and they mostly prevent mitochondrial fragmentation and oxidative stress protection roles of *GDAP1* (Niemann *et al*., 2005, 2009; Pedrola *et al*., 2008). The subtype of CMT for recessively inherited GDAP1 mutations is named as CMT4A (Baxter *et al*., 2002). Both the features of demyelinating and axonal neuropathies are seen in this autosomal recessive form of CMT like in motor NCV values. Patients suffering from CMT4A show early childhood onset and may even become wheelchair dependent on their second decade (Boerkoel *et al*., 2003).

In peripheral nerves, one of the pathways essential for synaptic transmission, respiratory function or cellular stress responses are mitochondrial dynamics-related pathways (Niemann *et al*., 2014; Chan, 2012). Mitochondrial dynamics are described as the continuous change in the position, size and shape of mitochondria within the cells (Chan, 2012). Neurons are particularly dependent on proper mitochondrial function and positioning due to the rapid changes in metabolic requirements arising from their

excitability. In many nervous system disorders such as dominant optic atrophy, amyotrophic lateral sclerosis, Parkinson's, Alzheimer's and Huntington's diseases and CMT, dysfunction of mitochondrial dynamics has been implicated as a pathogenic factor (Chen & Chan, 2009; Detmer & Chan, 2007).

The opposing processes of fusion and fission are the balancing events maintaining the mitochondrial morphology and population in equilibrium. These events not only control mitochondrial morphology and population but also regulate their function. The fusion event, which is the mixing of the membranes, the intermembrane space, and the matrix, occurs almost simultaneously both for the outer and inner membrane of mitochondria. Three proteins are required for mitochondrial fusion in mammals; the mitofusins Mfn1 and Mfn2 that are docked in the mitochondrial outer membrane and OPA1 that is associated with the inner mitochondrial membrane and intermembrane space (Chan, 2012). While mitofusins mediate outer membrane fusion with the adjacent mitochondria, OPA1 regulates inner membrane and intermembrane space fusion (Figure 1.3a). The mitochondrial fission event, on the other hand, is mediated by a dynamin-related protein, Drp1. Drp1 is a cytosolic protein and it is thought to regulate constriction of mitochondrial tubules by assembling on them (Chan, 2012). Recruitment of Drp1 for fission is mediated by a second protein such as Fis1, Mff, MiD49 or MiD51 (Figure 1.3b).

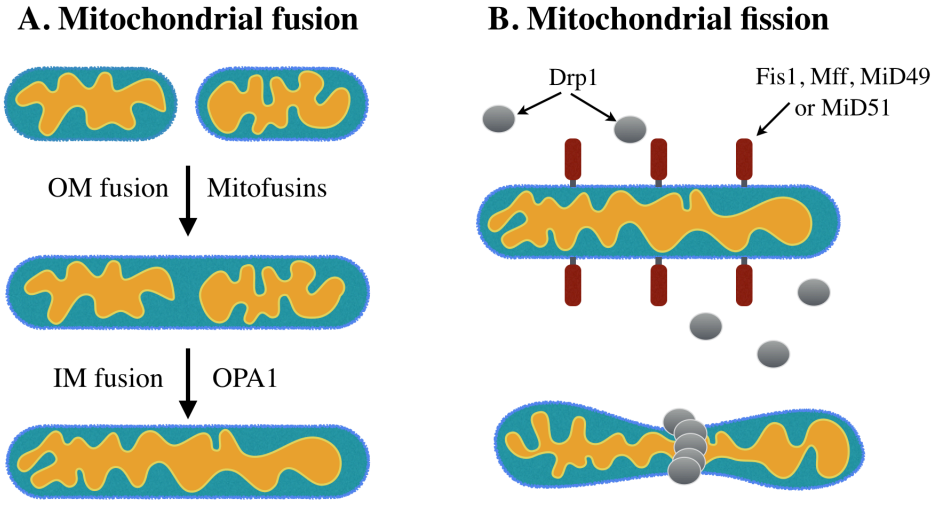

Figure 1.3. Schematic view of mitochondrial fusion and fission events. (A) Mitofusins in outer membrane (OM) and OPA1 in inner membrane (IM) fusion. (B) Recruitment of Drp1 to the mitochondrial surface. The candidate Drp1 receptors, Fis1, Mff, MiD49 and MiD51 are also depicted on the surface.

GDAP1 is located on the outer mitochondrial membrane to function as a fission factor and it is also categorized as a member of a new glutathione S-transferase family (Marco *et al*., 2004; Niemann *et al*., 2005, 2009; Pedrola *et al*., 2005, 2008; Shield *et al*., 2006; Huber *et al*., 2013). Many of the initial studies related with its function focus on its role in mitochondrial dynamics. In cultured cells, recessive *GDAP1* mutants showed reduced fission activity, while dominant mutants showed impairments in fusion (Niemann *et al*., 2005; Pedrola *et al*., 2005; Wagner *et al*., 2009). It was also found that mitochondrial fragmentation was induced when *GDAP1* was overexpressed, whereas tubular mitochondria were found when its downregulated (Niemann *et al*., 2005). Researchers also discovered that the CMT-related truncated forms of GDAP1 did not target mitochondria. Additionally, many of the recessive *GDAP1* mutations caused reduced activity compared to the dominant mutations that are mainly affecting the fusion activity (Niemann *et al*., 2005, 2009). Perturbation in transport, energy production, and calcium buffering were also detected in cells with *GDAP1* mutant alleles (Cassereau *et al*., 2011; Pla-Martin *et al*., 2013).

Aside from cell culture analyses, experiments performed with mice carrying the homozygous null mutant form of *Gdap1* allowed researchers to investigate CMT disease mechanisms (Niemann *et al*., 2014). The very first signs of a peripheral neuropathy, which are decreased nerve conduction velocity and hypo-myelination, began in 19-month-old *Gdap1* null mutant mice, indicating the progressive phenotype of CMT. These features recapitulated the phenotypes when *GDAP1* was only ablated in Schwann cells. In *Gdap1* null mutant mice, the morphology of intra-axonal mitochondria were altered, however, in the central nervous system (CNS), loss of *GDAP1* was compensated by the mitochondrial translocation of *GDAP1-like 1* (*GDAP1L1*), which is the paralogue of *GDAP1* and is only expressed in the CNS. Dorsal root ganglia explant cultures adapted from *Gdap1* null mutant mice also showed mild mitochondrial transport impairment (Niemann *et al*., 2014).

In addition to the mouse model, Dr. Galindo and his group in Centro de Investigacion Principe Felipe, Spain, conducted experiments in *Drosophila* in which the fly homolog of *GDAP1* (*CG4623*) expression was altered. Overexpression of *Drosophila Gdap1* resulted in fragmented mitochondria in the retina and muscle; on the contrary, downregulation of *Drosophila Gdap1* induced mitochondrial tubularization in the same tissues. The distribution of mitochondria within the cell was also altered in the fly retina

when *Drosophila Gdap1* was up-or-down regulated. Alteration of the expression levels of *Drosophila Gdap1* also caused neurodegeneration, abnormal synapse formation and muscular degeneration. All these mitochondrial defects and tissue degenerations were seen more severely in the old flies (five weeks old) as compared to the young flies (ten days old), indicating the progressive pathophysiology of the CMT disease (Lopez Del Amo *et al*., 2014). Not only cell culture experiments but also mouse and fly model experiments that were conducted to reveal *GDAP1*'s function suggest that the *GDAP1* protein is a mitochondrial fission factor and its loss or altered expression induces nervous or muscular system tissue degeneration due to alterations in mitochondrial dynamics.

Aside from GDAP1's involvement in mitochondrial dynamics, its two glutathione S-transferase (GST) domains are suggested to play a role in oxidative stress mechanisms (Marco *et al*., 2004). GSTs are enzymes that are working for the detoxification of xenobiotics, reactive oxygen species (ROS) and other cellular byproducts by catalyzing the conjugation of those charged substrates to glutathiones (GSHs) (Eaton & Bammler, 1999). GSTs are also known to be involved in cell signaling and post-transcriptional modification pathways (Laborde, 2010; Mcllwain *et al*., 2006).

In cell culture, *GDAP1* expression has a pro-survival effect in neuronal cell death models. In fact, overexpression of *GDAP1* in those cells resulted in reduced oxidative stress and protected mitochondrial integrity (Noack *et al*., 2012). Unlike many other GSTs, GDAP1 and its paralogue GDAP1L1 have a transmembrane domain, a hydrophobic domain, and an extra loop of alpha helices. Interestingly, they also lack any sequence similarity with other GSTs. These facts together with bioinformatics analyses group GDAP1 and GDAP1L1 as distinct GSTs (Marco *et al*., 2004). In *Gdap1* null mutant mice, it has been shown that mitochondrial DNA biogenesis and content were increased in the peripheral nervous system (PNS). This increase was associated with the increase in oxidative stress due to GDAP1 ablation, indicating that GDAP1 is required for maintaining redox status. It was also shown that an increase in mitochondrial DNA was only seen in the PNS but not in central nervous system (CNS). This phenomenon was explained as GDAP1L1's response to elevated levels of oxidized glutathione by its translocation from the cytosol to the mitochondrial outer membrane to substitute for GDAP1 ablation (Niemann *et al*., 2014). This suggests a novel function for GDAP1-family members, which is to function as a sensor in case of altered oxidative stress levels. In the *Drosophila* model,

a protective effect of *Drosophila Gdap1* over reactive oxygen species was also shown. Downregulation of *Drosophila Gdap1* resulted in a lower antioxidant defense in old flies (Lopez Del Amo *et al*., 2014).

1.1.1. *CG4623* is the Drosophila Homolog of *GDAP1*

CG4623 is the *Drosophila melanosgaster* homolog of vertebrate *GDAP1* gene according to the NCBI's protein blast tool, BLASTP 2.2.28+. Protein products of these two genes show 29% amino acid identity and 46% amino acid similarity (Altschul *et al*., 1997; 2005). A phylogenetic analysis of the GST family proteins showed that *CG4623* is the candidate homolog of both *GDAP1* and *GDAP1L1* (Marco *et al*., 2004). *CG4623* gene spans 2.3 kb of genomic DNA and it has four exons. It encodes a 328 amino acids long protein with 37.6 kDa in weight. CG4623 and GDAP1 proteins also share the same α4–α5 loop and C-terminal transmembrane domains.

In *Drosophila*, *CG4623* is expressed in imaginal discs, salivary glands, head and carcass at very low levels; in testis and larva at low levels, and in accessory gland and adult digestive system at moderate levels according to the ModENCODE database (Cherbas *et al*., 2011). Expression pattern analysis with DsRed tagged CG4623 *Drosophila* fly line showed that CG4623 is expressed in midgut, hindgut, malpighian tubules, anal pads, and antenna-maxillary sense organs (Lopez Del Amo *et al*., 2014). This expression pattern of *CG4623* resembles the expression pattern of the genes involved in reactive oxygen species (ROS) defense mechanisms, pointing at a role for *CG4623* in the defense against ROS (Lopez Del Amo *et al*., 2014). Overexpression of human *GDAP1* in flies lacking *CG4623,* partially rescues neurodegeneration phenotypes in the fly eye (Lopez Del Amo *et al*., 2014). These findings indicate that the human *GDAP1* can substitute the *CG4623* function as being its homolog.

1.2. *MTMR2*

Myotubularin-related protein 2 (*MTMR2*) is a phosphatase that is suggested to regulate vesicular trafficking in the nervous system (Wishart & Dixon, 2002). Loss of *MTMR2* causes autosomal recessive demyelinating CMT type 4B1 with myelin outfoldings (Bolino *et al*., 2000). The CMT4B subtype includes CMT4B1, CMT4B2 and

CMT4B3, which are caused by loss of function mutations in *MTMR2*, *MTMR13,* and *MTMR5,* respectively. CMT4B is the first neuropathy that was recognized with focally folded myelin. Disease onset is in early infancy, starting with a progressive atrophy and distal weakness in all limbs. By early adulthood, patients might be wheelchair dependent (Parman *et al*., 2004). In some cases, diaphragmatic and facial weakness, and scoliosis may occur (Tyson *et al*., 1997; Verny *et al*., 2004). NCV values of the patients are markedly reduced, ranging from 9 to 20 m/s with prolonged distal latency and reduced amplitudes (Quattrone *et al*., 1996). Pathological hallmark of CMT4B is the focally folded myelin sheaths and severe depletion of myelinated nerves (Tyson *et al*., 1997).

The *MTMR2* gene is a member of the *myotubularin* (*MTM*) gene family; it is located on chromosome 11q22 in the human genome and is ubiquitously expressed (Bolino *et al*., 2000). MTMR2 is a 643 amino acids long protein with a PH-GRAM domain, a phosphatase domain, a coiled-coil domain, and a PSD-95-Dlg-ZO-1 binding domain (PDZ-BD) at the carboxyl end (Figure 1.4) (Robinson & Dixon, 2006). PH-GRAM, phosphatase domain and coiled-coil domains of MTMR2 are conserved among many MTM proteins. PH-GRAM domain binds to phosphoinositides and are required for protein-lipid and protein-protein interactions to target proteins to specific cell membranes (Doerks *et al*., 2000). While the phosphatase domain dephosphorylates phosphoinositides (PIs), the coiled-coil domain is necessary for homo- and heterodimerization with other members of the *MTM* family (Berger *et al*., 2003). The PDZ-binding domain is required for transmembrane protein interactions thus suggesting a role in membrane metabolism for MTMR2.

MTM family of proteins shares homology with protein tyrosine phosphatases (PTPs) (Wishart & Dixon, 2002). This family is highly conserved among different species and includes fifteen members in humans (*MTM1* and *MTMR1-14*) (Kerk & Moorhead, 2010). Mutations in different *MTM* genes are linked with several diseases such as X-linked centronuclear myopathy due to *MTM1* mutations (Laporte *et al*., 1996), autosomal centronuclear myopathy associated with *MTMR14* (Tosch *et al*., 2006), CMT4B2 because of altered *MTMR13* (Azzedine *et al*., 2003), and CMT4B3 linked with *MTMR5* mutations (Nakhro *et al*., 2013). MTM family proteins consist of nine catalytically active (e.g. MTM1, MTMR1-4, MTMR6-7 and MTMR14) and six catalytically inactive members

(e.g. MTMR13). While active MTMs dephosphorylate their target, inactive MTMs determine the subcellular localization of active members via forming homo- and heterodimers with each other. Catalytically active MTMR2 protein is thought to be regulated by inactive MTMR13. This suggests that, not only loss of function mutations in different domains of MTMR2, but also mutations in MTMR13 resulting in dysregulation of MTMR2, might cause CMT phenotype with focally folded myelin sheaths (Previtali *et al*., 2003).

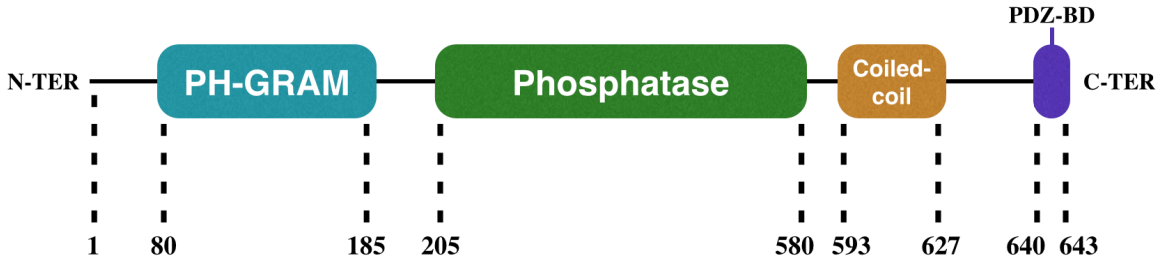

Figure 1.4. Schematic representation of the MTMR2 protein and its domains. Numbers represent the aminoacid numbers.

MTMR2 has a role in phosphatidyl inositol (PI) mechanism. PIs are distributed at specific intracellular membranes as potent signaling molecules and their actions are controlled by kinases and phosphatases (Vicinanza *et al*., 2008; Di Paolo & De Camilli, 2006). Membrane trafficking and dynamics, vesicle movement, tethering and fusion are regulated by PIs. PIs interact with cellular membrane proteins and cytosolic proteins via their PH-domains. Phospholipid phosphatase *MTMR2* interacts with PIs thorugh its PH-GRAM domain. MTMR2 specifically dephosphorylates both PtdIns3*P* (PI3P) and PtdIns(3,5)P_2 [PI(3,5)P2] phosphoinositides from their D3 position of the inositol ring, generating PtdIns5*P* (PI5P) (Tronchere *et al*., 2004; Cao *et al*., 2008). It has been shown that *MTMR2* co-localizes with Rab7 GTPase, which regulates the late endosomal membrane trafficking (Cao *et al*., 2008). Also, downregulation of *MTMR2* resulted in accumulation of epidermal growth factor receptor (EGFR) in late endosomes and increased levels of PI3P, which localizes to early and late endosomes. These findings suggest that MTMR2 might function in late endocytosis by negatively regulating membrane production. Thus, myelin outfoldings in case of CMT4B1 could be the consequence of the loss of negative control on membrane production in Schwann cells (Bolis *et al*., 2009).

In the *Mtmr2*-null mice, which were previously confirmed to recapitulate the CMT4B1 phenotype of myelin outfolding, Mtmr2 was shown to be interacting with Dlg1, a protein expressed in Schwann cells (Bolino *et al*., 2004). Also, downregulation of *Mtmr2* only in Schwann cells resulted in the same phenotype with *Mtmr2*-null mice, which suggests that Dlg1 and Mtmr2 interaction might be crucial for membrane homeostasis in Schwann cells. Fig4, which is required for PI(3,5)P2 generation, and Mtmr2 interaction was shown in Schwann cells and neurons of *Mtmr2*/*Fig4* double null mutant mice. This interaction suggests a role for Mtmr2 also in neurons, which might be functioning antagonistically with Fig4 to regulate membrane formation (Vaccari *et al*., 2011). Interaction of MTMR2 with neurofilament light chain protein expressed in neurons (Previtali *et al*., 2003) and PSD-95, a post-synaptic scaffolding protein, which is mainly localized in excitatory synapses in neurons (Lee *et al*., 2010), were also shown. These findings provide further evidence for functioning of MTMR2 in neurons.

1.2.1. *mtm* is the *Drosophila* Homolog of *MTMR2*

According to NCBI's protein blast tool (BLASTP 2.2.28+), *mtm* is the *Drosophila melanogaster* homolog of vertebrate *MTMR2*. Protein products of these two genes are 58% identical and 76% similar in amino acid content. Similar to MTMR2, mtm has also a PH-GRAM domain and a phosphatase domain. The *mtm* gene encodes a 69.8 kDa weighed protein.

In 2010, Velichkova *et al*., reported a *Drosophila* model of the mtm protein. They have shown that mtm has a role in policing traffic at the late endosome by regulating the PI(3)P pool and PI(3)P-mediated endolysosomal homeostatis. They have also shown that human MTMR2 rescues the lethality associated with mtm depletion in different tissues (Velichkova *et al*., 2010). Our former lab member Merve Kılınç also performed experiments with the *mtm*-null mutant flies that were generated by Velichkova and her colleagues. Merve Kılınç has shown that *mtm*-null mutant third instar larvae revealed satellite boutons and submembrane inclusions in its neuromuscular junctions (NMJs) (Kılınç, 2013). These morphological defects might be related with the problems in synaptic

transmission that are linked with mtm depletion. All these findings highlight the potential homology in between vertebrate MTMR2 and *Drosophila* mtm proteins.

1.3. *Drosophila melanogaster* as a Model Organism

The arthropod *Drosophila melanogaster*, which belongs to a subspecies of *Drosophilidae*, has long been recognized as one of the most powerful genetic system for studying multi-cellular eukaryotic biology. Although the arthropod lineage was separated from the vertebrate lineage more than 600 million years ago, genetic, molecular, and behavioral analyses with *Drosophila* over more than a century suggest that these flies are fruitful genetic tools (Hirth, 2010).

Drosophila has four morphologically distinct developmental stages, which are embryo, larva (three different instar stages), pupa, and adult stages. They represent the discrete developmental stages of embryonic development, juvenile growth phase, sexual maturation, and reproductive adulthood that are similar to many other animals. Flies that are kept at 25°C pass embryogenesis, first (L1) and second (L2) larval instar phases in three days, each phase lasting one day. The third instar larval phase (L3) lasts two days and is followed by the puparium formation, which includes four days of metamorphosis. Sexually active adult flies are formed after ten days of *Drosophila* egg fertilization. Flies have distinct anatomical features such as compound eyes, wings and bristles. These organs can attain different phenotypic features, which can be used to study neurodegeneration without affecting the survival of the fly (Hirth, 2010).

One of the major advantages of using *Drosophila* as a model organism is its cheap and easy maintenance in the laboratory as well as the ease of making genetic manipulations such as deletions, insertions, knockdowns or transgenics as compared to mammals. Additionally, a single mating couple of fruit flies can give rise to a large number of genetically identical progeny and they also have lifespan of 40-120 days depending on their diet and stress factors. Fundamental aspects of cellular processes like regulation of gene expression, subcellular trafficking, synaptic transmission, synaptogenesis and cell death events are very similar in between humans and flies. Besides, it is known that many

of the key regulatory pathways are conserved in between humans and flies such as Wnt, Ras/Extracellular Regulated Kinase (ERK), and Toll-like pathways. In fact, these pathways were first identified in flies and later their mammalian homologs were found (Ambegaokar *et al*., 2010). As compared to 23 pairs of homologous chromosomes (containing ~20000 genes) in humans, flies have only 4 pairs (containing ~12000 genes) making their genetics simpler. Nonetheless, approximately 77% of all known human disease genes have at least one fly homolog (Reiter *et al*., 2001). Amino acid identity of two homologous genes is nearly 40%, though this value is up to 90% for some of the conserved domains (Pandey & Nichols, 2011). Flies have ~200.000 neurons with simpler and compact nervous systems as opposed to ~100 billion neurons in humans in a complex network and anatomy (Ambegaokar *et al*., 2010). In spite of these differences, flies still show complex behavior of learning and memory; they perform complex motor behaviors like walking, climbing, flying, grooming and flight navigation. Compared to other organisms like *Caenorhabditis elegans*, *Drosophila* brain is complex enough to analyze human diseases and behavioral disorders. However, fly brain is still small enough compared to mouse for an in-depth structural and functional analysis (Hirth, 2010).

Many of the impractical genetic manipulations in mammals are possible to be performed in *Drosophila*, with the help of naturally found transposable elements. These elements are called P elements and consist of inverted repeats surrounding transposase genes, allowing them to hop into endogenous chromosomes. Researchers engineer P elements for genomic insertions to create disease models. On the other hand, a gene of interest can be overexpressed spatiotemporally with the GAL4/UAS system in which the binding of yeast-derived transcription factor GAL4 to the Upstream Activation Sequence (UAS) enhancer element activates transcription of the relevant gene (Ambegaokar *et al*., 2010).

Drosophila is a powerful model organism to study neurodegenerative diseases. *Drosophila* models of motor neuron diseases (spinobulbar muscular atrophy, spinal muscular atrophy, myotonic dystrophy), neurological disorders (Huntington's, Alzheimer's, Parkinson's diseases, Fragile-X syndrome, Frienreich's Ataxia, ALS) and myopathies (Duchenne muscular dystrophy, myotonic dystrophy) have been generated. By replicating key features of the human diseases, these models led insights into

understanding the pathogenesis of these diseases (Lloyd & Taylor, 2010). *Drosophila* models of CMT disease include tyrosyl-tRNA synthetase genes (*YARS* and *GARS*), *RAB7,* and *Drosophila Gdap1* (Storkebaum *et al*., 2009; Ermanoska et al. 2014; Cherry et al., 2013; Lopez Del Amo *et al*., 2014). All these disease models are also excellent *in vivo* systems for the testing of therapeutic compounds.

1.3.1. GAL4/UAS Binary System

The GAL4/UAS binary system is one of the most important genetic tool kit of *Drosophila*. Analogous to Cre-Lox system in mice, this system allows spatio-temporal expression of any gene. In this system, promoter of a gene is cloned and inserted upstream of GAL4, which is a transcription factor that is derived from yeast. UAS (Upstream Activating Sequence), on the other hand, is a yeast promoter element that can be recognized by GAL4 transcription factor.

In the flies bearing the transgene expressing GAL4, the chosen promoter drives GAL4 transcription factor expression in the desired tissue (Figure 1.5). Naturally, GAL4 does not have any target in *Drosophila* thus it is not functional by its own. GAL4 is only functional when it is bounded to the yeast promoter element, UAS (Figure 1.5). In this system, the gene of interest is cloned downstream of the UAS. In order for an organism to have both GAL4 and UAS; GAL4 fly strain (driver line) should be crossed with the UAS fly strain (responder line). In the resulting progeny, our gene of interest is expressed under the control of UAS in all the cells that express GAL4 (Jones, 2009).

UAS can be ectopically activated in many different tissue types, depending on the tissue-specific promoter used to express the GAL4 gene. This makes GAL4/UAS system very advantageous when generating neurodegeneration models since different phenotypes can be observed in different tissues or even in different cell types within the same tissue caused by the misexpression of the same gene. GAL4 lines that allow expression at different developmental stages are also available. It is also possible to terminate transcriptional activation of the gene of interest by using GAL80 that is the inhibitor of GAL4. Compared to direct promoter-fused transgenes, GAL4/UAS system has much

higher yield since it is possible to add more copies of either the driver or the UAS in the generated constructs.

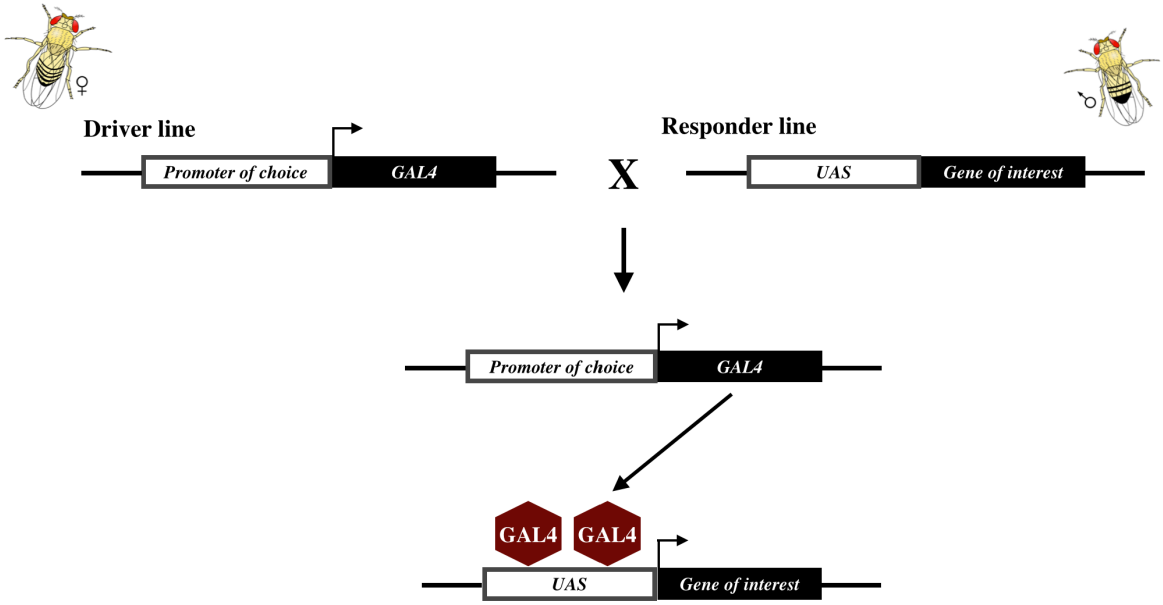

Figure 1.5. The GAL4/UAS binary system. Driver line expresses GAL4 in the cells that the promoter of choice is active. Responder line has gene of interest downstream of an UAS element. When these two lines are crossed, F1 progeny bearing the both driver and responder could express our gene of interest in the cells that express GAL4 under the control of promoter of choice.

P element transposons can be used as vectors for the generation of the transgenic GAL4 and UAS lines. P element transposons provide insertions in at least 40% of *Drosophila* genes. Different types of transposons have been generated allowing their random integration into the fly genome to find enhancers using enhancer trap screens, allow mutagenesis via insertions to disrupt genes, and to generate overexpression lines.

P elements insert randomly into the genome by their nature. However, some P element vectors can be engineered to contain short sequences called *attB*, which are bacterial attachment sites. *attB* sites allow site specific integration into the genome. The overexpression vectors of *pUAST* (random integration) and *pUASTattB* (site specific integration) are commonly used P element vectors. They not only allow overexpression of a gene but also promote overexpression of siRNAs against mRNAs of a target gene, which are in turn downregulated by those siRNAs.

1.3.2. The *Drosophila* Larval Neuromuscular Junction as a Model

In order to understand the essence of the neurodegenerative diseases, we must understand the fundamental mechanisms of neuromuscular function in synaptic transmission. *Drosophila* third instar larval body wall muscles harboring the neuromuscular junctions (NMJs) are ideal models to study synaptic transmission. The fundamental mechanisms of neuromuscular function are very well conserved across the species that include the processes of action potential generation, synaptic transmission at the NMJ and excitation-contraction in the muscle (Lloyd & Taylor, 2010). Almost all vertebrate proteins implicated in synaptic communication exist in flies (Lloyd *et al*., 2000).

The morphology of *Drosophila* larval NMJ is very well documented. NMJs are embedded in body wall muscles. Figure 1.6a shows the filleted larva, in which its body wall muscles are exposed as well as the nervous system comprised of two lobes of the brain (**) and the ventral nerve cord (*). Axons of the motor nerves (Figure 1.6a, arrow) project from ventral nerve cord to innervate muscles to form NMJs (Figure 1.6b). The largest NMJs reside in between muscles 6 and 7 in the abdominal segment 3 or 4 (Figure 1.6b). Synaptic boutons of the NMJs are shown in Figure 1.2c, in green. Boutons are composed of multiple active zones, each containing multiple synaptic vesicles. The presynaptic terminals projecting from the neurons (Figure 1.6c, in magenta) are surrounded by a synaptic cleft of the receiving muscle cell.

NMJs provide easy access to synapsis and boutons that can measure up to 5 μm in diameter. Immunostaining, electron microscopy, and electrophysiology are feasible assays of NMJ tissue to understand the functions of the proteins in the synaptic transmission.

The electrophysiological recordings are the most fundamental measurements for CMT diagnosis. Clinicians preferentially use motor nerve conduction velocities (mNCVs) of the patients as one of the diagnostic criteria. In fact, synaptic transmission studies in *Drosophila* include electrophysiological analyses, where the electrical signal elicited at the postsynaptic terminal in response to presynaptic release reveals presynaptic function.

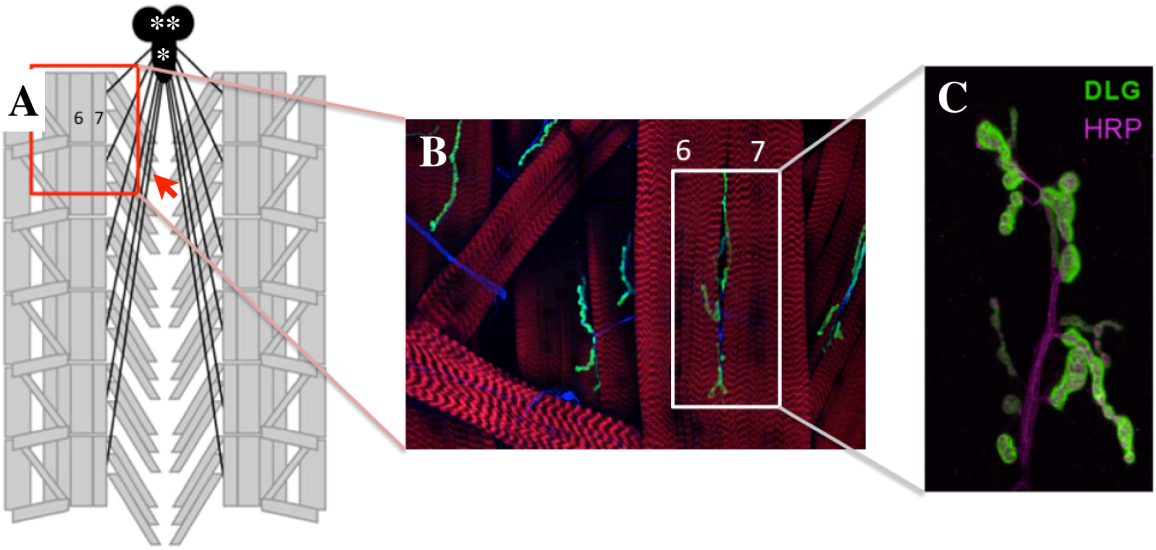

Figure 1.6. Larval body wall muscles and neuromuscular system. (A) Filleted larva, in which its body wall muscles and nervous system are exposed (adapted from Imlach and McCabe, 2009). (B) NMJ residing between muscle 6 and 7 in the abdominal segment. (C) NMJ labeled with anti-HRP (magenta) and anti-DLG (green). HRP stains neuronal membranes and DLG stains post-synaptic areas (Kılınç, 2013).

Individual muscles and nerve bundles can be easily visualized in the *Drosophila* larva. Glutamatergic synapses of the third instar larval NMJ is a robust model system to study synaptic transmission. In larvae, it is possible to measure excitatory junction potentials (EJPs), which is an upswing in the membrane potential due to the current influx upon vesicular release of glutamate neurotransmitter from the neurons at the synapses. EJP values can be recorded with a measurement electrode in the muscle while another electrode stimulates the neuron to induce vesicular release (Imlach and McCabe, 2009). Upon stimulation of the motor neuron, signals are transmitted across the NMJ synapse and are recorded in the muscle as a shift in the membrane potential upon neurotransmitter release (Figure 1.7).

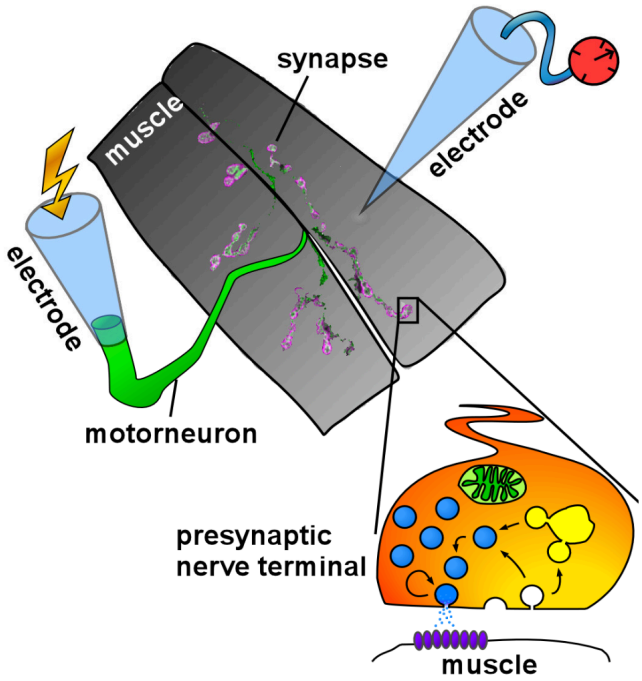

Figure 1.7. Schematic overview of measuring EJPs at the *Drosophila* NMJ. Motor neuron projecting to the muscle is sucked with an electrode. It is then stimulated to induce neurotransmitter release at the synapse. Change in the muscle cell membrane potential upon neurotransmitter release is measured with a measurement electrode (adapted from Uytterhoeven, 2012).

EJPs are detected as changes in the muscle cell membrane potential. This is due to ion flux (neurotransmitter glutamate and ions) through muscle glutamate receptors. In normal conditions, inside of a cell is electrically negative when compared with the outside, thus the resting membrane potential of a wild type larva is at least ~50-80 mV less than the outside. Nerve stimulation causes release of neurotransmitters and entry of the ions into the muscle cell, resulting in a shift in the membrane potential (EJP). EJP amplitude of wild type larva is around 30-40 mV (Figure 1.8). Change in the amplitude of EJP's can be referred to the differences in synaptic function and structure.

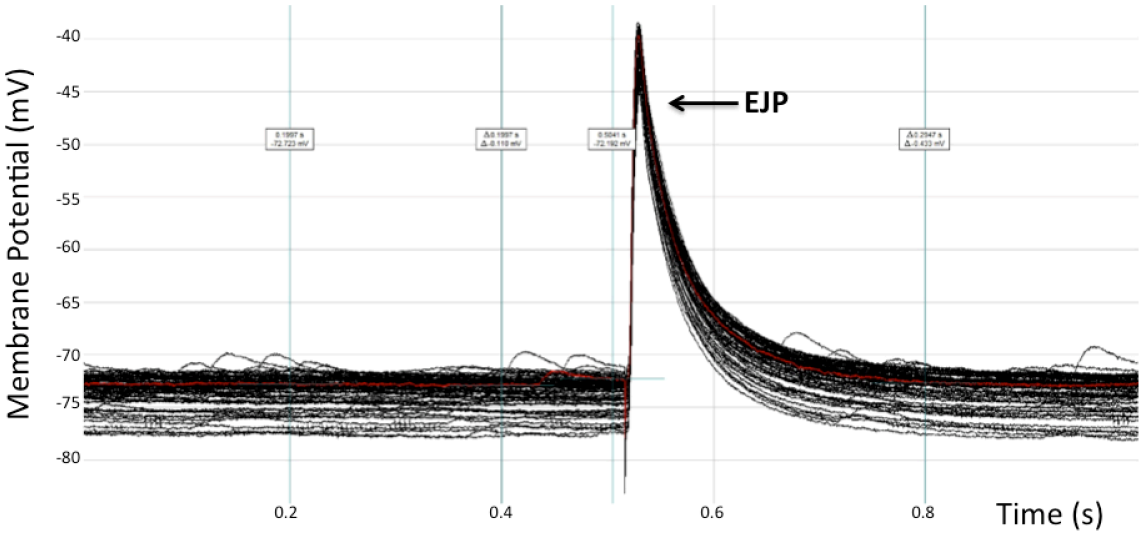

Figure 1.8. Representative intracellular EJP recordings from muscles of the third instar *Drosophila* larva. Wild type larva has a membrane potential of -60 to -80 mV, whereas the EJP amplitude of the larva is around 30-40 mV.

2. AIM OF THE STUDY

This study aims to generate *Drosophila* models for Charcot-Marie-Tooth disease, specifically for its subtype CMT4, by altering the expression levels of *ganglioside-induced differentiation associated protein 1* (*GDAP1)* and *myotubularin-related 2* (*MTMR2*) genes. GDAP1 is a mitochondrial fission factor with glutathione S-transferase activity and involved in mitochondrial dynamics. MTMR2, on the other hand, is a phosphatase that is suggested to regulate vesicular trafficking in nervous system.

For this purpose, we planned to downregulate *Drosophila* homologs of *GDAP1* and *MTMR2* that are known as *CG4623* and *mtm*, respectively. The expressions of these genes were silenced either ubiquitously or in a tissue specific manner using RNA interference method. Overexpression of *CG4623* and *mtm*, on the other hand, has been achieved using our newly generated overexpression fly lines.

In the first part of the study, we have produced a polyclonal antibody for CG4623, since it is not available commercially. The antibody developed has been tested using Western blot analyses and immunohistochemistry assays and used to assess CG4623 expression levels and pattern in *Drosophila*.

In the second part, we aimed to perform synaptic electrophysiology recordings to elucidate functional roles of CG4623 and mtm in synaptic transmission based on a collaborative study with Prof. Patrik Verstreken's Laboratory in University of Leuven.

Lastly, we have investigated changes in neuromuscular junction (NMJ) morphology to analyze the effects of altered expression levels of CMT causative genes in synapse-to-muscle interaction zones. Additionally, mitochondrial dynamics analyses of CG4623 were performed to investigate its role in mitochondrial fission mechanism.

3. MATERIALS

3.1. Biological Materials

3.1.1. The Model Organism: *Drosophila melanogaster*

Drosophila melanogaster lines used in this study are listed in Table 3.1. All fly lines were commercially available except that *UAS-CG4623 OE* and *UAS-mtm OE* lines were generated by former M.Sc. student Kaya Akyüz and *CG4623::DsRed* line was generated by Dr. Galindo and his group in Centro de Investigacion Principe Felipe, Spain. They were maintained in nine cm long plastic vials filled with approximately 10 ml Nutri-Fly Bloomington Formulation that was prepared according to manufacturer's instructions. The flies in vials were kept in incubators that are set to 12:12 day:night cycle at 25°C in 80% humidity unless stated otherwise. Stock flies were flipped to the fresh fly food containing vials in every 17-18 days.

Table 3.1. List of *Drosophila melonagaster* lines used in this study.

Genotype	Chromosome	Description
Canton-S	-	Red eye
w^{1118}	I	White eye
y, v	I	Yellow body, vermillion eye
y, w	I	Yellow body, white eye
Act5C-GAL4	II	Ubiquitous driver
OK6-GAL4	II	Motor neuron driver
CyO	II	Balancer chromosome with curly wings
CyO, GFP	II	Balancer chromosome with GFP expression
UAS-CG4623 KK RNAi	II	Overexpresses dsRNA targeting *CG4623*

Table 3.1. List of *Drosophila melonagaster* lines used in this study (cont.).

UAS-KK Control	II	Control line that does not contain KK RNAi sequence
CG4623::DsRed	II	DsRed tagged CG4623
elav-GAL4	III	Neuronal driver
repo-GAL4	III	Glial driver
repo-GAL4, UAS-mitoGFP	III	Glial driver that overexpresses GFP with mitochondria import signal
UAS-Dicer;;nSyb-GAL4	III	Neuronal driver with Dicer enzyme
TM6, tb, hu	III	Balancer chromosome with tubby larvae and additional macrochaetas on the humeri in adults
TM6B, tb, sb	III	Balancer chromosome with tubby larvae and short bristle marker in adults
UAS-CG4623	III	Overexpresses *CG4623*
UAS-Drp1 TRIP RNAi	III	Overexpresses dsRNA targeting Drp1
UAS-Marf TRIP RNAi	III	Overexpresses dsRNA targeting Marf
UAS-TRIP Control	III	Control line that does not contain TRIP RNAi sequence

3.1.2. Rabbits

Two New Zealand white rabbits were used in this study for antibody generation against a desired antigen. They were purchased from Boğaziçi University, Center for Life Sciences and Technologies. Rabbits were bred in the animal facility of the Center on a 12:12 day:night cycle at room temperature. Food, water and maintenance supplies were also provided by the animal facility until the termination of the study. All use and handling of animals were in accordance with Boğaziçi University Ethics Committee guidelines.

3.2. Chemicals and Enzymes

Chemicals and enzymes used in this study are listed in Table 3.2. Their supplier and catalog number information are also given in the table.

Table 3.2. List of chemicals and enzymes used in this study.

Chemical	**Supplier and Catalog Number**
β-mercaptoethanol	Merck Millipore, Germany (8057400250)
Acetic acid	Merck Millipore, Germany (1.00056.2500)
Acetone	Sigma-Aldrich, USA (650501)
Acrylamide	Sigma-Aldrich, USA (A3553)
Ammonium chloride	BDH, England (271495R)
Ammonium peroxodisulfate	Fluka, Germany (09914)
Benzonase nuclease	Merck Millipore, Germany (70664)
Bis-acyrlamide	Sigma-Aldrich, USA (M7279)
Bovine Serum Albumin	Sigma-Aldrich, USA (A2153)
Bromophenol blue	Merck Millipore, Germany (111746)
Calcium chloride	Sigma-Aldrich,USA (C1016)
Chloramphenicol	Applichem, Germany (7495)
Citric Acid	Sigma-Aldrich, USA (251275)
Coomassie Brillant Blue R250	Merck, Germany (112553)
D-glucose	Sigma-Aldrich, USA (G8270)
EDTA	Riedel-de Haen, Germany (32140)
Ethanol	Panreac, Spain (131086.1214)
Formaldehyde	Sigma-Aldrich, USA (47608)
Freund's Adjuvant, Complete	Sigma-Aldrich, USA (F5881)
Freund's Adjuvant, Incomplete	Sigma-Aldrich, USA (F5506)
Glycerol	Sigma-Aldrich, USA (G5516)
Glycine	Sigma-Aldrich, USA (G8898)
HEPES	Sigma-Aldrich, USA (H4034)
Hydrochloric acid	BDH, England (2850744)
Imidazole	Sigma-Aldrich, USA (I5513)

Table 3.2. List of chemicals and enzymes used in this study (cont.).

ImmunoCruz Western Blotting Luminol Reagent	Santa Cruz Biotechnology, UAS (sc-2048)
Isopropanol	Sigma-Aldrich, USA (24137)
Isopropyl β-D-1-thiogalactopyranoside	Promega, USA (V395A)
Kanamycin	Life Technologies, USA (11815-024)
LB broth	Difco, France, (244620)
Magnesium chloride	Carlo Erba Reagenti, Italy (349357)
Methanol	Sigma-Aldrich, USA (24229)
Monosodium phosphate	Merck Millipore, Germany (1.06576.1000)
Normal goat serum (NGS)	Merck Millipore, Germany (S26-100ML)
NP-40	Fluka, Germany (74385)
PageRuler Prestained Protein Ladder	Thermo Scientific, USA (26616)
Phenylmethanesulfonyl fluoride	Sigma Aldrich, USA (P7626)
Phosphate buffered saline (10X)	Life Technologies, USA (70011-036)
Potassium acetate	Sigma-Aldrich, USA (P1190)
Potassium chloride	Merck Millipore Germany (1.04935.1000)
Potassium Phosphate	Merck Millipore, Germany (529568)
Propionic acid	Merck Millipore, Germany (8.00605.0500)
Protease inhibitor cocktail	Roche, Germany (14268500)
Sodium azide	Sigma-Aldrich, USA (438456)
Sodium bicarbonate	Sigma-Aldrich, USA (S5761)
Sodium chloride	Sigma-Aldrich, USA (13423)
Sodium citrate	Merck Millipore, Germany (106448)
Sodium dodecyl sulfate	Merck Millipore, Germany (822050)
Sodium hydroxide	Riedel-de Haen, Germany (06203)
Sucrose	Sigma-Aldrich, USA (S0389)
TEMED	Sigma-Aldrich, USA (T7024)
Trehalose	Sigma-Aldrich, USA (T9531)
Trichloraacetic acid	Merck Millipore, Germany (100807)
Tris	Sigma-Aldrich, USA, (T1503)
Triton X-100	Sigma-Aldrich, USA (T8787)

Table 3.2. List of chemicals and enzymes used in this study (cont.).

Tween 20	Riedel-de Haen, Germany (63158)
Urea	Sigma Aldrich, USA (U5378)

3.3. Buffers and Solutions

Buffers and solutions used in this study are listed in Tables 3.3 - 3.5. The contents of these preparations are also given in the tables.

Table 3.3. Buffers and solutions used in protein purification and antibody generation assays.

Buffer or Solution	**Content**
Buffer B (pH 8.0)	0.1 M NaH_2PO_4 7 M Urea 0.01 M Tris-Cl (pH 8.0) 0.1 mM PMSF 3 unit/ml Benzonase nuclease
Buffer C (pH 5.9)	0.1 M NaH_2PO_4 8 M Urea 0.01 M Tris-Cl (pH 6.3) 0.1 mM PMSF
Buffer E (pH 4.5)	0.1 M NaH_2PO_4 8 M Urea 0.01 M Tris-Cl (pH 4.5) 0.1 mM PMSF
Binding Buffer (pH 7.5)	50 mM HEPES (pH 7.5) 300 mM KCl 1% Triton X-100 10 mM Imidazole (pH 8.0) 0.1 mM PMSF

Table 3.3. Buffers and solutions used in protein purification and antibody generation assays (cont.).

Wash Buffer (pH 7.5)	50 mM HEPES (pH 7.5) 300 mM KCl 1% Triton X-100 30 mM Imidazole 0.1 mM PMSF 1M NH_4Cl
Elution Buffer (pH 7.5)	50 mM HEPES (pH 7.5) 300 mM KCl 1% Triton X-100 500 mM Imidazole 0.1 mM PMSF
BBT Buffer	1X PBS 0.1% BSA 0.1% Tween 20
Gel Extraction Elution Buffer (pH 7.5)	50 mM Tris-Cl 150 mM NaCl 0,1 mM EDTA
Sodium Citrate-Glucose Solution	2.3 g Sodium citrate 0.8 g Citric acid 2.2 g D-glucose
Strip Buffer for Nickel Column Cleaning	50 mM KH_2PO_4 0.3 M NaCl 0.1 M EDTA

Table 3.4. Buffers and solutions used in Western Blot analysis.

Buffer or Solution	**Content**
Blocking Solution	5% BSA in TBS-T
Coomassie Blue Destaining Solution	30% Isopropanol 10% Acetic acid

Table 3.4. Buffers and solutions used in Western Blot analysis (cont.).

Coomassie Blue Staining Solution	50% Methanol 10% Acetic acid 0.05% Coomassie Brillant Blue R250
Non-ionic Fly Lysis Buffer	20 mM Tris-Cl (pH 6.8) 50 mM NaCl 1% NP-40 2 mM EDTA 1X Protease inhibitor cocktail
Protein Sample Buffer (6X)	300 mM Tris-Cl (pH 6.8) 12 mM EDTA 60% Glycerol 12% SDS 6% β-mercaptoethanol 0.04% Bromophenol blue
Running Buffer	25 mM Tris-Cl 250 mM Glycine 0.2% SDS
SDS-Polyacrylamide Gel (10%)	375 mM Tris-Cl (pH 8.8) 10% Acrylamide:Bisacrylamide (37.5:1) 0.1% SDS 0.1% APS 0.1% TEMED
SDS-Polyacrylamide Gel (5%)	125 mM Tris-Cl (pH 6.8) 5% Acrylamide:Bisacrylamide (37.5:1) 0.1% SDS 0.1% APS 0.1% TEMED
Stripping Solution	62,5 mM Tris-Cl (pH 6.8) 2% SDS 0.7% β mercaptoethanol

Table 3.4. Buffers and solutions used in Western Blot analysis (cont.).

Transfer Buffer	25 mM Tris-Cl 200 mM Glycine 15 % Methanol
TBS with Tween 20 (TBS-T)	0.1 % Tween 20 in TBS
Tris-Buffered Saline (TBS)	20 mM Tris-Cl (pH 8.0) 150 mM NaCl

Table 3.5. Buffers and solutions used in immunohistochemistry assays.

Buffer or Solution	**Content**
Blocking Solution	10% NGS in PBX4
Fixative Solution	3.7% Formaldehyde in HL-3 solution
HL-3 Solution (pH 7.2)	110 mM NaCl 5 mM KCl 10 mM $NaHCO_3$ 5 mM HEPES 30 mM Sucrose 5 mM Trehalose 10 mM $MgCl_2$
PBS (1X)	10% PBS (10X) in dH_2O
PBX4	0.4% Triton X-100 in 1X PBS

3.4. Antibodies

Antibodies used in Western Blot Analysis are listed in Tables 3.6 (primary antibodies) and 3.8 (secondary antibodies). Antibodies used in Immunohistochemistry assays are listed in Tables 3.7 (primary antibodies) and 3.9 (secondary antibodies).

Table 3.6. List of primary antibodies used in Western Blot Analysis.

Antigen	**Host**	**Dilution**	**Producer**
Actin	Goat	1000	Santa Cruz Biotechnology, USA (sc1616)

Table 3.6. List of primary antibodies used in Western Blot Analysis (cont.).

CG4623	Rabbit	2500	Our laboratory (CMT Lab)
CG4623 (pre-adsorbed)	Rabbit	1000	Our laboratory (CMT Lab)
His-probe	Mouse	1000	Santa Cruz Biotechnology, USA (sc8036)

Table 3.7. List of primary antibodies used in Immunohistochemistry.

Antigen	**Host**	**Dilution**	**Producer**
CG4623	Rabbit	100	Our laboratory (CMT Lab)
DLG1	Mouse	50	DSHB
DsRed	Rabbit	500	Clontech
GFP	Rabbit	500	Torrey Pines Biolabs
HRP	Rabbit	1000	Jackson Laboratories
HRP (Cy3 conjugated)	Goat	500	Dianova
Repo	Mouse	20	DSHB

Table 3.8. List of secondary antibodies used in Western Blot Analysis.

Target	**Host**	**Tag**	**Dilution**	**Producer**
Goat	Donkey	Horse radish peroxidase	5000	Santa Cruz Biotechnology, USA (sc2620)
Rabbit	Goat	Horse radish peroxidase	3000	Santa Cruz Biotechnology, USA (sc2030)
Mouse	Donkey	Horse radish peroxidase	2000	Santa Cruz Biotechnology, USA (sc2314)

Table 3.9. List of secondary antibodies used in Immunohistochemistry.

Target	**Host**	**Tag**	**Dilution**	**Producer**
Rabbit	Goat	Alexa 488	500	Invitrogen
Mouse	Donkey	Alexa 633	800	Invitrogen

3.5. Laboratory Equipment

Laboratory equipment used in this study is listed in Table 3.10.

Table 3.10. List of laboratory equipment used in this study.

Equipment	Producer
Autoclave	Astell Scientific Ltd., UK
Blotting Apparatus	Mini Trans-Blot Cell, Bio-Rad, USA
Centrifuges	Allegra X-22R, Beckman Coulter, USA Centrifuge 5415, Eppendorf, Germany J2-21 Centrifuge, Beckman, USA
Chemiluminescence Detection System	Stella, Raytest, Germany
Cold Room	Birikim Elektrik Soğutma, Turkey
Confocal Microscope	SP5, AOBS, Leica, Germany
Dissection Forceps	FST, USA
Dissection Scissors	Wannas Fine Scissors, WPI, USA
Electronic Balance	UW6200H, Shimadzu, Japan
Electrophoresis	Mini PROTEAN Tetra Cell, Bio Rad, USA PROTEAN II xi Cell, Bio-Rad, USA
The Flowbuddy	Flystuff, Genesee Scientific, USA
Fly CO_2 Pads	Flystuff, Genesee Scientific, USA
Fly Homogenizer	Kontes Pellet Pestile Motor, Fisher Scientific, UK
Fly Homogenizer Heads	Fisher Scientific, UK
Fly Incubators	TK 120, Nüve, Turkey TK 600, Nüve, Turkey
Fluorescence Stereomicroscope	MZ16FA, Leica, Germany
Freezers	-20 ºC, Arçelik, Turkey -80 ºC, Thermo Forma, USA
Glass Capillary Puller, Model P2000	Sutter Instrument Co., USA
HisTrap FF Nickel Column	GE Healthcare, England
Hybridization Oven	Hybaid Shaken Stack, Thermo Scientific

Table 3.10. List of laboratory equipment used in this study (cont.).

Laboratory Bottles	Isolab, Germany
Magnetic Stirrers	Speed Safe, Hanna Instruments, USA MK 418, Nüve, Turkey
Micropipettes	Gilson, USA
Microwave Oven	Arçelik, Turkey
Multiclamp 700B, Axon Instruments	Molecular Devices, USA
Nickel Column	Qiagen, Netherlands
Peristaltic Pump	LKB Bromma, Sweeden
pH Meter	HI 208 Hanna Instruments, Romania
Power Supply	Power Pac, Bio-Rad, USA
Refrigerators	+4º C Arçelik, Turkey
Shakers	SL 350, Nüve, Turkey Orbital Shaker, Thermo Scientific, USA
Sonicator	Sonoplus, Bandelin, Germany
Spectrophotometers	ND-1000, NanoDrop, USA DU 730, Beckman Coulter, USA
Stereomicroscope	SZ61, Olympus, Japan
Stimulus Isolater	WPI, USA
Thermal Cycler	C1000 Thermal Cycler, Bio-Rad, USA
Vortex Mixer	Nuvemix, Nüve, Turkey

3.6. Disposable Labware

Disposable labware used in this study are listed in Table 3.11.

Table 3.11. List of disposable labware used in this study.

Disposable Labware	**Producer**
Centrifuge tubes, 15 ml	Becton, Dickinson and Company, USA
Centrifuge tubes, 50 ml	Becton, Dickinson and Company, USA
Culture tubes, 14 ml	Greiner Bio-One, Belgium

Table 3.11. List of disposable labware used in this study (cont.).

Filtered tips	Fisher Scientific, UK
Flugs	Flystuff, Genesee Scientific, USA
Fly tubes	Gür Plastik, Turkey
Glass capillaries with flament	Hilgenberg, Germany
Microcentrifuge tubes, 0.5 ml	Fisher Scientific, UK
Microcentrifuge tubes, 1.5 ml	Fisher Scientific, UK
Microcentrifuge tubes, 2 ml	Fisher Scientific, UK
Pasteur pipettes	Isolab, Germany
Pestle and mortar	Boeco, Germany
Petri dishes (60 mm)	Isolab, Germany
Pipette tips	Fisher Scientific, UK
PVDF Western Blotting Membrane	Roche, Germany
Scalpel	Bayha, Germany
Serological pipette, 50 ml	Greiner Bio-One, Belgium
Syringe, 50 ml	Set, Turkey
Syringe Filter, 0.22 um	Sartorius Stedim Biotech, Germany
Syringe Filter, 0.45 um	Sartorius Stedim Biotech, Germany

4. METHODS

4.1. Downregulation of *CG4623*

CG4623 gene expression level was downregulated using RNA interference pathway. *CG4623 KK RNAi Drosophila* line was purchased from Vienna *Drosophila* Resource Center (VDRC) and was crossed with ubiquitous or tissue specific driver lines. As a control to RNAi line, *KK Control*, which was purchased from the same company, was crossed with the same driver lines.

4.1.1. Ubiquitous Downregulation of *CG4623*

Ubiquitous downregulation of *CG4623* was achieved under the control of actin5C promoter using UAS-GAL4 system. To generate flies that express interfering RNA for *CG4623; CyO, GFP* (curly winged flies expressing GFP) balanced *Act5C-GAL4* driver line was crossed with *CG4623 KK RNAi* line and its control line *KK Control*. Crosses were kept at 25°C in 80% humidity. Among the F1 progeny, L3 larvae were selected against GFP signal (Figure 4.1).

$$♂;UAS-CG4623\ KK\ RNAi;\quad \mathbf{X}\quad ;\frac{Act5C-GAL4}{CyO,GFP};♀$$

$$↓$$

$$♀/♂\ ;\frac{UAS-CG4623\ KK\ RNAi}{Act5C-GAL4};$$

Figure 4.1. Crossing scheme used for ubiquitous downregulation of *CG4623*. L3 larvae were selected against GFP signal among the progeny.

4.1.2. Tissue Specific Downregulation of *CG4623*

CG4623 was downregulated in different tissues of *Drosophila* by using tissue specific drivers. For this purpose, *CG4623 KK RNAi* and *KK Control* lines were crossed with these driver lines. Crosses were kept at 25°C in 80% humidity (except for the cross with *UAS-Dicer;;nSyb-GAL4* driver, which was kept at 29°C). In the *elav-GAL4* driver line, GAL4 protein is generated under the control of *elav* promoter that is used as a neuronal driver. In the *UAS-Dicer;;nSyb-GAL4* driver line, GAL4 protein is generated under the control of *nSyb* promoter that is also used as a neuronal driver, additionally dicer enzyme is overexpressed in this driver line for increasing the effectiveness of the sequence-specific degradation of the target mRNA. GAL4 protein is generated under the control of *OK6* promoter that is restricted to motor neurons in the *OK6-GAL4* driver line. *repo-GAL4* driver line was used to ensure downregulation in glial lineage cells. Since *elav-GAL4* (Figure 4.2), *UAS-Dicer;;nSyb-GAL4* (Figure 4.3) *OK6-GAL4* (Figure 4.4) driver lines were homozygous, there was no need for larval selection. On the other hand, *repo-GAL4* (Figure 4.5) driver line was balanced with *TM6B, tb, sb* (tubby larva, short bristles in adults), thus in the resulting progeny, L3 larvae were selected against tubby (tb) character.

$$♂;UAS-CG4623\ KK\ RNAi;\quad \mathbf{X}\quad ;;elav-GAL4\ ♀$$

$$↓$$

$$♀/♂\ ;\ \frac{UAS-CG4623\ KK\ RNAi}{+};\frac{elav-GAL4}{+}$$

Figure 4.2. Crossing scheme for neuronal *CG4623* downregulation using *elav-GAL4* line.

$$♂;UAS-CG4623\ KK\ RNAi;\quad \mathbf{X}\quad UAS-Dicer;;nSyb-GAL4♀$$

$$↓$$

$$♀/♂\ \frac{UAS-Dicer}{+}\ ;\ \frac{UAS-CG4623\ KK\ RNAi}{+};\frac{nSyb-GAL4}{+}$$

Figure 4.3. Crossing scheme for neuronal *CG4623* downregulation using *UAS-Dicer;;nSyb-GAL4* line.

$$♂;UAS-CG4623\ KK\ RNAi;\quad \mathbf{X}\quad ;OK6-GAL4;♀$$

$$\downarrow$$

$$♀/♂\ ;\frac{UAS-CG4623\ KK\ RNAi}{OK6-GAL4};$$

Figure 4.4. Crossing scheme for motor neuron specific *CG4623* downregulation.

$$♂;UAS-CG4623\ KK\ RNAi;\quad \mathbf{X}\quad ;;\frac{repo-GAL4}{TM6B,tb,sb}\ ♀$$

$$\downarrow$$

$$♀/♂\ ;\frac{UAS-CG4623\ KK\ RNAi}{+};\frac{repo-GAL4}{+}$$

Figure 4.5. Crossing scheme for glial *CG4623* downregulation.

4.1.3. Glial Downregulation of *CG4623* for Analysis of Mitochondria Dynamics

In order to analyze mitochondria dynamics, *CG4623* was downregulated with the glia driver *repo-GAL4, UAS-mitoGFP* that has mitochondria-targeted GFP. *CG4623 KK RNAi* and *KK Control* lines were crossed with *repo-GAL4, UAS-mitoGFP* driver line and the crosses were kept at 25°C in 80% humidity. Since *repo-GAL4, UAS-mitoGFP* driver line was balanced with *TM6, tb, hu* (tubby larva, additional macrochaetas on the humeri in adults), L3 larvae were selected against tubby (tb) character among the progeny (Figure 4.6).

$$♂;UAS-CG4623\ KK\ RNAi;\quad \mathbf{X}\quad ;repo4.3;\frac{repo-GAL4,mitoGFP}{TM6,tb,hu}\ ♀$$

$$\downarrow$$

$$♀/♂\ ;\frac{UAS-CG4623\ KK\ RNAi}{repo4.3};\frac{repo-GAL4,mitoGFP}{+};$$

Figure 4.6. Crossing scheme for glial *CG4623* downregulation.

4.2. Overexpression of *CG4623*

CG4623 was overexpressed ubiquitously or in a tissue specific manner by crossing *UAS-CG4623 OE* line, which was generated by former M.Sc. student Kaya Akyüz, with the ubiquitous or tissue specific driver lines. As a control to overexpression line, w^{1118} was crossed with appropriate driver lines.

4.2.1. Ubiquitous Overexpression of *CG4623*

Ubiquitous overexpression of *CG4623* was achieved under the control of actin5C promoter using UAS-GAL4 system. To generate flies that overexpress *CG4623; CyO, GFP* (curly winged flies expressing GFP) balanced *Act5C-GAL4* driver line was crossed with *UAS-CG4623 OE* line and its control line w^{1118}. Crosses were kept at 25°C in 80% humidity. Among the F1 progeny, L3 larvae were selected against GFP signal (Figure 4.7).

$$♂;;UAS-CG4623\ OE \quad \mathbf{X} \quad ;\frac{Act5C-GAL4}{CyO,GFP};♀$$

$$↓$$

$$♀/♂\ ;\frac{Act5C-GAL4}{+};\frac{UAS-CG4623\ OE}{+}$$

Figure 4.7. Crossing scheme used for ubiquitous overexpression of *CG4623*. L3 larvae were selected against GFP signal among the progeny.

4.2.2. Tissue Specific Overexpression of *CG4623*

CG4623 gene was overexpressed in all neurons, in only motor neurons, or in only glial cells. To generate these overexpression lines, *UAS-CG4623 OE* and w^{1118} lines were crossed with fly lines with the appropriate drivers. Crosses were kept at 25°C in 80% humidity (except for the cross with *UAS-Dicer;;nSyb-GAL4* driver, which was kept at 29°C). The *elav-GAL4* driver line was used as a neuronal driver, *UAS-Dicer;;nSyb-GAL4*

driver line was also used as a neuronal driver additionally dicer enzyme is overexpressed in this driver line for increasing the effectiveness of the sequence-specific degradation of the target mRNA. *OK6-GAL4* driver line restricted overexpression to motor neurons and *repo-GAL4* driver line allowed overexpression in glial lineage cells. Since *elav-GAL4* (Figure 4.8*), UAS-Dicer;;nSyb-GAL4* (Figure 4.9) *OK6-GAL4* (Figure 4.10) driver lines were homozygous, there was no need for larval selection. On the other hand, *repo-GAL4* (Figure 4.11) driver line was balanced with *TM6B, tb, sb* (tubby larva, short bristles in adults), thus in the resulting progeny, L3 larvae selected against tubby (tb) character.

$$♂;;UAS-CG4623\ OE \quad \mathbf{X} \quad ;;elav-GAL4\ ♀$$

$$\downarrow$$

$$♀/♂ \quad ;;\frac{UAS-CG4623\ OE}{elav-GAL4}$$

Figure 4.8. Crossing scheme for neuronal *CG4623* overexpression using *elav-GAL4* line.

$$♂;;UAS-CG4623\ OE \quad \mathbf{X} \quad UAS-Dicer;;nSyb-GAL4♀$$

$$\downarrow$$

$$♀/♂ \quad \frac{UAS-Dicer}{+} \;;\frac{UAS-CG4623\ OE}{nSyb-GAL4}$$

Figure 4.9. Crossing scheme for neuronal *CG4623* overexpression using UAS-Dicer;;*nSyb*-GAL4.

$$♂;;UAS-CG4623\ OE \quad \mathbf{X} \quad ;OK6-GAL4;\ ♀$$

$$\downarrow$$

$$♀/♂ \quad ;\frac{OK6-GAL4}{+};\frac{UAS-CG4623\ OE}{+}$$

Figure 4.10. Crossing scheme for motor neuron specific *CG4623* overexpression.

$$♂;;UAS-CG4623\ OE \quad \mathbf{X} \quad ;;\frac{repo-GAL4}{TM6B,tb,sb}\ ♀$$

$$♀/♂\ \ ;;\frac{UAS-CG4623\ OE}{repo-GAL4}$$

Figure 4.11. Crossing scheme for glial *CG4623* overexpression.

4.2.3. Glial Overexpression of *CG4623* for Analysis of Mitochondria Dynamics

In order to analyze mitochondria dynamics, *CG4623* was overexpressed with the glia driver *repo-GAL4*, *UAS-mitoGFP* that has mitochondria-targeted GFP. *UAS-CG4623 OE* and w^{1118} lines were crossed with *repo-GAL4*, *UAS-mitoGFP* driver line and the crosses were kept at 25°C in 80% humidity. Since *repo-GAL4*, *UAS-mitoGFP* driver line was balanced with *TM6*, *tb*, *hu* (tubby larva, additional macrochaetas on the humeri in adults), L3 larvae selected against tubby (tb) character in the resulting progeny (Figure 4.6).

$$♂;;UAS-CG4623\ OE \quad \mathbf{X} \quad ;repo4.3;\frac{repo-GAL4,mitoGFP}{TM6,tb,hu}\ ♀$$

$$♀/♂\ \ ;\ \frac{repo4.3}{+};\frac{UAS-CG4623\ OE}{repo-GAL4,mitoGFP};$$

Figure 4.12. Crossing scheme for glial *CG4623* overexpression.

4.3. Downregulation of Mitochondrial Factors: *Drp1* and *Marf*

Mitochondrial fission factor *Drp1* and mitochondrial fusion factor *Marf* gene expression levels were downregulated using RNA interference pathway. *Drp1 TRIP RNAi* and *Marf TRIP RNAi* lines were purchased from Vienna *Drosophila* Resource Center (VDRC). These flies were crossed with ubiquitous or tissue specific driver lines. As a

control to RNAi line, *TRIP Control*, which was purchased from the same company, was crossed with the same driver lines. Analysis of mitochondria in the progeny generated by these crosses was used to compare and contrast the effect of up-or-down-regulation of *CG4623* gene expression levels on mitochondrial morphology.

4.3.1. Ubiquitous Downregulation of Mitochondrial Factors: *Drp1* and *Marf*

Ubiquitous downregulation of *Drp1* and *Marf* was achieved under the control of actin5C promoter using UAS-GAL4 system. To generate flies that express interfering RNA for *Drp1* or *Marf; CyO, GFP* (curly winged flies expressing GFP) balanced *Act5C-GAL4* driver line was crossed with *Drp1 TRIP RNAi* and *Marf TRIP RNAi* lines and their control line *TRIP Control*. Crosses were kept at 25°C in 80% humidity. Among the F1 progeny, L3 larvae were selected against GFP signal (Figure 4.13).

a.

$$♂;;UAS-Drp1\ TRIP\ RNAi \quad \mathbf{X} \quad ;\frac{Act5C-GAL4}{CyO,GFP};♀$$

$$↓$$

$$♀/♂\ ;\frac{Act5C-GAL4}{+};\frac{UAS-Drp1\ TRIP\ RNAi}{+};$$

b.

$$♂;;UAS-Marf\ TRIP\ RNAi \quad \mathbf{X} \quad ;\frac{Act5C-GAL4}{CyO,GFP};♀$$

$$↓$$

$$♀/♂\ ;\frac{Act5C-GAL4}{+};\frac{UAS-Marf\ TRIP\ RNAi}{+};$$

Figure 4.13. Crossing scheme of *Drp1* (a) and *Marf* (b) ubiquitous downregulation. L3 larvae selected against GFP signal among the progeny.

4.3.2. Tissue Specific Downregulation of Mitochondrial Factors: *Drp1* and *Marf*

Drp1 and *Marf* were downregulated in neuronal tissues of *Drosophila* by using neural driver *UAS-Dicer;;nSyb-GAL4*. For this purpose, *Drp1 TRIP RNAi* and *Marf TRIP RNAi* together with their control line of *TRIP Control* were crossed with this driver line. Crosses were kept at 29°C in 80% humidity. In the *UAS-Dicer;;nSyb-GAL4* driver line, GAL4 protein is generated under the control of *nSyb* promoter that is also used as a neuronal driver, additionally dicer enzyme is overexpressed in this driver line for increasing the effectiveness of the sequence-specific degradation of the target mRNA. Since *UAS-Dicer;;nSyb-GAL4* (Figure 4.14) driver line was homozygous, there was no need for larval selection.

a.

$$♂;;UAS-Drp1\ TRIP\ RNAi \quad \mathbf{X} \quad UAS-Dicer;;nSyb-GAL4\ ♀$$

$$♀/♂\ \frac{UAS-Dicer}{+};;\frac{UAS-Drp1\ TRIP\ RNAi}{nSyb-GAL4}$$

b.

$$♂;;UAS-Marf\ TRIP\ RNAi \quad \mathbf{X} \quad UAS-Dicer;;nSyb-GAL4\ ♀$$

$$♀/♂\ \frac{UAS-Dicer}{+};;\frac{UAS-Marf\ TRIP\ RNAi}{nSyb-GAL4}$$

Figure 4.14. Crossing scheme for neuronal *Drp1* (a) and *Marf* (b) downregulation.

4.3.3. Glial Downregulation Mitochondrial Factors of *Drp1* and *Marf* for Analysis of Mitochondria Dynamics

In order to analyze mitochondria dynamics, *Drp1* and *Marf* were downregulated with the glia driver *repo-GAL4, UAS-mitoGFP* that has mitochondria-targeted GFP. *Drp1*

TRIP RNAi, *Marf TRIP RNAi* and *TRIP Control* lines were crossed with *repo-GAL4, UAS-mitoGFP* driver line and the crosses were kept at 25°C in 80% humidity. Since *repo-GAL4, UAS-mitoGFP* driver line was balanced with *TM6, tb, hu* (tubby larva, additional macrochaetas on the humeri in adults), L3 larvae selected against tubby (tb) character in the resulting progeny (Figure 4.15).

a.

$$♂;;UAS-Drp1\ TRIP\ RNAi\ \ \mathbf{X}\ \ ;repo4.3;\frac{repo-GAL4,mitoGFP}{TM6,tb,hu}\ ♀$$

$$♀/♂\ ;\frac{repo4.3}{+};\frac{UAS-Drp1\ TRIP\ RNAi}{repo-GAL4,mitoGFP}$$

b.

$$♂;;UAS-Marf\ TRIP\ RNAi\ \ \mathbf{X}\ \ ;repo4.3;\frac{repo-GAL4,mitoGFP}{TM6,tb,hu}\ ♀$$

$$♀/♂\ ;\frac{repo4.3}{+};\frac{UAS-Marf\ TRIP\ RNAi}{repo-GAL4,mitoGFP}$$

Figure 4.15. Crossing scheme for glial *Drp1* (a) and *Marf* (b) downregulation.

4.4. Downregulation of *mtm*

mtm gene expression level was downregulated using RNA interference pathway. *mtm TRIP RNAi Drosophila* line was purchased from Vienna *Drosophila* Resource Center (VDRC). These flies were crossed with ubiquitous or tissue specific driver lines. As a control to RNAi line, *TRIP Control*, which was purchased from the same company, was crossed with the same driver lines.

4.4.1. Ubiquitous Downregulation of *mtm*

Ubiquitous downregulation of *mtm* was achieved under the control of actin5C promoter using UAS-GAL4 system. To generate flies that express interfering RNA for *mtm; CyO, GFP* (curly winged flies expressing GFP) balanced *Act5C-GAL4* driver line was crossed with *mtm TRIP RNAi* line and its control line *TRIP Control*. Crosses were kept at 25°C in 80% humidity. Among the F1 progeny, L3 larvae were selected against GFP signal (Figure 4.16).

$$♂;;UAS-mtm\ TRIP\ RNAi\ \ \mathbf{X}\ \ ;\frac{Act5C-GAL4}{CyO,GFP};♀$$

$$\downarrow$$

$$♀/♂\ \ ;\frac{Act5C-GAL4}{+};\frac{UAS-mtm\ TRIP\ RNAi}{+}$$

Figure 4.16. Crossing scheme used for ubiquitous downregulation of *mtm*. L3 larvae were selected against GFP signal among the progeny.

4.4.2. Tissue Specific Downregulation of *mtm*

The gene *mtm* was downregulated in different tissues of *Drosophila* by using tissue specific driver lines. For this purpose, *mtm TRIP RNAi* and *TRIP Control* lines were crossed with these driver lines. Crosses were kept at 25°C in 80% humidity. In the *elav-GAL4* driver line, GAL4 protein is generated under the control of *elav* promoter that is used as a neuronal driver. GAL4 protein is generated under the control of *OK6* promoter that is restricted to motor neurons in the *OK6-GAL4* driver line. In the *repo-GAL4* driver line, GAL4 protein is generated under the control of *repo* promoter that belongs to glial lineage cells. Since *elav-GAL4* (Figure 4.17*)* and *OK6-GAL4* (Figure 4.18) driver lines were homozygous, there was no need for larval selection. On the other hand, *repo-GAL4* (Figure 4.19) driver line was balanced with *TM6B, tb, sb* (tubby larva, short bristles in adults), thus in the resulting progeny, L3 larvae selected against tubby (tb) character.

$$♂;;UAS-mtm\,TRIP\,RNAi \quad \mathbf{X} \quad ;;elav-GAL4\,♀$$

$$♀/♂ \quad ;;\frac{UAS-mtm\,TRIP\,RNAi}{elav-GAL4}$$

Figure 4.17. Crossing scheme for neuronal *mtm* downregulation.

$$♂;;UAS-mtm\,TRIP\,RNAi \quad \mathbf{X} \quad ;OK6-GAL4;\,♀$$

$$♀/♂ \quad ;\frac{OK6-GAL4}{+};\frac{UAS-mtm\,TRIP\,RNAi}{+}$$

Figure 4.18. Crossing scheme for motor neuron specific *mtm* downregulation.

$$♂;;UAS-mtm\,TRIP\,RNAi \quad \mathbf{X} \quad ;;\frac{repo-GAL4}{TM6B,tb,sb}\,♀$$

$$♀/♂ \quad ;;\frac{UAS-mtm\,TRIP\,RNAi}{repo-GAL4}$$

Figure 4.19. Crossing scheme for glial *mtm* downregulation.

4.5. Overexpression of *mtm*

The gene *mtm* was overexpressed ubiquitously or in a tissue specific manner by crossing *UAS-mtm OE* line, which was generated by former M.Sc. student Kaya Akyüz, with the ubiquitous or tissue specific driver lines. As a control to overexpression line, w^{1118} was crossed with appropriate driver lines.

4.5.1. Ubiquitous Overexpression of *mtm*

Ubiquitous overexpression of *mtm* was achieved under the control of actin5C promoter using UAS-GAL4 system. To generate flies that overexpress *mtm; CyO, GFP* (curly winged flies expressing GFP) balanced *Act5C-GAL4* driver line was crossed with *UAS-mtm OE* line and its control line w^{1118}. Crosses were kept at 25°C in 80% humidity. Among the F1 progeny, L3 larvae were selected against GFP signal (Figure 4.20).

$$♂;;UAS-mtm\ OE\ \ \mathbf{X}\ \ ;\frac{Act5C-GAL4}{CyO,GFP};♀$$

$$↓$$

$$♀/♂\ \ ;\frac{Act5C-GAL4}{+};\frac{UAS-mtm\ OE}{+}$$

Figure 4.20. Crossing scheme used for ubiquitous overexpression of *mtm*. L3 larvae were selected against GFP signal among the progeny.

4.5.2. Tissue Specific Overexpression of *mtm*

Drosophila mtm gene was overexpressed in all neurons, in only motor neurons, or in only glial cells. To generate these overexpression lines, *UAS-mtm OE* and w^{1118} lines were crossed with fly lines with the appropriate driver lines. Crosses were kept at 25°C in 80% humidity. The *elav-GAL4* driver line was used as a neuronal driver, *OK6-GAL4* driver line restricted overexpression to motor neurons and *repo-GAL4* driver line allowed overexpression in glial lineage cells. Since *elav-GAL4* (Figure 4.21) and *OK6-GAL4* (Figure 4.22) driver lines were homozygous, there was no need for larval selection. On the other hand, *repo-GAL4* (Figure 4.23) driver line was balanced with *TM6B, tb, sb* (tubby larva, short bristles in adults), thus in the resulting progeny, L3 larvae selected against tubby (tb) character.

♂ ; ; $UAS - mtm\ OE$ **X** ; ; $elav - GAL4$ ♀

♀/♂ ; ; $\frac{UAS - mtm\ OE}{elav - GAL4}$

Figure 4.21. Crossing scheme for neuronal *mtm* overexpression.

♂ ; ; $UAS - mtm\ OE$ **X** ; $OK6 - GAL4$; ♀

♀/♂ ; $\frac{OK6 - GAL4}{+}$; $\frac{UAS - mtm\ OE}{+}$

Figure 4.22. Crossing scheme for motor neuron specific *mtm* overexpression.

♂ ; ; $UAS - mtm\ OE$ **X** ; ; $\frac{repo - GAL4}{TM6B, tb, sb}$ ♀

♀/♂ ; ; $\frac{UAS - mtm\ OE}{repo - GAL4}$

Figure 4.23. Crossing scheme for glial *mtm* overexpression.

4.6. Histological Methods

4.6.1. Larval Neuromuscular Junction Dissection

Freshly prepared, ice-cold HL-3 was poured on a silicone plate that has dissection pins stuck on it. A wandering third instar larva was put on the plate and the food around the larva was cleaned if any. A dissection pin was placed onto the anterior part of the larva near the mouth hook. Larva was stretched out lengthwise with another pin while placing the pin in between posterior spiracles. With a fine forceps, an incision was made in the

middle of anterior to posterior pin on the dorsal cuticle side. A vertical cut was made towards both ends of the larva. Gut, fat tissue and tracheal system were removed carefully without touching the muscles. The larva was spread open by placing four pins to every corner of the body wall while stretching the animal vertically and horizontally. This allowed ventral muscles to be exposed. More of gut, fat and tracheal tissue cleaned. Brain, discs and the ventral nerve cord were cut carefully with a fine scissors from the attachment side of the ventral motor nerve bundles to nerve cord. Pinned larva was washed with fresh HL-3 to remove floating organs.

4.6.2. Immunohistochemistry of Larval Neuromuscular Junction

The third instar larvae dissected as described in Section 4.6.1 was fixed with 3.7% formaldehyde solution for 20 minutes in room temperature. Fixation solution was discarded and larvae were washed with HL-3 for two times without pouring HL-3 directly onto larvae body wall. Pins were removed carefully without harming the body wall and starting from the posterior side. Larvae with different genotypes were labeled by cutting the tail at the posterior side. All larvae were put together into one eppendorf tube containing 1 ml of PBX. Samples were washed with PBX four times changing solution in every 15 minutes. PBX was discarded and 10% normal goat serum containing blocking solution was added to the tube in order to block non-specific binding sides on samples. Samples were blocked for 1 hour at room temperature. Primary antibodies of interest were prepared by diluting antibodies in desired concentrations in the blocking solution. Larvae were incubated overnight at 4°C with primary antibodies. Next day, antibody solution was removed and samples were washed with PBX five times changing the solution in every 10 minutes. Proper secondary antibodies were prepared by diluting antibodies in desired concentrations in blocking solution. Larvae were incubated with secondary antibodies for 2 hours in room temperature in the dark. After that, secondary antibody solution was discarded and samples were washed with PBX for 2 hours changing solutions in every 15 minutes. Larvae were prepared for microscopy. Twenty μl of vectashield mounting medium was put on a microscopy glass slide and larvae were placed in this vectashield drop muscles facing upwards. A coverglass was put on top and the preparation was sealed with nail polish. Prepared slides were stored at 4°C.

4.6.3. Quantitative Analyses of Larval Neuromuscular Junction

Neuromuscular junctions (NMJs) were analyzed using Leica TCS SP5 confocal microscope, LAS AF software. NMJs residing in abdominal segment 3 (A3) or abdominal segment 4 (A4) in between the muscle 6 and 7 were imaged with 63X objective. NMJ images were taken with 1X digital zoom while bouton images were taken with 4X digital zoom. Line average was set to 8.

Images were processed and analyzed using ImageJ 1.48V software. For each NMJ, the length of NMJ and its ratio to innervated muscle area was determined. The mean values of controls and experiments were compared using two-tailed t-test.

4.6.4. Larval Ventral Nerve Cord Dissection and Immunohistochemistry for Analysis of Mitochondrial Dynamics

The wandering third instar larvae were dissected as described in Section 4.6.1 until the step of removing brain, imaginal discs and the ventral nerve cord. Brain and disc structures together with the ventral nerve cord were left allowing ventral motor nerve bundles to be attached to the ventral nerve cord. This enables tracing of each nerve bundle while imaging. Immunohistochemistry of the larvae were performed as described in Section 4.6.2.

4.6.5. Quantitative Analyses of Larval Ventral Motor Neuron Bundles for Analysis of Mitochondria Dynamics

Larval ventral motor neuron bundles were analyzed using Leica TCS SP5 confocal microscope, LAS AF software. Motor neuron bundles that are projecting to abdominal segment 3 (A3) or abdominal segment 4 (A4) were imaged. 63X objective and 3X digital zoom were used during imaging. Line average was set to 6.

Images were processed and analyzed using Fiji 2.0 software. Within each nerve bundle, elongation and circularity factors of mitochondria were determined. The mean values of controls and experiments were compared using two-tailed t-test.

4.7. Synaptic Electrophysiology of Larval Neuromuscular Junction

4.7.1. Preparation of the Electrodes

Glasscapillaries were produced using a capillary puller. For the suction electrode preparation, one of the pulled capillary was polished to make the end blunt and be in the thickness of a nerve bundle. The other pulled capillary was left sharp for measurement. Suction electrode was filled with fresh HL-3 solution while measurement electrode was filled with the buffer containing 2.7 M KCl and 0.3 M KAc. Both suction and measurement electrodes were attached to corresponding wire handles. The wire corresponding to measurement electrode was chloride up before with the 3M KCl solution for 10 minutes at 5 amper.

4.7.2. Larval Neuromuscular Dissection for Electrophysiology

The wandering third instar larva was dissected as described in Section 4.6.1 until the removal of brain, imaginal discs and the ventral nerve cord. HL-3 solution was replaced with fresh HL-3 solution that additionally contains 0.5 mM $CaCl_2$. Brain, imaginal discs and the ventral nerve cord of the larva were removed in this solution.

4.7.3. Larval Neuromuscular Junction Recording

Silicon plate containing dissected larva preparation was put into the recording apparatus. Reference electrodes were placed into the silicon plate without touching the larva. Resistance value of the measurement electrode was checked with MultiClamp 700B Commander software. Electrodes that are not having 20-30 MΩ resistance value were discarded.

Nerve bundle that is projecting to the abdominal segment 3 or 4 was sucked with the suction electrode without disturbing the muscle. Measurement electrode was placed on top of muscle 6 to which the sucked nerve bundle is projecting. With the measurement electrode, membrane potential of the muscle was measured on Clampex 10.3 software. Once the membrane potential of -60 mV was reached, excitatory junctional potentials (EJPs) in external calcium concentrations were evoked by stimulation of the cut segmental nerve at 2X threshold. At this stage, motor neurons were stimulated at 1 Hz for 0.3 ms with the stimulus isolator. Basal EJP amplitudes were determined in Clampfit 10.3 by calculating the average of 60 traces. At least five recordings from five different larvae were taken for each genotype. One-way Anova test was applied with the GraphPad software.

4.8. Polyclonal Antibody Generation

4.8.1. IPTG Induction

Five to ten ml LB Broth medium containing Kanamycin and Chloramphenicol, diluted to a ratio of 1:1000, was inoculated with *E. coli* cells harboring the IPTG inducible expression plasmid. Cells were grown in a rotary shaker at 37°C, 200 rpm overnight. Next day, overnight culture was diluted to a 1:60 ratio with fresh LB Broth medium containing Kanamycin and Chloramphenicol diluted with a 1:1000 ratio. Cells were grown at 37°C, 200 rpm until the OD_{600} reaches to 0.6. Ten ml of culture medium was taken to a fresh culture tube, to be used as uninduced control. IPTG was added to a final concentration of 500 μM and the culture was grown either at 20°C for 16 hours or 37°C for 4 hours since induction condition depends on the purification method. After termination of IPTG induction, 1 ml of culture medium was taken from both uninduced and induced samples, and centrifuged at 13200 rpm for 5 minutes. Supernatant was discarded and pellets were stored at -20°C for TCA Assay to control IPTG induction. Rest of the culture medium was centrifuged at 7000 rpm for 15 minutes to harvest the cells. Supernatant was discarded and cell pellet was stored at -80°C.

4.8.2. Trichloroacetic Acid (TCA) Assay

Previously collected uninduced and IPTG induced pellets (pelleted from 1 ml culture medium) were dissolved in 100 μl TCA (100%) with vigorous vortexing. Samples were kept on ice for 15 minutes and later centrifuged at 13200 rpm for 2 minutes. Supernatant was carefully discarded and 1 ml of acetone was added. Pellet was lifted with slight vortexing and centrifuged again in 13200 rpm for 2 minutes to remove acid. Acetone was discarded and tube was left lid open to evaporate remaining acetone. Dried pellets were dissolved in protein sample buffer and stored at -20°C until they were analyzed for IPTG induction on SDS-PAGE.

4.8.3. Nickel Column Protein Purification with Urea Containing Buffers

Both the peristaltic pump and the column were cleaned before protein purification. For peristaltic pump cleaning, 15-20 ml 4M NaOH was passed through the cables then 50 ml of dH_2O was passed with the maximum speed. For the column cleaning, 10 ml of dH_2O, 15 ml of strip buffer, 50 ml of dH_2O, 4 ml of 0.5 M $NiSO_4$ and 30 ml dH_2O were passed through the column in the given order.

Pelleted and stored cells were thawed for 15 minutes in 5 ml Buffer B containing 3 unit/ml of Benzonase Nuclease for protein purification. The cells were then incubated with agitation for 15 minutes at room temperature. The lysate was centrifuged at 4500 rpm, 4°C for 20 minutes and the supernatant was collected. Two hundred μl of supernatant was saved for SDS-PAGE analysis. Column was equilibrated with 10 ml of Buffer B. Lysate supernatant was loaded up onto pre-equilibrated column and flow-through was collected. Column was washed with 30-40 ml of Buffer C to get rid of unbound protein. Wash fractions were collected in every 10 ml. Bound proteins to the Nickel column were eluted with 15 ml of Buffer E. Elution fractions were collected in every 2 ml. Pellet after lysis, lysate supernatant, lysate flow through, wash fractions and elution fractions were stored at -20°C until they were analyzed with SDS-PAGE.

4.8.4. Nickel Column Protein Purification with Imidazole Containing Buffers

Both the peristaltic pump and the column were cleaned before starting protein purification as described in Section 4.8.3. For protein purification, cells were thawed for 15 minutes in 5 ml Binding Buffer containing 0.1 mM PMSF and then incubated with agitation for 15 minutes at room temperature. The mixture was sonicated at 95 V for 2 cycles of 1 minute. Lysate was centrifuged at 4500 rpm, 4°C for 20 minutes and supernatant was collected. Two hundred μl of supernatant was saved for SDS-PAGE analysis. Starting from the column equilibration step, protein purification protocol was followed as described in Section 4.8.3, however, this time Binding Buffer (10 mM imidazole), Wash Buffer (30 mM imidazole) and Elution Buffer (500 mM imidazole) were used instead of urea containing Buffer B, Buffer C and Buffer E, respectively.

4.8.5. Polyacrylamide Gel Electrophoresis (SDS-PAGE)

10% SDS-Polyacrylamide running gel was poured in between 1.5 mm thick glass plates. Isopropanol was distributed on top of running gel to align gel level evenly. After 20 minutes of waiting for the running gel to polymerize, isopropanol was discarded and 5% SDS-Polyacrylamide stacking gel was poured in between the glass plates. One and a half mm thick gel comb was placed right after and we waited for polymerization for 20 minutes.

1X protein sample buffer containing cell lysates were incubated at 95°C for 5 minutes to denature proteins. Lysate was loaded to the SDS-polyacrylamide gel. PageRuler Prestained Protein Ladder and BSA with known concentration were also loaded into gel to determine protein size and concentration, respectively. Gel was run at 80 V until samples pass the stacking gel, afterwards 100 V for 2 hours. Coomassie Blue staining solution was used to stain polyacrylamide gel for 2 hours at room temperature. Gel was shaken with the destaining solution for 4 hours by changing the solution in every 30 minutes. Destained gel was visualized using white light box.

4.8.6. Protein Purification from Polyacrylamide Gels

For bulky purification of the protein, IPTG induced, pelleted and stored cells were thawed for 15 minutes in 5 ml 1X PBS with 1% Triton-X containing 3 unit/ml of Benzonase Nuclease. The mixture was sonicated at 95 V for 2 cycles of 1 minute. Lysate was centrifuged at 4500 rpm, 4°C for 20 minutes and the supernatant was collected. Pellet was dissolved in 5 ml of 1X PBS with 1% Triton-X. Centrifugation, removal of supernatant and addition of 5 ml 1X PBS with 1% Triton-X steps were repeated three times. 5 ml of 1X PBS was used in the last step to get rid of excess detergent. Final pellet was dissolved in 2 ml of 1X PBS and stored at -20°C together with supernatants until they were analyzed with SDS-PAGE.

Polyacrylamide gel was prepared as described in Section 4.8.5. However, eight wells of the ten-well comb were combined with a tape to generate a greater space for cell lysate to be loaded. Remaining two wells were saved for PageRuler Prestained Protein Ladder and a sample cell lysate to be stained and aligned with the bulk cell lysate. 1X protein sample buffer containing cell lysate pellet was incubated at 95°C for 5 minutes to denature proteins and loaded to the gel later on. After gel electrophoresis, protein ladder and sample cell lysate lanes were cut off with a clean scalpel and stained with Coomassie Blue staining solution as described in Section 4.8.6. Rest of the gel was wrapped in plastic and wet with running buffer to prevent it from drying until the strip of protein ladder and sample cell lysate was stained. Stained strip of gel was aligned with the unstained gel portion. The band of the gel that aligns with the stained protein of interest was cut out. Excised gel pieces were put on a mortar and immersed in 1.5 ml of gel extraction elution buffer. Gel pieces were crushed with a clean pestle vigorously. Mixture was placed in 15 ml test tube and incubated in a rotary shaker at 30°C overnight. Next day, mixture was centrifuged at 7500 rpm for 10 minutes and supernatant containing purified protein was pipetted into a new tube. An aliquot of the supernatant was tested for the presence of protein by subjecting it to SDS-PAGE.

4.8.7. Antigen Injection and Serum Collection

Polyacrylamide gel purified protein solution, which was tested for the presence of desired the protein by SDS-PAGE, was used as an antigen source for injections into two New Zealand white rabbits. Protein concentration of purified protein solution was determined with NanoDrop. Freund's Complete Adjuvant mixed with 200 μl of 1X PBS containing 50 μg of purified protein and prepared for injection. Two ml of blood was collected from each rabbit as prebleed to compare later on with the 3rd, 5th and 6th bleeds. Protein-adjuvant mix was injected into rabbits in every two weeks for three times. Purified protein solution was mixed with Freund's Complete Adjuvant only for the first injection. Freund's Incomplete Adjuvant was used in the remaining injections as the same amount. One ml of blood was collected from each rabbit three days after 3rd injection. The 4th and 5th injections were performed in the following second and fourth weeks after third injection, respectively. Twenty-five ml of blood was collected from each rabbit three days after 5th injection. The 6th injection was performed four weeks after the 5th one and the rabbits were sacrificed 3 days after 6th injection. Seventy-five to one hundred ml of blood was collected and saved for antibody purification. Sodium citrate-glucose solution was added in 1:10 ratio into all bleeds immediately after blood collection to prevent coagulation. After that, blood was centrifuged at 10000 rpm, 4°C for 20 minutes. Serum was collected after centrifugation and stored at -20°C for antibody purification.

4.8.8. Purification of Polyclonal Antibody from Rabbit Sera

Blood sera that were collected from rabbits after 5th and 6th injections were sent to Assoc. Prof. Fatma Yücel in TUBİTAK MAM in Kocaeli. Assoc. Prof. Yücel and her group purified the polyclonal antibody that was raised against our antigen by using a HiTrap protein G column. Sera were run through the column and bound antibodies were eluted later on. Elutes were analyzed with Enzyme-Linked ImmunoSorbent Assay (ELISA) to determine the ones containing high antibody concentrations. High antibody containing elutes were received from Assoc. Prof. Yücel and used as polyclonal antibody source against the desired protein. Those elutes were used in Western Blot analysis and immunohistochemistry assays.

4.8.9. Protein Extraction from Flies

Fourteen young adult flies (approximately 10 days old) of the same genotype were anesthetized, collected into 1.5 ml Eppendorf tubes, and stored at -80°C for 10 minutes. Flies were homogenized thoroughly in 210 μl of Non-ionic Fly Lysis Buffer containing 1X protease inhibitor. Tissues were kept on ice for 30 minutes and then centrifuged at 10000 rpm, 4°C for 10 minutes. Supernatant was collected without disturbing the pellet and the oily upper layer that is rich in lipids. Protein concentration of the fly cell lysate was determined by using Pierce BCA Protein Assay Kit (Thermo Scientific, USA, 23227) according to manufacturer's instructions. Fly cell lysates were stored at -20°C until they were used for Western Blot analysis.

4.8.10. Western Blot Analysis

Cell lysates containing 1X protein sample buffer were incubated at 95°C for 5 minutes to denature proteins. Cell lysates were diluted to contain 50-100 μg of protein. Lysate was loaded to the SDS-polyacrylamide gel and the gel was run as described in Section 4.8.5. After gel electrophoresis, proteins were electroblotted to PVDF membranes in transfer buffer at 100 V for 45 minutes (transfer time depends on the size of the protein of interest). Protein blotted membrane was washed with TBS-T for three times changing the solution in every 5 minutes. Non-specific binding sites on membrane were blocked with 5% BSA containing TBS-T for 1 hour. Primary antibody of interest was diluted in appropriate amount in 5% BSA in TBS-T. Membrane was incubated with that primary antibody solution at 4°C overnight. Next day, primary antibody solution was discarded and membrane was washed with TBS-T for three times changing the solution in every 5 minutes. Membrane was incubated with the secondary antibody in 5% BSA containing TBS-T for 1 hour at room temperature and washed with TBS-T for three times changing the solution in every 5 minutes. For visualization, membranes were incubated in ImmunoCruz Western Blotting Luminol reagent. They were visualized by using Stella Raytest. Bands corresponding to the target protein were normalized to actin levels.

4.8.11. PVDF Membrane Stripping

The membrane with the antibodies was put on a hybridization glass tube. Ten ml of stripping solution was poured on top of the membrane. It was incubated at 50°C for 30 minutes in rotating hybridization oven and afterwards washed with TBS-T for three times changing the solution in every 10 minutes. It was continued with the blocking of membrane as described in Section 4.8.10.

4.8.12. Pre-adsorbing Antibodies

A wandering third instar larva, in which the gene of interest was downregulated, was put on a silicon plate that was filled with freshly made, ice-cold HL-3 solution. Food around the larva was cleaned if any. Larva was cut through half with fine scissors and cuticle around the half of the larva, which was composed of mount hook, brain, discs and ventral nerve cord, were removed with fine forceps. In this way, brain, discs and leftover muscles were exposed. Fifty or more larvae were dissected in this way and fixed with 4% formaldehyde solution for 20 minutes in room temperature. Fixed larvae were transferred into an Eppendorf tube and washed with BBT solution for four times changing the solution in every 20 minutes. Antibody was diluted in BBT solution in 1:10 ratio and incubated with larvae at 4°C overnight, rotating. Next day, larvae were allowed to settle and the supernatant (pre-adsorbed antibody) was removed to a fresh tube. Pre-adsorbed antibody was mixed with 0.3% NaN_3 and stored at 4°C.

5. RESULTS

5.1. Expression Pattern Analysis of CG4623

Since our aim was to model CMT disease pathogenicity in *Drosophila* by altering the expression levels of *CG4623*, it is crucial to identify its expression pattern in different tissues of flies. Unfortunately, an antibody for CG4623 protein was not commercially available and trials with available human GDAP1 and GDAP1L1 antibodies did not show any significant cross-reactivity with *Drosophila* proteins. Therefore, we have decided to generate a polyclonal antibody against CG4623 protein and used it in Western blot and immunohistochemistry analyses to reveal expression pattern of the protein in *Drosophila*. We have also performed immunohistochemistry assays with *CG4623::DsRed* fly strain, which is a line expressing DsRed tagged version of CG4623 protein under endogenous control kindly provided by Dr. Galindo in Centro de Investigacion Principe Felipe, Spain.

5.1.1. Polyclonal CG4623 Antibody Generation

High amounts of CG4623 protein were required to be used as an antigen source for polyclonal antibody generation. For this, our former lab member Kaya Akyüz cloned *CG4623* into pET30a vector, which allows IPTG induced overexpression of a recombinant protein with six histidine residues (His-tag) at the amino or carboxyl terminus. He transformed pET30aX6HIS-CG4623 plasmid into competent Rosetta strain of *Escherichia coli* (Akyüz, 2013). To test whether the cells are inducible, they were incubated with 500 μM of IPTG for 4 hours at 37°C. Later they were treated with TCA and the cell lysates were run on 10% polyacrylamide gel (Figure 5.1). A thicker band, which corresponds to the overexpression of CG4623, was observed in the induced sample as compared to that of the uninduced cells.

In order to achieve a high yield of CG4623 protein expression, IPTG concentration, duration of induction, and temperature parameters were optimized (Figure 5.2). To determine the optimal IPTG concentration, cells were incubated with 50, 500 or 1000 μM

of IPTG at 20°C, O/N (Figure 5.2A). The optimum, non-toxic IPTG concentration was set to 500 μM accordingly. Once the IPTG concentration was determined, duration of induction (4 hours or O/N) and temperature (20°C or 37°C) were optimized (Figure 5.2B). This time both the supernatant and the pellet were run on the polyacrylamide gel to observe the phase the protein remained. Highest expression of CG4623 was observed in 4 hours at 37°C condition and the protein mainly remained in the pellet, whereas the second highest expression was observed in O/N at 20°C condition and the protein equally remained in both supernatant and pellet. Since pellet cannot run through the column later in the purification steps, we have decided to use O/N at 20°C with 500 μM of IPTG condition as the optimum induction condition.

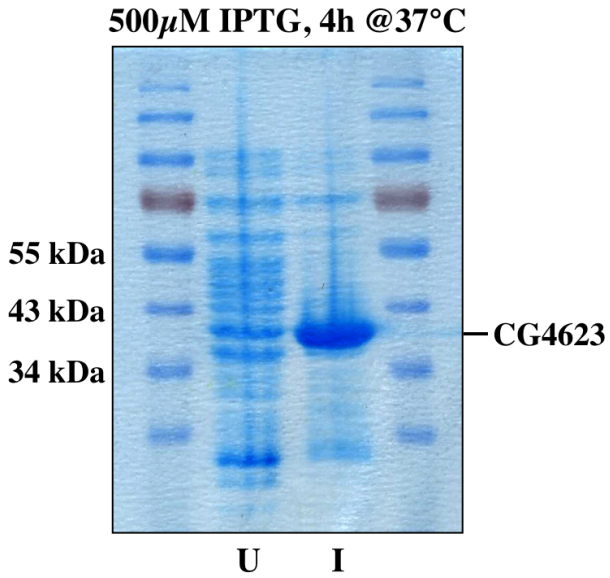

Figure 5.1. TCA treatment of pET30aX6HIS-CG4623 transformed Rosetta cells. Molecular mass of His-tagged CG4623: 41.9 kDa. U: Uninduced, I: Induced.

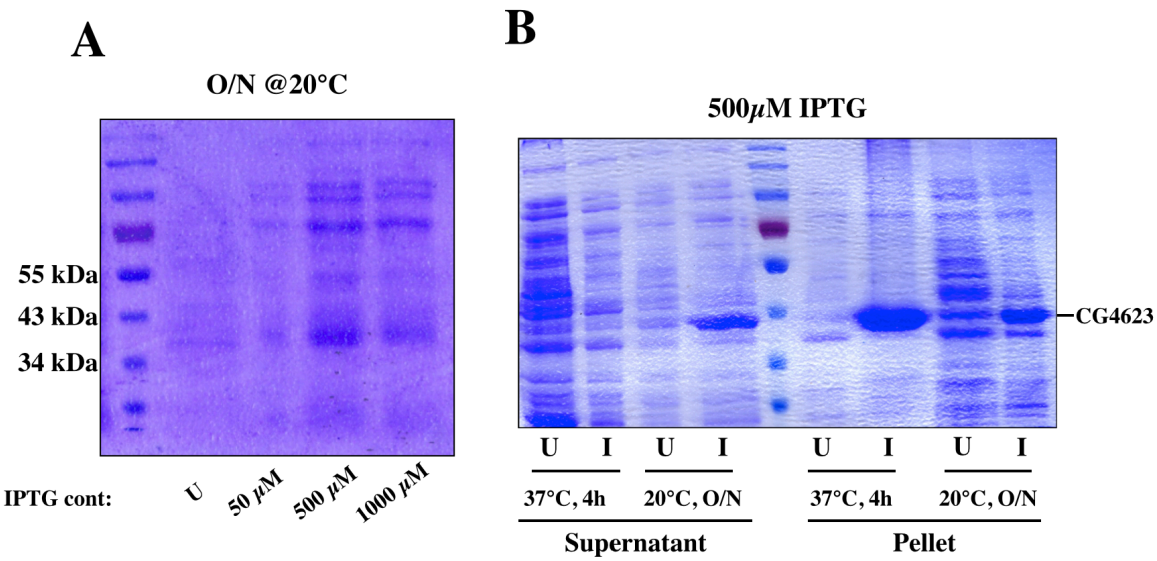

Figure 5.2. IPTG induction optimizations for high yield CG4623 protein expression. Molecular mass of His-tagged CG4623: 41.9 kDa. U: Uninduced, I: Induced. (A) pET30aX6HIS-CG4623 transformed Rosetta cells were incubated with 50, 500 or 1000 μM of IPTG at 20°C, O/N. (B) pET30aX6HIS-CG4623 transformed Rosetta cells were incubated with 500 μM of IPTG either at 37°C for 4 hours or 20°C, O/N.

For protein purification, cell lysates, in which the recombinant CG4623 protein (41.9 kDa) was overexpressed with the optimum IPTG condition, were run through the Nickel column. Initially, purification buffers with high urea concentration (8M) were used. Cells were lysed in Buffer B, which was adjusted to pH 8.0 to allow binding of polyhistidine tagged proteins to the immobilized nickel ions in the column. Column was washed with Buffer C, which has a reduced pH of 5.9, to discard non-specifically bound proteins. Finally, acidic Buffer E with the pH of 4.5 was used to elute bound proteins by decreasing the affinity of His-tag for nickel ions. Sample of induced and uninduced lysates together with the flow through (collected after running the bulk lysate through the column), wash fractions and elution fractions were run on a polyacrylamide gel (Figure 5.3). CG4623 protein can be observed in elution fractions (Figure 5.3B) yet its concentration was low. Therefore, we have decided to change purification buffers to allow higher amounts of protein to bind to the column.

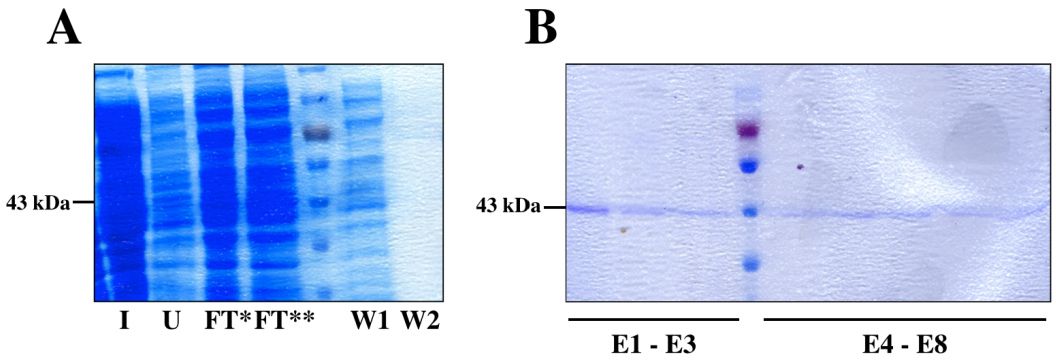

Figure 5.3. Nickel column purification of CG4623 protein using urea buffers. (A) Samples of induced (I), uninduced (U), flow through fractions collected after bulk lysate run (FT*, FT**) and wash fractions (W1, W2) were run on polyacrylamide gel. (B) Elution fractions collected after column wash (E1-E8).

Urea buffers were replaced with imidazole purification buffers. Cells were lysed in binding buffer containing 10 mM of imidazole to allow binding of His-tagged protein to the column in the presence of low imidazole. Wash buffer containing 30 mM of imidazole dislocates the non-specifically bound proteins. Elution buffer with the 500 mM imidazole elutes the bound protein by competing with the polyhistidine tag for binding to the Nickel ions. Sample of induced and uninduced lysates together with the flow through (collected after running the bulk lysate through the column), wash fractions and elution fractions were run on a polyacrylamide gel (Figure 5.4). CG4623 protein could be observed only in first elution fraction, moreover, its concentration was low and elution fraction itself was not pure enough as several other bands were observed on the gel (Figure 5.4B).

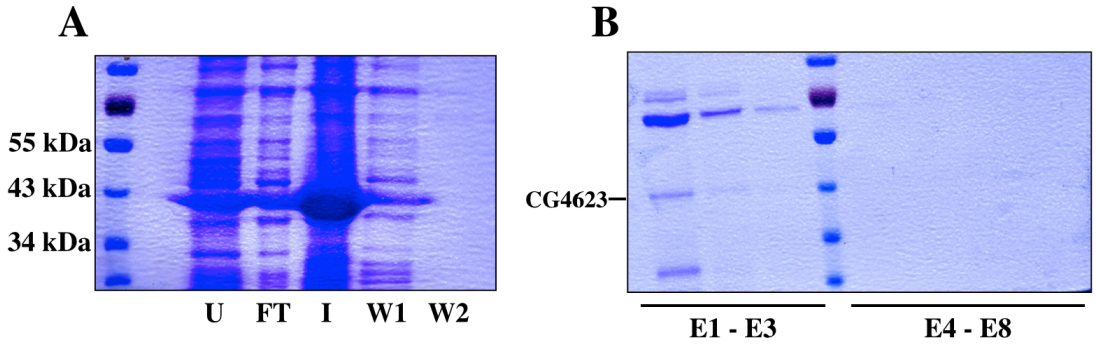

Figure 5.4. Nickel column purification of CG4623 protein using imidazole buffers. (A) Samples of induced (I), uninduced (U), flow through fraction collected after bulk lysate run (FT) and wash fractions (W1, W2) were run on polyacrylamide gel. (B) Elution fractions collected after column wash (E1-E8).

Regarding the difficulties in column purification methods and low yield of purified protein, we have changed our method of protein purification to polyacrylamide gel extraction. Induction conditions were also changed to 4 hours at 37°C with 500 μM of IPTG condition to reach higher yield of CG4623 expression since in this method any fraction of cells, pellet or supernatant, can be used for purification. After cell lysis, both the supernatant and the pellet were run on polyacrylamide gel to determine the phase of CG4623 (Figure 5.5A-B). As shown in figure 5.5B, CG4623 mainly remained in the pellet rather than the supernatant. Therefore, pellet was used in further studies of protein purification. Western blotting of purified protein with primary His-probe antibody revealed a single band of ~42 kDa corresponding to his-tagged CG4623 (Figure 5.5C).

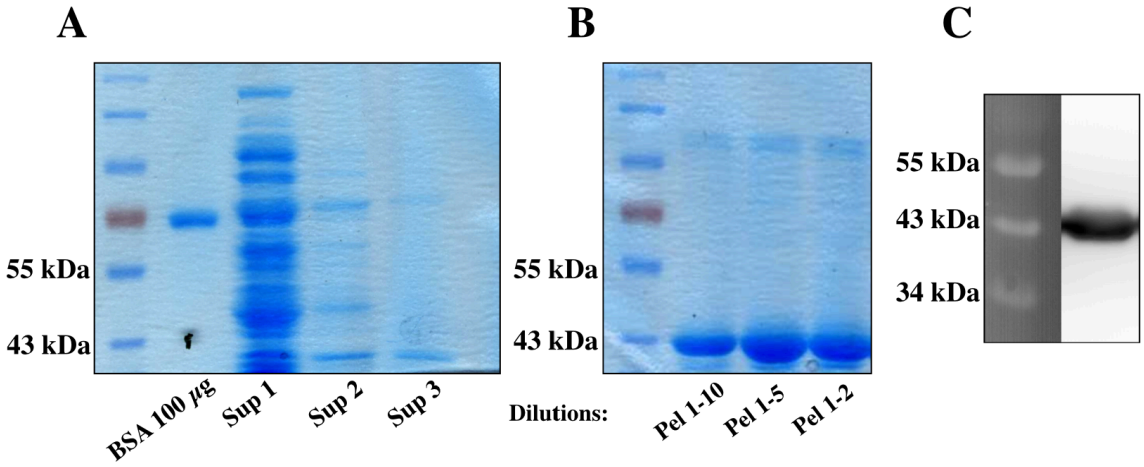

Figure 5.5. Purification of CG4623 from polyacrylamide gel. (A-B) Samples lysed for purification from gel extraction. (A) 100 μg BSA marker together with supernatants after three washing steps. (B) Polyacrylamide gel image of pellet samples diluted in PBS 1-10, 1-5 and 1-2 ratios. (C) Western blotting of purified CG4623 with anti-His antibody.

Western blotting confirmed the purified sample to be the recombinant CG4623 protein and allowed its use as an antigen source for injection into rabbits. Comparison of pre-bleed serum with the sera collected after third and fifth injections were also confirmed that rabbits raised an antibody against the injected protein (data not shown). Polyclonal antibody purification from the blood sera of the rabbits was performed by Assoc. Prof. Fatma Yücel and her group in TUBITAK MAM, Kocaeli. They have used HiTrap protein G column to purify immunoglubulins raised against CG4623. Elution fractions were analyzed with Enzyme-Linked ImmunoSorbent Assay (ELISA) to determine the ones containing high antibody concentration. High antibody containing elution fractions were

received from Assoc. Prof. Yücel and used as polyclonal antibody source against CG4623 in Western blot and immunohistochemistry assays.

5.1.2. Western Blot Analysis of *Drosophila* Protein Samples with CG4623 Antibody

Western blot analysis of *Drosophila* proteins extracted from ten days old adult flies were performed with the primary antibody of purified CG4623 polyclonal antibody. Before testing CG4623 antibody on fly extracts, Western blotting of CG4623 antigen was also performed to confirm reactivity of the CG4623 antibody with the antigen (Figure 5.6). A single band higher than 40 kDa was observed, indicating that the purified CG4623 antibody recognizes and cross-reacts with the antigen we have purified.

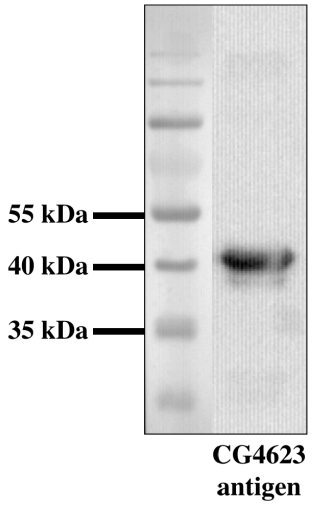

Figure 5.6. Western blotting of CG4623 antigen with the CG4623 antibody.

CG4623 antibody was tested on protein samples extracted from wild type, *act > CG4623 RNAi*, and *act > CG4623 Overexpression (OE)* flies. Downregulation and overexpression of *CG4623* was achieved by crossing the *CG4623 RNAi* and *CG4623 OE* lines with the ubiquitous driver *actin5C-GAL4* line. In all fly lines, a band was observed at around 40 kDa that might correspond to endogenous CG4623 protein (37.6 kDa) (Figure 5.7A). However, no change was observed in between *act > CG4623 RNAi* and *act > CG4623 OE* fly extracts in terms of band intensity even though the loading control (actin) levels were the same. Non-specific bindings were also observed at around 35 kDa and ~80 kDa levels. In order to reduce non-specificity, CG4623 antibody was pre-adsorbed by incubating with third instar larvae, in which *CG4623* was downregulated. Western blot

analysis with pre-adsorbed CG4623 antibody showed that ~80 kDa band intensity was reduced (Figure 5.7B). However, we did not observe any improvements for other non-specific bindings. Similar to previous blot, a band around 40 kDa, which might correspond to CG4623, was observed in all fly lines. However, pre-adsorbing the antibody did not improve specificity against endogenous CG4623 since there was only slight increase in band intensity of *act > CG4623 OE* compared to *act > CG4623 RNAi*.

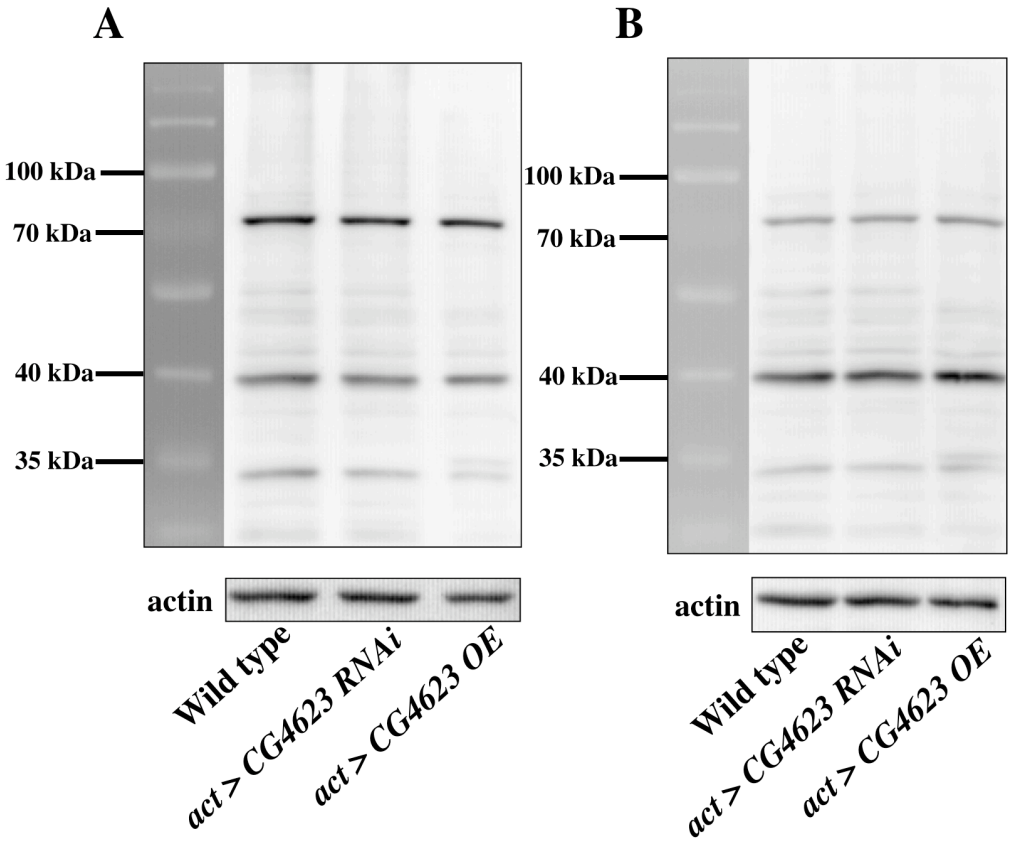

Figure 5.7. Western blotting of wild type (w^{1118}), *act > CG4623 RNAi*, and *act > CG4623 OE* fly line extracts with CG4623 antibody (A) and pre-adsorbed CG4623 antibody (B).

5.1.3. Immunohistochemistry Analysis of Third Instar Larvae with CG4623 Antibody

In order to reveal the expression pattern of CG4623 in third instar larva, immunohistochemistry assays were performed with the CG4623 antibody that we have generated. Localization of CG4623 in the whole body and in the neuromuscular junctions (NMJs) together with its colocalization with neuronal and synaptic markers was investigated. To test the staining property of CG4623 antibody and to eliminate the risk of

getting false positive signals from the secondary antibody, wild type *Canton-S* larvae were stained in two different conditions. In the first experiment, only the secondary antibody that would recognize the CG4623 antibody was used (Figure 5.8A-A''). In the second experiment, both the CG4623 antibody and the secondary antibody were used (Figure 5.8B-B''). Additionally, neuronal marker HRP was used in both conditions. Signal was observed only from the CG4623 antibody staining in the second experiment indicating that the stainings performed with CG4623 antibody did not originate from the false positive signals of secondary antibody staining (Figure 5.8A'' and B'').

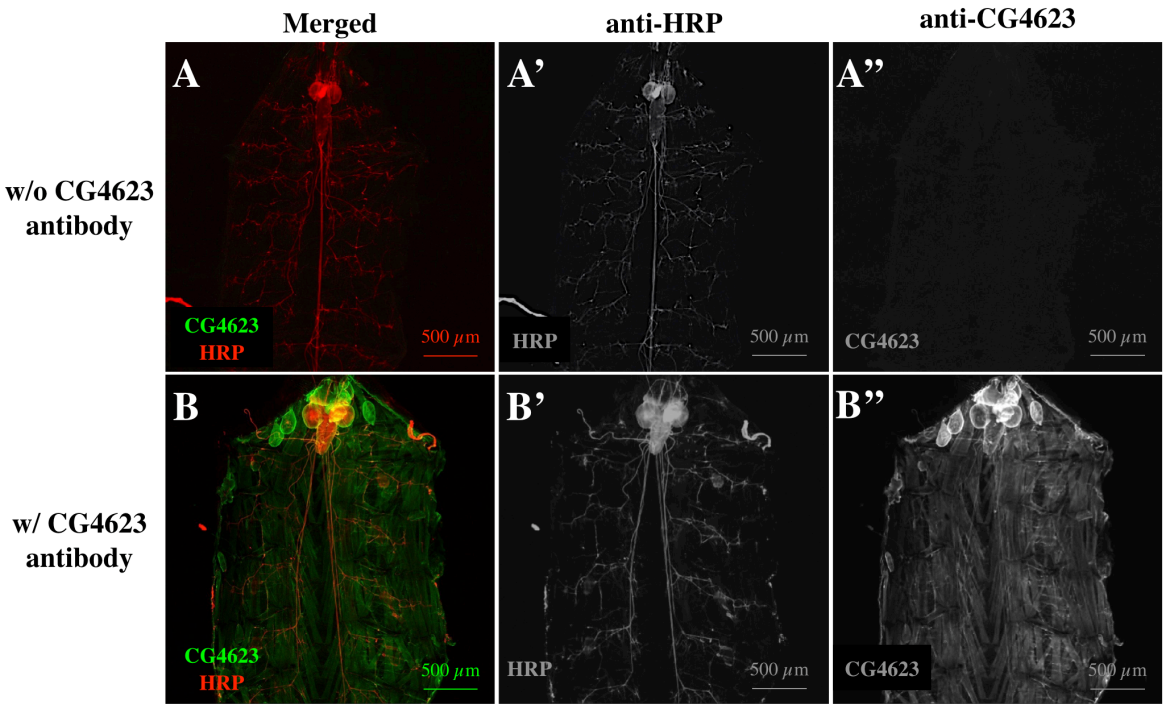

Figure 5.8. Third instar larva staining with CG4623 antibody. Wild type *Canton-S* larvae were stained with (B-B'') or without (A-A'') CG4623 antibody. (A and B) are the merged images of CG4623 (green) and HRP (red). (A' and B') and (A'' and B'') are anti-HRP and anti-CG4623, respectively.

CG4623 antibody staining of wild type *Canton-S* larva showed that CG4623 was expressed ubiquitously (Figure 5.9A). Muscle network, two lobes of brain, ventral nerve cord, motor nerve bundles and imaginal discs were stained with CG4623 antibody. Signal intensity was especially high in brain lobes, ventral nerve cord and imaginal discs. CG4623 also colocalizes with HRP that is a neuronal marker staining neuron membranes. CG4623 was also observed in neuromuscular junctions (NMJs) of third instar larva (Figure 5.9B-E).

Distinctive muscle 6 and 7 pattern in abdominal segment 3 was completely stained with CG4623 antibody (Figure 5.9E). CG4623 also colocalizes with HRP in NMJ that reside in between muscle 6 and 7 (Figure 5.9B, C, E), whereas, it does not colocalize with the post-synaptic marker DLG (Figure 5.9B, D, E).

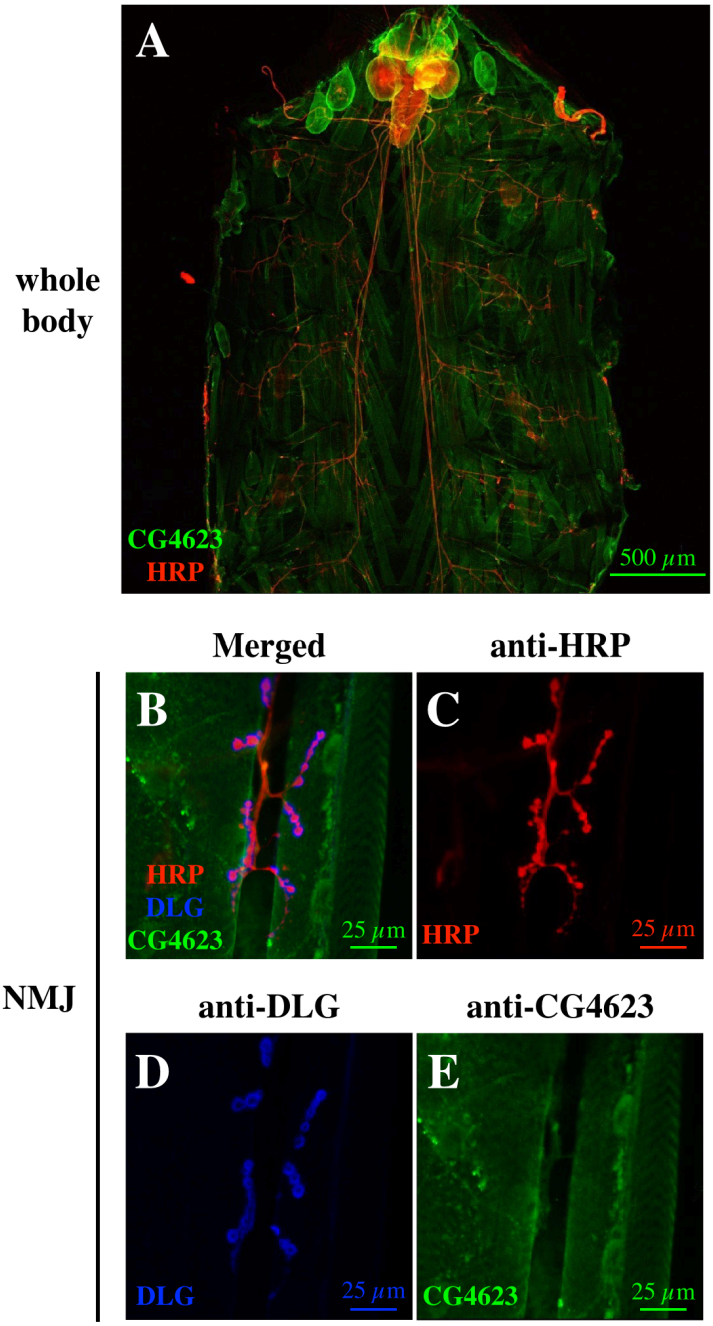

Figure 5.9. CG4623 (green), HRP (red), and DLG (blue) staining of the third instar, wild type *Canton-S* larva. (A) Whole body image of the filleted larva. (B-E) Staining of NMJ that resides in between muscle 6 and 7 of abdominal segment three.

Immunohistochemistry assays with CG4623 antibody were also performed with *act > CG4623 RNAi* and *act > CG4623 OE* flies. Downregulation and overexpression of *CG4623* was achieved by crossing the *CG4623 RNAi* and *CG4623 OE* lines with the ubiquitous driver *actin5C-GAL4* line. Changes in expression pattern of the protein and sensitivity of the newly developed antibody upon altered expression of *CG4623* were tested in the third instar larvae. CG4623 colocalizes with HRP, muscle network, central nervous system (brain lobes), and peripheral nervous system (ventral nerve cord, motor nerve bundles and imaginal discs) of both *act > CG4623 RNAi* and *act > CG4623 OE* larvae (Figure 5.10). Downregulation or overexpression of *CG4623* mildly decreased (Figure 5.10A, B) or increased (Figure 5.10C, D) the signal intensity of CG4623 staining, respectively, as compared to controls, revealing non-specific binding of the antibody.

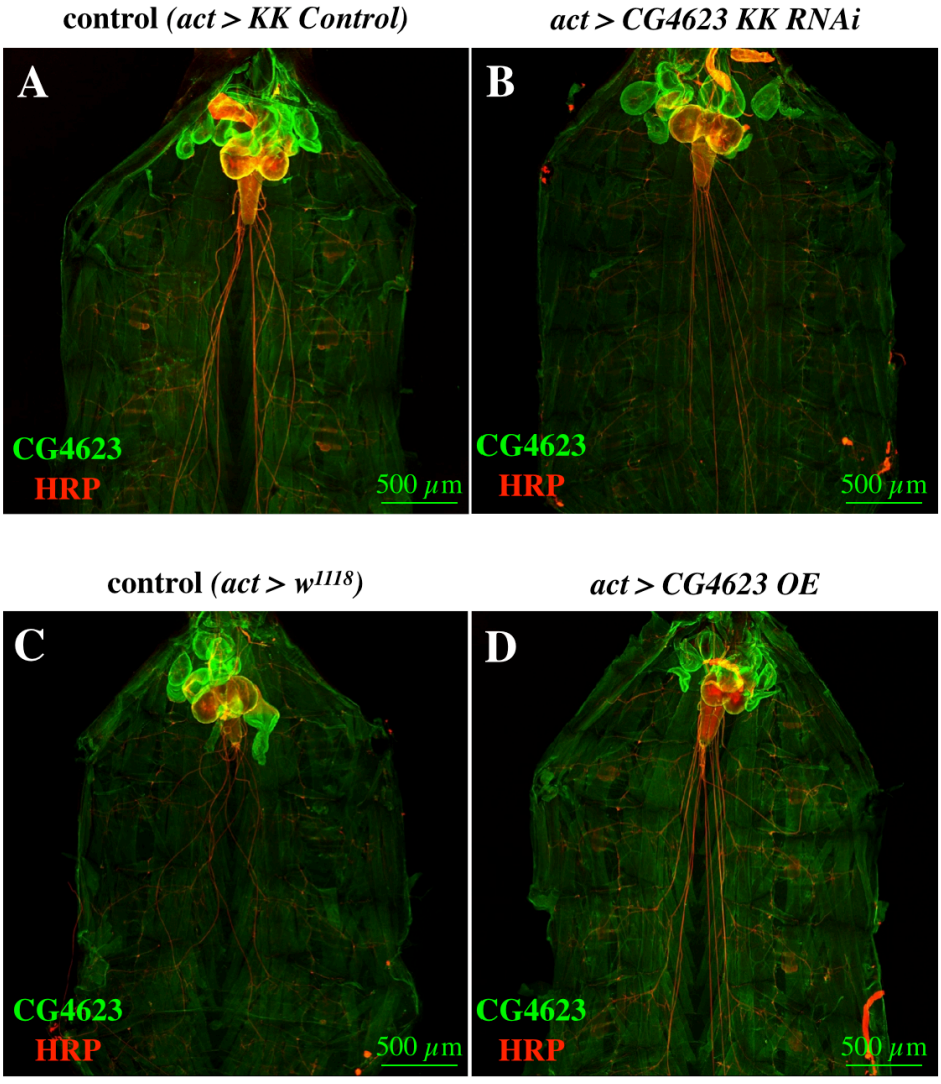

Figure 5.10. CG4623 (green) and HRP (red) staining of third instar larvae, in which *CG4623* was downregulated (A, B) or overexpressed (C, D).

5.1.4. Immunohistochemistry Analysis of *CG4623::DsRed* Flies

In addition to expression pattern analysis of CG4623 protein with the antibody generated in our laboratory, immunohistochemistry assays were performed with *CG4623::DsRed* flies. Coding sequence of *DsRed* was introduced just downstream of *CG4623* start codon in *CG4623::DsRed* flies. This allows expression of DsRed tagged version of the protein that can be used to detect the localization of CG4623 (Lopez Del Amo *et al*., 2014). For these stainings, *CG4623::DsRed* third instar larvae were dissected and stained with DsRed and DLG (post-synaptic marker) antibodies. Unfortunately, no signal was detected in DsRed channel, which supposedly corresponds to CG4623, in the whole larval body (data not shown). Then, NMJ imaging was performed to see if it is possible to detect CG4623::DsRed protein at the muscle segments or synapses (Figure 5.11). Post-synaptic areas of NMJs were stained with DLG antibody in both *CG4623::DsRed* and control (w^{1118}) larvae as expected (Figure 5.11A', B'). However, no signal was detected in DsRed channel as compared to control larva (Figure 5.11A'', B''). These findings showed that CG4623::DsRed protein could not be detected when tissues were dissected and fixed. Therefore, *CG4623::DsRed* flies have not been used in further experiments.

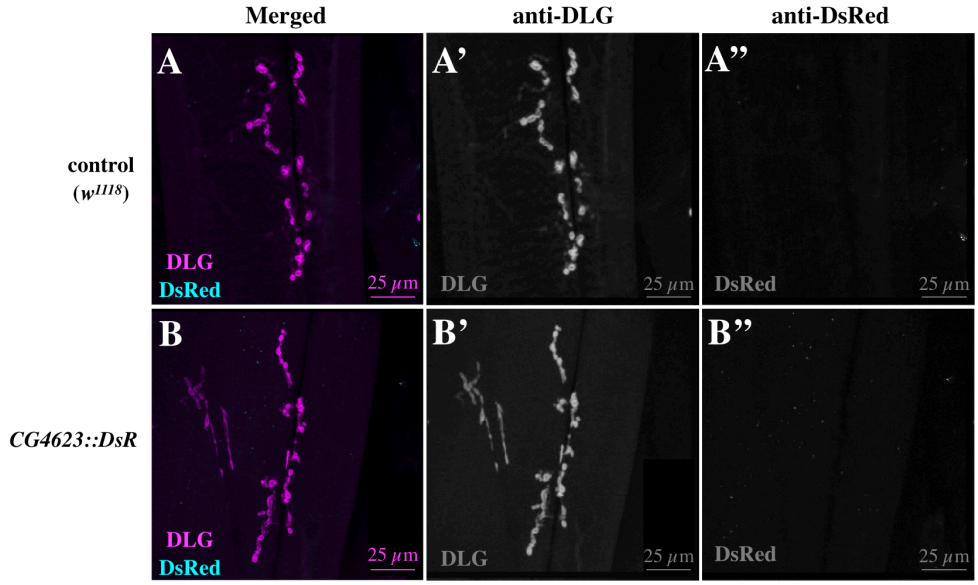

Figure 5.11. DLG (magenta) and DsRed (cyan) staining of third instar larvae expressing the DsRed tagged version of CG4623 protein. Merged anti-DLG and anti-DsRed (A and B), anti-DLG only (A' and B'), and anti-DsRed only (A'' and B'') stainings of control (w^{1118}) and *CG462::DsRed* larvae are shown.

5.2. Synaptic Electrophysiology of Larval NMJs

To determine if downregulation or overexpression of *CG4623* and *mtm* affect synaptic transmission, we electrically stimulated motor neurons at 1 Hz while recording the muscle membrane potential. The amplitude of excitatory junctional potentials (EJPs) was recorded from the muscle membrane in bath solution with 0.5 mM calcium. EJP is an upswing in the muscle cell membrane potential due to the current influx upon vesicular release of glutamate neurotransmitter from the neurons at the synapses. Therefore, amplitude of EJP is directly correlated with the amount of neurotransmitter release. Changes in the amplitude of EJP's can be referred to the differences in synaptic function and structure.

RNAi and overexpression lines of *CG4623* and *mtm* genes together with the driver lines that were planned to be used in synaptic electrophysiology experiments have different genetic backgrounds such that w^{1118}, *yw* or *yv*. Therefore, before starting to measure the EJP amplitudes of RNAi and overexpression flies, control experiments with flies having different genetic backgrounds were performed to eliminate the possibility of genetic background effect on measurements. Driver lines of *act5C-GAL4, OK6-GAL4, elav-GAL4* and *repo-GAL4* were crossed with these wild type flies and progeny flies carrying the driver allele were also used in EJP measurements to eliminate the risk of getting false data out of genetic background changes in driver lines. Fortunately, EJP amplitudes of the stated fly lines did not differ significantly, indicating that the differences in genetic background did not affect the experimental measurements (Figure 5.12).

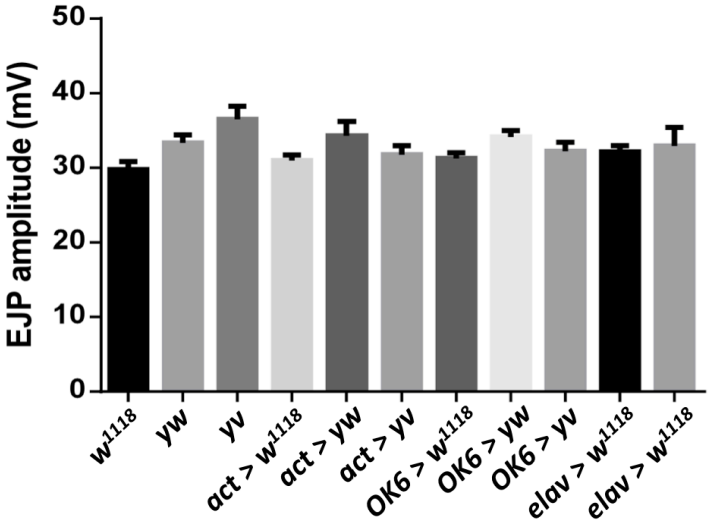

Figure 5.12. EJP amplitudes of w^{1118}, *yw,* and *yv* fly lines together with the progeny resulting from crosses of these lines with the driver lines of *act5C-GAL4, OK6-GAL4, elav-GAL4,* and *repo-GAL4*. n ≥ 5 animals per condition. Error bars: SEM; one-way ANOVA.

5.2.1. Changes in EJP Amplitude upon Up-or-Down Regulation of *CG4623*

CG4623 was downregulated or overexpressed ubiquitously (with *act5C driver*), only in neurons (with *elav-GAL4 driver*), only in motor neurons (with *OK6-GAL4*), or only in glia cells (with *repo-GAL4 driver*) to identify changes in synaptic transmission by measuring EJP amplitudes. EJP amplitudes significantly increased as compared to controls when *CG4623* was downregulated in the whole body and/or only in neurons, motor neurons or glia cells. On the other hand, when *CG4623* was overexpressed in the same tissues, EJP amplitudes significantly decreased as compared to controls (Figure 5.13A-D). These results indicate that *CG4623* is needed for proper synaptic transmission since its downregulation or overexpression, increases or decreases neurotransmitter release, respectively. This effect of *CG4623* is cell-autonomous since tissue specific driver lines also caused abnormal EJP amplitude changes.

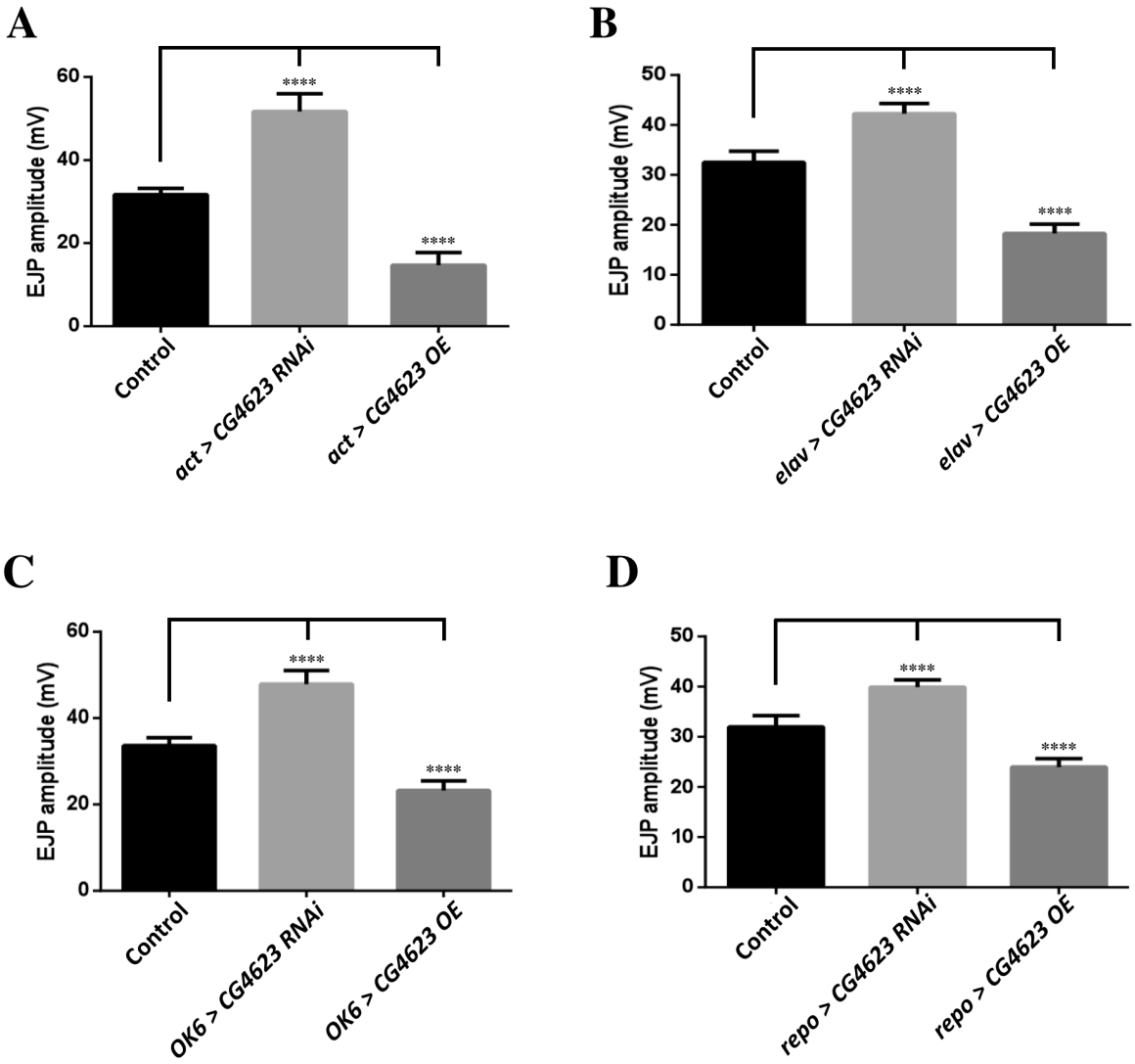

Figure 5.13. Analysis of EJP amplitude changes upon up-or-down regulation of *CG4623* in whole body (A) and/or only in neurons (B), motor neurons (C), and in glia cells (D). $n \geq 5$ animals per condition. Error bars: SEM; one-way ANOVA: ****: $p \leq 0.0001$

5.2.2. Changes in EJP Amplitude upon Up-or-Down Regulation of *mtm*

EJP amplitudes of third instar larvae, in which the *mtm* gene was downregulated or overexpressed in the whole body with the ubiquitous driver *act5C-GAL4*, in neurons with *elav-GAL4* driver, in motor neurons with *OK6-GAL4*, or in glia cells with *repo-GAL4* driver, were measured to analyze the changes in synaptic transmission. When *mtm* was downregulated in the whole body and/or only in neurons, motor neurons or glia cells, EJP amplitudes significantly decreased as compared to controls, whereas, overexpression of

mtm in the same tissues resulted in significantly increased EJP amplitudes (Figure 5.14). These findings suggest that *mtm* is required for healthy synaptic transmission since the up-or-down regulation of *mtm* increases or decreases neurotransmitter release, respectively, in a cell autonomous way.

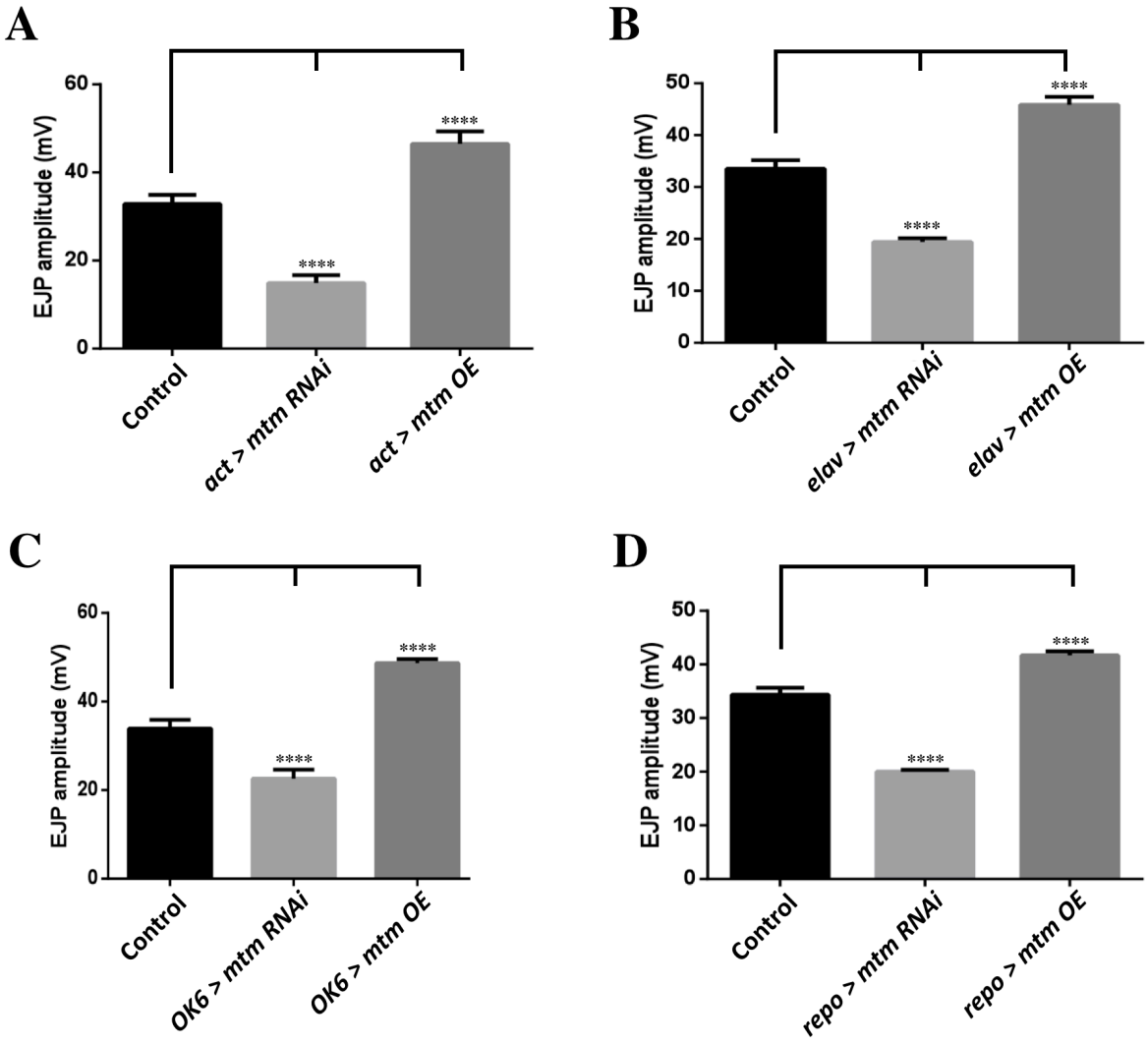

Figure 5.14. Analysis of EJP amplitude changes upon up-or-down regulation of *mtm* in whole body (A) and/or only in neurons (B), motor neurons (C), and in glia cells (D). $n \geq 5$ animals per condition. Error bars: SEM; one-way ANOVA: ****: $p \leq 0.0001$

5.3. NMJ Morphology Analysis upon *CG4623* Up-or-Down Regulation

Drosophila NMJ is an excellent structure to study pathophysiological features of the peripheral neurons affected in CMT disease. Many proteins are involved in NMJ development and proteins associated with neurodegenerative diseases were shown to affect

the NMJ morphology (Bayat *et al*., 2011). As alterations in *CG4623* expression levels were shown to be affecting EJP amplitudes recorded from NMJs, its up-or-down regulation might also affects the NMJ morphology or morphological changes in NMJs might be the cause of defective EJP amplitudes. In order to further analyze this phenomenon, immunohistochemistry experiments were performed in NMJs found on the muscles 6 and 7 in the segments A3 or A4 of third instar larva. Anti-HRP and anti-DLG markers were used to stain the neuronal membrane and the post-synaptic areas, respectively. The length of NMJ and its ratio to innervated muscle area was determined. We have also investigated the morphological changes in boutons at which the neuron-muscle interaction occurs.

Ubiquitous downregulation or overexpression of *CG4623* was achieved by crossing *CG4623 RNAi* and *CG4623 OE* lines with *act5C-GAL4* driver, respectively. *CG4623* was downregulated or overexpressed only in neurons by crossing *CG4623 RNAi* and *CG4623 OE* lines with *UAS-Dicer;;nSyb-GAL4*. In addition to *CG4623 RNAi* and *CG4623 OE* lines, morphology analysis of *Drp1 RNAi* and *Marf RNAi* lines were also performed. Drp1 is a mitochondrial fission factor and Marf (*Drosophila* homolog of human mitofusin) is a mitochondrial fusion factor. Analyses of NMJs with the known mitochondrial factors were used as a positive control for CG4623 that is suggested to be a mitochondrial fission factor. RNAi lines of these genes were also crossed with *act5C-GAL4* and *UAS-Dicer;;nSyb-GAL4* driver lines.

5.3.1. Effects of Ubiquitous Downregulation/Overexpression of *CG4623* in NMJ Morphology

Ubiquitous downregulation of *CG4623* did not change NMJ morphology in terms of NMJ length to muscle area and bouton structure (Figure 5.15). We did not observe any premature NMJ structure or defects in boutons like satellite bouton formation. The ratio of NMJ length to muscle area did not differ significantly between RNAi larvae and controls. Ubiquitous overexpression of CG4623 also did not change NMJ morphology (Figure 5.16). Boutons had healthy round shape when *CG4623* was overexpressed and also NMJ length to muscle area did not differ significantly between overexpression larvae and controls. Not only altered expression of *CG4623* but also ubiquitous downregulation of

known mitochondrial factors *Drp1* and *Marf* did not disrupt bouton structure and length of NMJ to innervated muscle area (Figure 5.17). Therefore, results of CG4623 were consistent with the results obtained from the known mitochondrial factors.

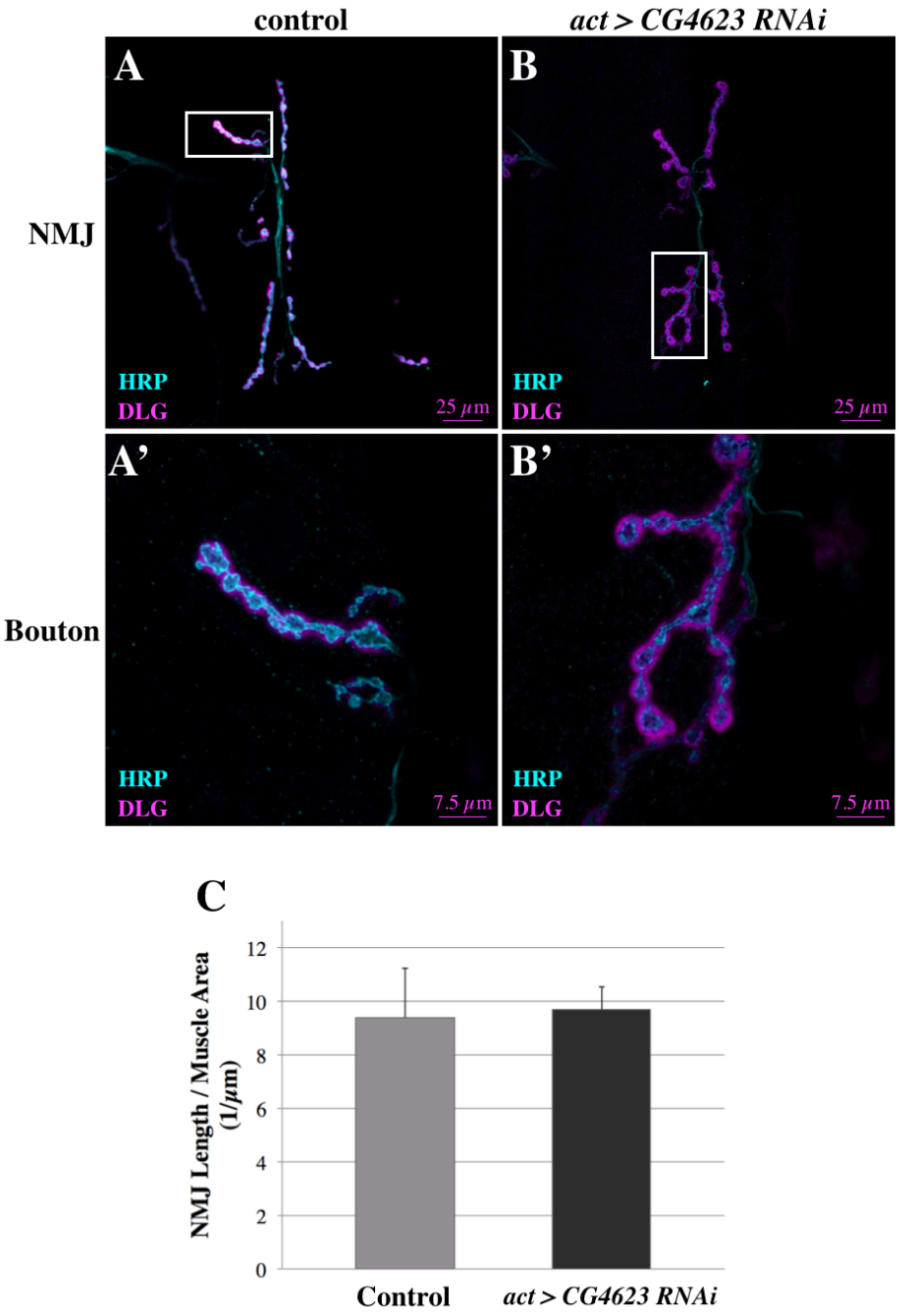

Figure 5.15. Effects of ubiquitous *CG4623* downregulation on NMJ morphology. (A, B) NMJ view of control (*act > KK Control*) and *act > CG4623 RNAi* larvae. Rectangles represent the magnified areas for bouton views. (A', B') Bouton view of control and *act > CG4623 RNAi* larvae. (C) The ratio of the NMJ length to the innervated muscle area. n ≥ 4 animals per condition. Error bars: SEM; two-tailed t-test = 0.883.

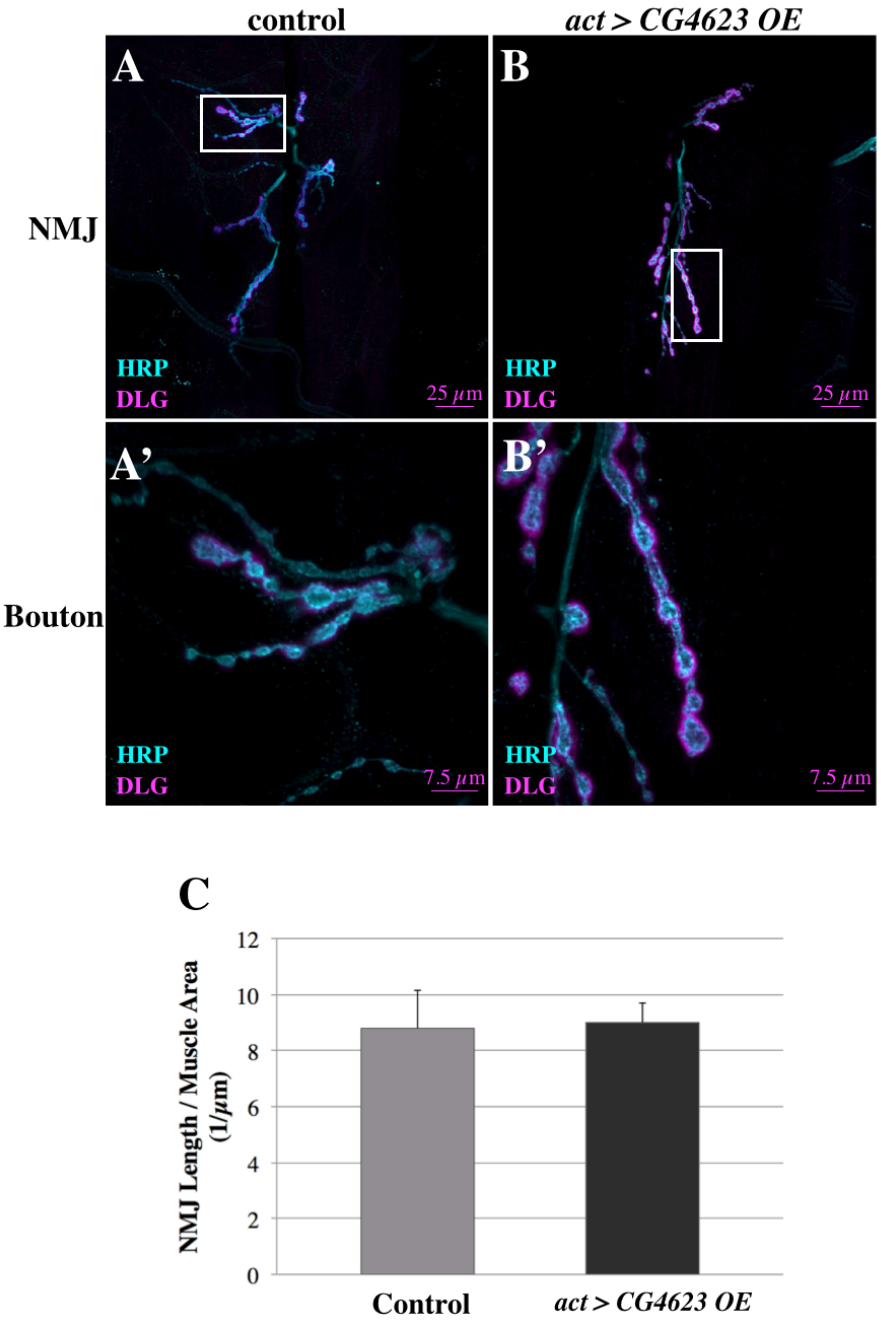

Figure 5.16. Effects of ubiquitous *CG4623* overexpression on NMJ morphology. (A, B) NMJ view of control (*act* > w^{1118}) and *act* > *CG4623 OE* larvae. Rectangles represent the magnified areas for bouton views. (A', B') Bouton view of control and *act* > *CG4623 OE* larvae. (C) The ratio of the NMJ length to the innervated muscle area. n ≥ 4 animals per condition. Error bars: SEM; two-tailed t-test = 0.803.

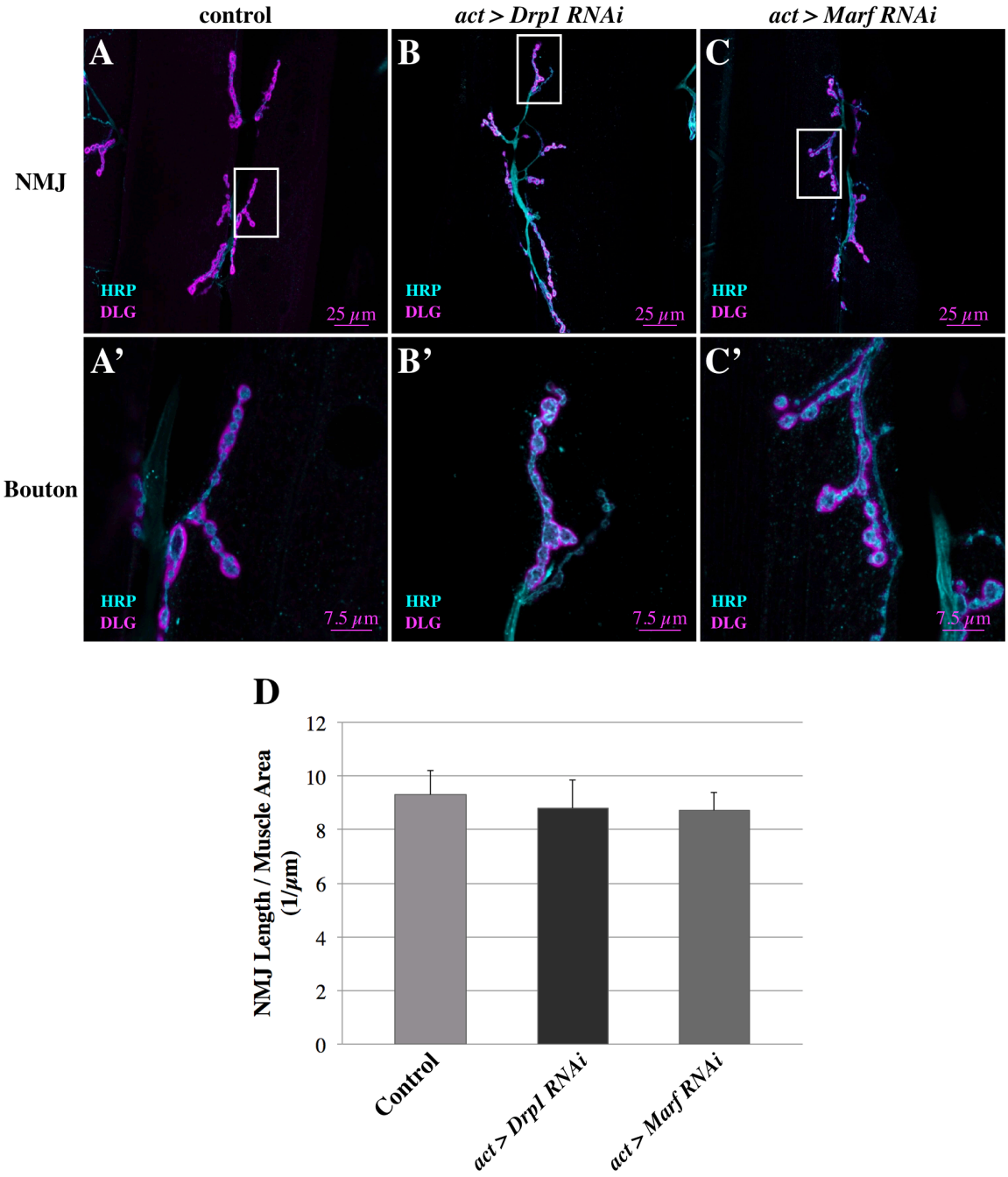

Figure 5.17. Effects of ubiquitous *Drp1* and *Marf* downregulation on NMJ morphology. (A, B and C) NMJs of control (*act>TRIP Control*), *act>Drp1 RNAi,* and *act>Marf RNAi* larvae. Rectangles represent the magnified areas for bouton views. (A', B' and C') Boutons of control, *act>Drp1 RNAi,* and *act>Marf RNAi* larvae. (D) The ratio of the NMJ length to the muscle area. n≥4 animals per condition. Error bars: SEM; one-way ANOVA.

5.3.2. Effects of Neuronal Downregulation/Overexpression of *CG4623* in NMJ Morphology

To identify if altered expression of *CG4623* has a cell-autonomous effect, *CG4623* was downregulated or overexpressed only in neurons by using neuronal driver *UAS-Dicer;;nSyb-GAL4*. Dicer enzyme was additionally overexpressed in this driver line for increasing the effectiveness of the sequence-specific degradation of the target mRNA. Despite the use of dicer, downregulation or overexpression of *CG4623* did not change the NMJ morphology (Figure 5. 18, Figure 5.19). Boutons had healthy round shapes as observed in controls (Figure 5.18A', B'; Figure 5.19A', B'). The ratio of NMJ length to innervated muscle did not differ significantly from controls in both conditions of *CG4623* downregulation and overexpression (Figure 5.18C, Figure 5.19C). These findings were consistent with the results obtained from neuronal downregulation of known mitochondrial factors *Drp1* and *Marf* (Figure 5.19). Bouton structure or NMJ length to muscle area ratio did not differ as compared to controls when *Drp1* or *Marf* were downregulated only in neurons.

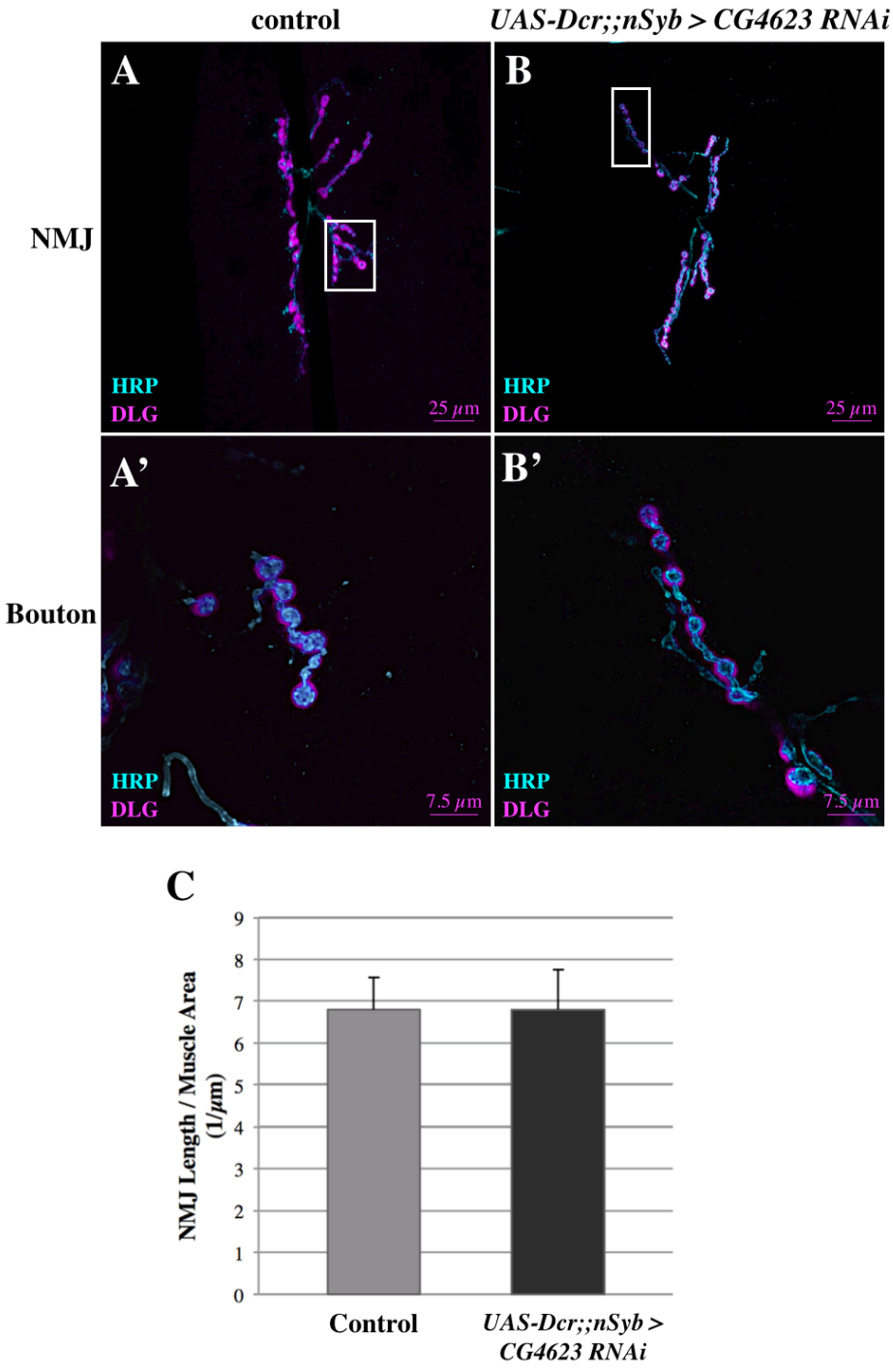

Figure 5.18. Effect of neuronal *CG4623* downregulation on NMJ morphology. (A, B) NMJ view of control (*UAS-Dcr;;nSyb-GAL4>KK Control*) and *UAS-Dcr;;nSyb-GAL4>CG4623 RNAi* larvae. Rectangles represent the zoomed areas for bouton views. (A', B') Bouton view of control and *UAS-Dcr;;nSyb-GAL4>CG4623 RNAi* larvae. (C) The ratio of NMJ length to muscle area. n≥4 animals per condition. Error bars: SEM; two-tailed t-test=0.981.

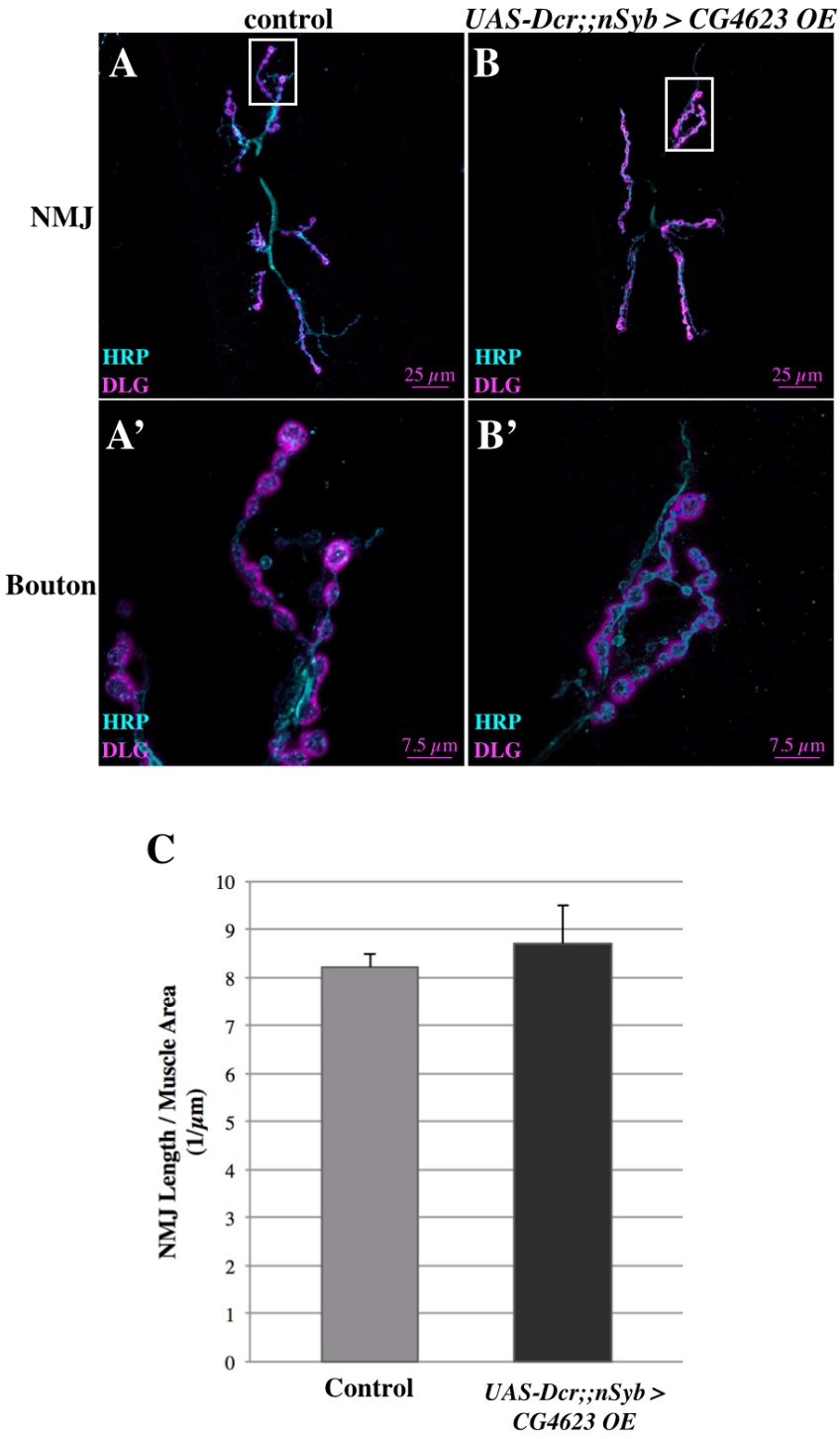

Figure 5.19. Effect of neuronal *CG4623* overexpression on NMJ morphology. (A, B) NMJ view of control (*UAS-Dcr;;nSyb-GAL4>w*^{1118}) and *UAS-Dcr;;nSyb-GAL4>CG4623 OE* larvae. Rectangles represent the zoomed areas for bouton views. (A', B') Bouton view of control and *UAS-Dicer;;nSyb-GAL4>CG4623 OE* larvae. (C) The ratio of NMJ length to muscle area. n≥4 animals per condition. Error bars: SEM; two-tailed t-test=0.578.

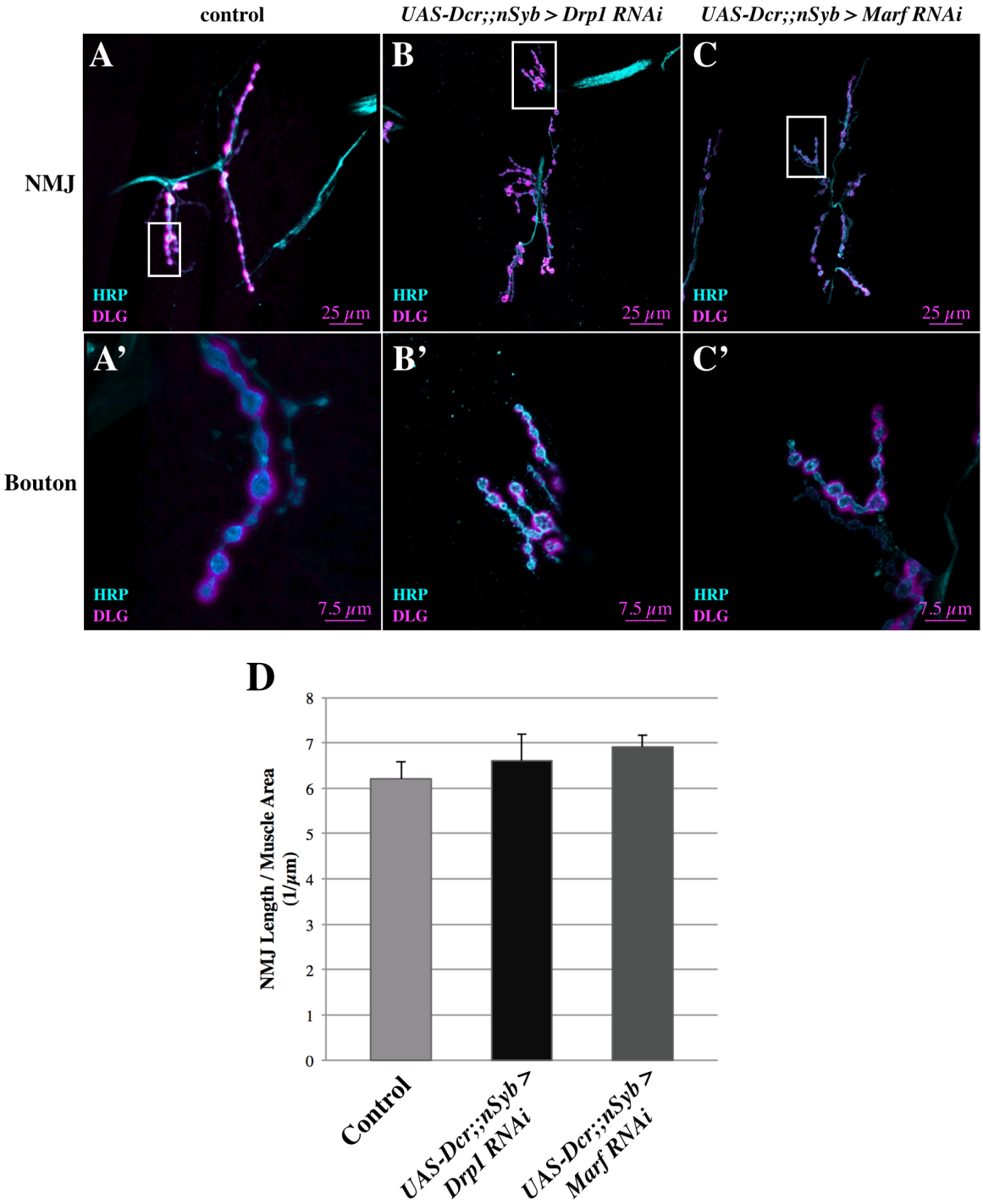

Figure 5.20. Effect of neuronal *Drp1* and *Marf* downregulation on NMJ morphology. (A, B and C) NMJ view of control (*UAS-Dcr;;nSyb-GAL4>TRIP Control*), *UAS-Dcr;;nSyb-GAL4>Drp1 RNAi,* and *UAS-Dcr;;nSyb-GAL4>Marf RNAi* larvae. Rectangles represent the zoomed areas for bouton views. (A', B' and C') Boutons of control, *UAS-Dcr;;nSyb-GAL4>Drp1 RNAi,* and *UAS-Dcr;;nSyb-GAL4>Marf RNAi* larvae. (D) The ratio of NMJ length to muscle area. n≥4 animals per condition. Error bars: SEM; one-way ANOVA.

5.4. Mitochondrial Dynamics Analysis upon *CG4623* Up-or-Down Regulation

In *Drosophila*, motor neurons stem from the ventral nerve cord (VNC) and migrate to the muscles to form NMJs. Although *Drosophila* has no myelin structure like that observed in mammals, it has a similar ensheathing glial structure surrounding peripheral neurons. Motor nerve bundles ensheathed by these glial cells can be used as a model for studying peripheral neuropathies. Since CG4623 is suggested to be a mitochondrial fission factor, we aimed to investigate its effect on mitochondrial dynamics in peripheral neurons. For this purpose, *CG4623* was downregulated and overexpressed in glia cells surrounding motor neurons using the glial driver *repo-GAL4*. Additionally, a mitochondrial marker construct under UAS control (*UAS-mitoGFP*) was included into the same background in order to visualize mitochondria. Immunohistochemistry experiments were performed in nerve bundles migrating to the muscles of segments A3 or A4 segments. Anti-repo and anti-GFP antibodies were used to stain glia cell nuclei and GFP tagged mitochondria, respectively. 3D Object Counter plug-in of Fiji software was used to calculate tubularization index of mitochondria.

CG4623 was downregulated or overexpressed only in glia cells by crossing *CG4623 RNAi* and *CG4623 OE* lines with *repo-GAL4, UAS-mitoGFP*. In addition to *CG4623 RNAi* and *CG4623 OE* lines, mitochondria dynamics analysis of *Drp1 RNAi* and *Marf RNAi* lines were also performed. Analyses of mitochondrial dynamics with the known mitochondrial factors were used as a positive controls for CG4623. RNAi lines of these genes were also crossed with *repo-GAL4, UAS-mitoGFP* driver line.

Mitochondrial dynamics did not differ upon glial downregulation or overexpression of *CG4623* (Figure 5.21, Figure 5.22). Mitochondria did not show any tendency to be more tubular or spherical in morphology (Figure 5.21A, B; Figure 5.22A, B). The tubularization index of larvae, in which *CG4623* was up-or-down regulated, also did not differ significantly as compared to controls (Figure 5.21C, Figure 5.22C). These findings were consistent with the results obtained from glial downregulation of known mitochondrial factors *Drp1* and *Marf* (Figure 5.23). Mitochondrial morphology or index of tubularization did not differ significantly as compared to controls when *Drp1* or *Marf* downregulated only in glia cells.

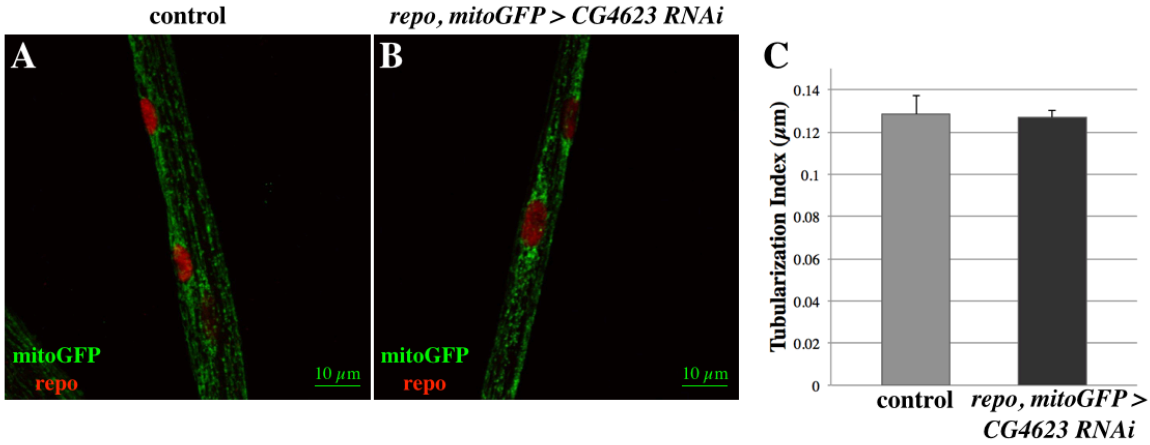

Figure 5.21. Effect of glial *CG4623* downregulation on mitochondrial dynamics. (A, B) Nerve bundle view of control (*repo-GAL4, UAS-mitoGFP > KK Control*) and *repo-GAL4, UAS-mitoGFP > CG4623 RNAi larvae*. (C) Tubularization index of control and *repo-GAL4, UAS-mitoGFP > CG4623 RNAi* larvae. n ≥ 4 animals per condition. Error bars: SEM; two-tailed t-test = 0.877.

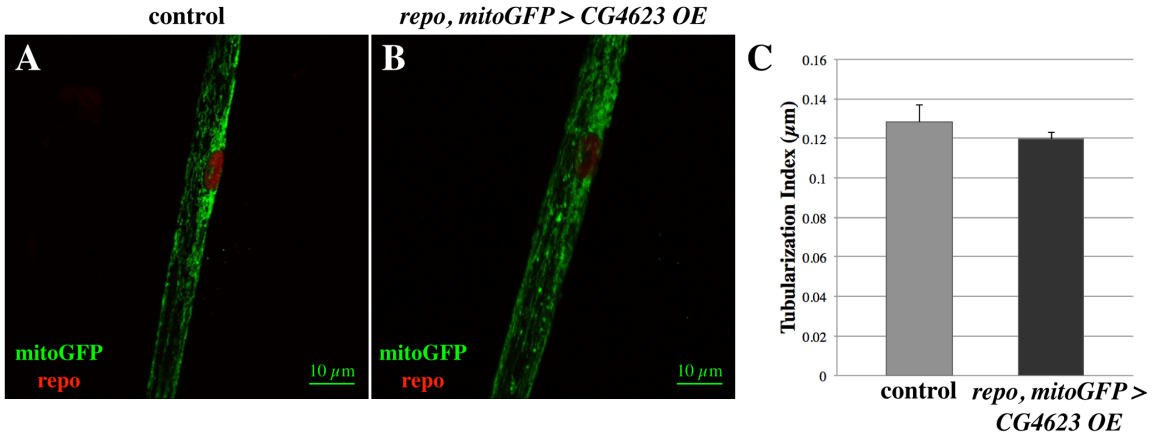

Figure 5.22. Effect of glial *CG4623* overexpression on mitochondrial dynamics. (A, B) Nerve bundle view of control (*repo-GAL4, UAS-mitoGFP > w^{1118}*) and *repo-GAL4, UAS-mitoGFP > CG4623 OE larvae*. (C) Tubularization index of control and *repo-GAL4, UAS-mitoGFP > CG4623 OE* larvae. n ≥ 4 animals per condition. Error bars: SEM; two-tailed t-test = 0.377.

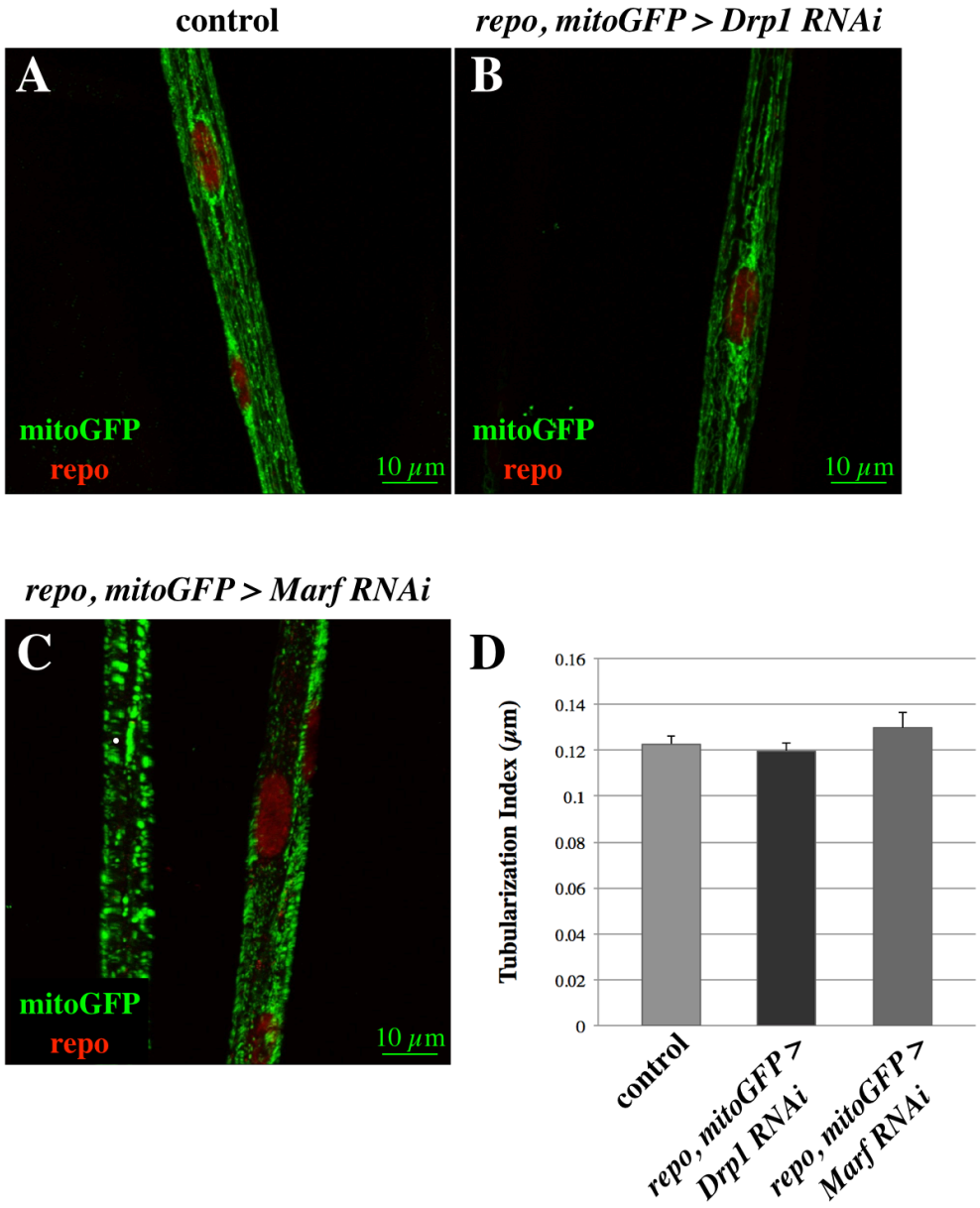

Figure 5.23. Effect of glial *Drp1* and *Marf* downregulation on mitochondrial dynamics. (A, B and C) Nerve bundle view of control (*repo-GAL4, UAS-mitoGFP>TRIP Control*), *repo-GAL4, UAS-mitoGFP>Drp1 RNAi*, and *repo-GAL4, UAS-mitoGFP>Marf RNAi* larvae. (D) Tubularization index of control, *repo-GAL4, UAS-mitoGFP>Drp1 RNAi*, and *repo-GAL4, UAS-mitoGFP>Marf RNAi* larvae. n ≥ 4 animals per condition. Error bars: SEM; one-way ANOVA.

6. DISCUSSION

In this study, we have focused on developing *Drosophila* models for Charcot-Marie-Tooth disease type 4 (CMT4) that includes all forms of autosomal recessive CMT. Because of widespread consanguinity, autosomal recessive forms of CMT are accounted more frequently in the Mediterranean and Middle Eastern countries like Turkey as compared to European population. Genes associated with CMT have diverse cellular functions and understanding the pathogenesis for each gene makes it necessary to develop *in vivo* models. For this purpose, we have chosen to model CMT4 in terms of *ganglioside-induced differentiation associated protein 1* (*GDAP1)* and *myotubularin-related 2* (*MTMR2*) genes, known for CMT4A and CMT4B1 types, respectively.

Mutations in *GDAP1* gene can be responsible for demyelinating, axonal or mixed forms of the disease with recessive or dominant modes of inheritance. Patients with *GDAP1* mutations show various clinical phenotypes of mild to very severe disease progression with late and early onset (Cassereau *et al*., 2011). These distinct forms of *GDAP1* phenotypes together with its involvement in mitochondrial dynamics and glutathione S-transferase activity make this gene promising to study and understand the underlying pathogenesis in CMT disease. On the other hand, mutations in *MTMR2* gene are associated with demyelinating recessive CMT with myelin outfoldings (Bolino *et al*., 2000). Studies show that MTRM2 is an important phospholipid phosphatase and has a role in endosomal trafficking (Cao *et al*., 2008; Tsujita *et al*., 2004). Loss of function mutations in *MTMR2* causes impaired phosphatidyl inositol (PI) mechanism, resulting in excess membrane formation and disturbed membrane trafficking.

Drosophila homologs of *GDAP1* and *MTMR2* genes are *CG4623* and *mtm*, respectively. In this study, our first goal was to analyze expression pattern of these genes by generating antibodies against them to show functional homology between their human homologs. Next, we have performed synaptic electrophysiology recordings to assess functional roles of CG4623 and mtm in synaptic transmission. Changes in neuromuscular junction (NMJ) morphology were also analyzed to see if those genes disrupt synapse-to-

muscle interaction zones. Additionally, mitochondrial dynamics analyses of CG4623 were performed to investigate its role in mitochondrial fission mechanism. We have modeled these genes' pathogenicity by altering their expression levels using available RNAi lines and our recently generated overexpression lines. Efficiency of these lines to successfully downregulate and overexpress *CG4623* and *mtm* were tested and confirmed by a colleague with quantitative RT-PCR (Küey, 2015). These lines were then crossed with the ubiquitous or tissue specific drivers to alter *CG4623* or *mtm* gene expression levels in the whole body or tissue-specifically depending on the assay.

The first part of the study was focused on generating a polyclonal antibody against CG4623 protein to reveal its expression level and pattern. Current literature knowledge about expression of CG4623 protein is not adequate enough to compare its function to the human homolog. Therefore, it is necessary to generate an antibody to study sub-cellular localization and interaction partners by immunohistochemistry experiments and Western blot assays. Before starting to generate antibody against CG4623, we had also tried Western blot analysis with available GDAP1 and GDAP1L1 antibodies on fly protein extracts, however, antibodies did not cross-react with *Drosophila* proteins significantly. This situation also urged us to study CG4623 expression levels and pattern using an anti-CG4623 antibody. The initial step was to overexpress CG4623 protein in bacteria and determine the optimum non-toxic IPTG condition, and then continue with the protein purification steps. Our initial plan for purification was to use nickel column since the protein has its own his-tag. Buffers containing high amounts of urea with varying pH values were used, however, only very low amount of protein was purified. Therefore, we have decided to change urea containing buffers to imidazole containing buffers to allow higher yield of protein binding to the column. The idea was to use high amounts of imidazole in elution buffer to allow competition with the histidine tag for binding to the nickel ions. However, with this method protein could have been observed only in first elution fraction, moreover, that fraction was not pure enough as several other bands were also observed in SDS-PAGE. Since we already knew that human GDAP1 had a transmembrane domain and formed dimers remaining insoluble in the cell, we have concluded that its *Drosophila* homolog CG4623 also behaved in the same manner (Pedrola *et al.,* 2005; Shield *et al.,* 2006). Same like GDAP1, transmembrane domain of CG4623 did not allow us to purify protein, as it probably remained insoluble within the cell lysate.

To overcome this problem, CG4623 construct could have been generated to express protein fragment lacking transmembrane domain rather than full-length.

Regarding the difficulties in column purification methods and low yield of purified protein, we have changed our method to protein purification from polyacrylamide gel extraction. We have successfully purified sufficient amount of protein with this method and confirmed that extracted sample was indeed containing CG4623 by performing Western blot analysis with his-probe antibody. Purified sample was used as an antigen source for injection into rabbits and a high concentration of antibody was produced that was later used for Western and immunohistochemistry assays.

The newly generated CG4623 antibody that was tested in Western blots yielded a product around 40 kDa that might correspond to endogenous CG4623 protein. However, there were no band intensity differences in between wild-type, downregulation and overexpression lines. Additionally non-specific bindings were observed at around 35 kDa and ~80 kDa levels. When the Western blot analysis was repeated with CG4623 antibody that was pre-adsorbed by incubating with *CG4623* downregulated third instar larvae, a slight increase was observed in the band intensity for overexpression compared to downregulation line. Even so, generated antibody is promising enough for further optimizations according to Western blot analysis, which were reproducible with clean background and without a smeared pattern or distorted bands. Furthermore, considering that GDAP1 is capable of forming dimers, its *Drosophila* homolog *CG4623* might also form dimers that might correspond to ~80 kDa band observed in Western blot analysis. Pre-adsorbing CG4623 antibody with the *CG4623* mutant larvae or with bacterial extracts might solve the problem of non-specificity.

Immunohistochemistry assays were also performed with the newly generated CG4623 antibody to reveal expression pattern of CG4623 in the third instar larvae. Wild type larvae stained with CG4623 antibody showed that CG4623 was expressed ubiquitously. Muscle network, two lobes of brain, ventral nerve cord, motor nerve bundles and imaginal discs were stained with CG4623 antibody. Considering that *GDAP1* is expressed predominantly in the peripheral nervous system (PNS) while its paralog *GDAP1L1* is expressed in the central nervous system (CNS), it is possible that *CG4623*,

which has approximately equal similarity to both genes, could have an important function in both parts of the nervous system since signal intensity was especially high in both brain lobes that are parts of CNS, and also in ventral nerve cord and imaginal discs that are related with PNS. At the neuromuscular junction (NMJ) level, CG4623 was localized to neurons innervating into the muscles of the third instar larva. Muscular structures were completely stained, especially longitudinal muscle 6 and 7 pattern in abdominal segment 3 was apparent. These findings, were taken into consideration with the absence of the colocalization with the post-synaptic marker DLG, indicating that CG4623 might be found in neuronal membranes but not in post-synaptic areas where neuron-to-muscle interactions occur. To track changes in expression pattern of *CG4623* and sensitivity of generated antibody, immunohistochemistry assays were also performed with *CG4623* downregulated and overexpressed larvae. Similar to results in wild type larva, CG4623 colocalizes with muscle network, central nervous system (brain lobes), and peripheral nervous system (ventral nerve cord, motor nerve bundles and imaginal discs) of both *CG4623* downregulated and overexpressed larvae. However, downregulation or overexpression of *CG4623* mildly decreased or increased the signal intensity of CG4623 staining, respectively, as compared to controls, probably due to non-specific binding of the antibody.

Both Western blot analysis and immunohistochemistry assays revealed that newly developed antibody is promising for determining sub-cellular localization or interaction partners of CG4623 with further optimizations. The reason why we did not observe any significant changes in the expression pattern of the protein upon up-or-down regulation of *CG4623* probably because of non-specific binding of the antibody. It might be possible to overcome this problem with antibody pre-adsorption techniques. Another possibility is incomplete silencing of *CG4623* by RNAi, however, this is less likely since we observed over 90 fold decrease at its mRNA level (Küey, 2015). It is also possible to perform antigen-specific antibody purification with the remaining batch of sera collected from rabbits. Overall, this antibody can be used in further analysis to assess mitochondrial fission factor role of CG4623 by showing its colocalization with mitochondria. Distribution of CG4623 in both PNS and CNS could also be searched to understand its dual role of substituting for both GDAP1 and GDAP1L1 in *Drosophila*.

We have also performed immunohistochemistry assays with the fly line expressing DsRed tagged version of the CG4623 that was kindly provided by Dr. Galindo. However, we did not observe any signal corresponding to CG4623 neither in the whole third instar larval body nor in the NMJ or muscles. We have concluded that CG4623::DsRed protein could not be detected when tissues were dissected and fixed. Alternatively, the expression level could be too low and thus its detection would require some amplification steps to allow visualization. As the results obtained with the antibody generated in the framework of this study were more promising, *CG4623::DsRed* flies have not been used in further experiments.

In the second part of the study, we have focused on recapitulating electrophysiological evidence of neuronal dysfunction observed in CMT patients. For this purpose, we have performed synaptic electrophysiology in NMJs of third instar larvae and tested whether downregulation or overexpression of *CG4623* and *mtm* affect synaptic transmission. We initially showed that different genetic backgrounds did not have any significant effect on the EJP amplitude recordings. We found that EJP amplitudes were significantly higher compared to controls when *CG4623* was downregulated in the whole body and/or only in neurons, motor neurons or glia cells. On the other hand, when *CG4623* was overexpressed in the same tissues, EJP amplitudes were significantly lower as compared to controls. These results indicate that CG4623 is crucial for proper synaptic transmission in a cell-autonomous way. Additionally, since amplitude of EJP is directly proportional with the amount of neurotransmitter release, downregulation or overexpression of *CG4623* might also affect neurotransmitter release mechanisms.

In contradiction, we observed just the opposite effects, when *mtm* was downregulated in the whole body and/or only in neurons, motor neurons or glia cells. In this case, EJP amplitudes were significantly low in *mtm* downregulated larvae and high in *mtm* overexpressed larvae. Even though the human homologs of *CG4623* and *mtm* show similar electrophysiological defects in humans, differences in their EJP amplitude abnormality pattern might be explained by other unknown cellular effects in flies. Similar to CG4623, mtm is also necessary for a healthy synaptic transmission in a cell-autonomous way in terms of these findings. Downregulation or overexpression of *mtm* also decreases or increases neurotransmitter release, respectively.

To the best of our knowledge, this is the very first study showing effects of up-or-down regulation of CMT causing genes via performing synaptic electrophysiology to measure EJP amplitudes. For this reason, our current knowledge is not sufficient to further evaluate electrophysiological measurements. It is also important to notice that EJP amplitude values are different then the nerve conduction velocities (NCVs) that are conventionally used by clinicians as one of the diagnostic criteria. Even so, significant changes in EJP amplitudes upon altered expression levels of *CG4623* and *mtm* indicate that these genes are capable to recapitulate electrophysiological evidence of neuronal dysfunction observed in CMT disease. Further experiments on the giant fiber axon system of adult flies to record response latency by using electrophysiology could also be performed.

To determine whether changes in EJP amplitudes were caused by morphological defects at the NMJ level, we have performed immunohistochemistry assays to visualize NMJs and boutons, where neuron-muscle interactions occur. Besides, NMJ is an excellent structure to study pathophysiological features of CMT since many proteins associated with neurodegenerative diseases are shown to affect the NMJ morphology. For this purpose, immunohistochemistry experiments were performed with RNAi and overexpression lines of *CG4623* whereas the compound heterozygous flies carrying two different null alleles of *mtm* were used during the assays.

RNAi knock-down of *CG4623* in the whole body or only in neurons did not display any reduction in bouton size or any disruption in NMJ morphology as compared to controls. NMJ or bouton phenotype also did not change when *CG4623* was overexpressed ubiquitously or only in neurons. The ratio of NMJ length to innervated muscle area did not differ significantly in those conditions as well. These results suggest that changes in EJP amplitudes upon up-or-down regulation of *CG4623* were not caused by disruption in NMJ/bouton morphology. Progressive characteristics of CMT pathophysiology in an age dependent manner can be taken into account at this point. It is possible that EJP abnormalities did not yet influence NMJ morphology at the third instar developmental stage. This phenomenon can also be supported with the findings of Lopez Del Amo *et al.,* and Niemann *et al.,* as they also reported progressive neurodegeneration in their *GDAP1*

fly and mouse models (Lopez Del Amo *et al.,* 2014; Niemann *et al.,* 2014). Another possibility is that changes in EJP amplitudes therefore neurotransmitter release, might be related with the levels of pre-synaptic glutamate and post-synaptic receptor cluster size rather than disruption in NMJ morphology. It is known that when the presynaptic terminals contain more glutamate, fewer glutamate receptors cluster post-synaptically at the NMJ. Conversely, when the motor neuron endings contain less glutamate, significantly more glutamate receptors cluster at the NMJ. Alterations in *CG4623* levels might cause disruptions in this fine mechanism, which is not possible to observe at the NMJ or bouton levels, instead of completely changing NMJ morphology. Calcium handling, ATP production and other mitochondrial mechanisms, which may influence synaptic vesicle pool organization and synaptic function, could have been disrupted also.

Conversely, immunohistochemistry assays performed by former lab member Merve Kılınç showed that the compound heterozygous flies carrying two different null alleles displayed abnormal NMJ structure and reduction in bouton size. Similar results were also obtained when *mtm* was downregulated. These findings of Merve Kılınç are reasonable to explain changes in EJP amplitudes upon up-or-down regulation of *mtm*. Abnormal NMJ and bouton structure might cause abnormal EJP amplitudes as well. This was expected when we take into account the early onset, rapid progression and severity of symptoms caused by mutations in *MTMR2*. Also, changes in neurotransmitter release might be the cause of disturbed recycling of vesicles considering mtm's role in the endosomal trafficking.

In the last part of the study, mitochondrial dynamics analyses were performed to reveal insights of the suggested role of CG4623 as a mitochondrial fission factor. However, mitochondrial dynamics did not differ upon glial downregulation or overexpression of *CG4623,* when the glial cells wrapping the motor nerve bundle were visualized. In these cells, mitochondria did not show any tendency to be more tubular or spherical in morphology. RNAi knock-down or overexpression of *CG4623* resulted in no significant difference in the tubularization index of larvae as compared to controls. Additionally, mitochondrial morphology or index of tubularization did not differ significantly when known mitochondrial factors *Drp1* or *Marf* were downregulated only in glia cells as well. On one hand, these results might be consistent with the progressive

characteristics of CMT disease since third instar larval stage might be an early developmental phase to show the effects of *CG4623* up-or-down regulation on mitochondrial morphology. This explanation is also parallel with the findings of Lopez Del Amo *et al.,* since they showed that overexpression of *CG4623* caused smaller mitochondria in the retina and muscle of five weeks old adult flies as compared to one week old adult flies (Lopez Del Amo *et al.,* 2014). On the other hand, confocal imaging of mitochondria might not be sufficient to visualize the organelle. Finer imaging using electron microscopy might help us to display mitochondria in a clearer way. Mitochondria at the NMJs can also be visualized since the organelle must be transported from the main body of the nerve cell to the tips of the axons to transmit impulses. This may not happen if mitochondria are in the wrong shape or size. It might be possible to visualize these abnormalities by electron microscopy.

In this study, we have aimed to develop *Drosophila* models for CMT disease by altering the expression levels of *CG4623* and *mtm* genes. Both RNAi knockdown and overexpression of CMT genes can model recessive and/or dominant forms of the disease for some aspects. In that context, we have successfully recapitulated some of the hallmarks of the human disease, including electrophysiological evidence of neuronal dysfunction. However, not only altering the expression levels of the genes but also the generation of the null mutants or knock-in flies carrying the mutant forms of *GDAP1* and *MTMR2* are necessary to delineate the mechanism through which these mutations cause the pathogenesis of CMT. It is also crucial to optimize the newly produced CG4623 antibody to reveal the sub-cellular localization and interaction partners of the protein. We are confident that with the enhancement of the techniques, it will be possible to gain mechanistic insight into the pathogenesis of CMT and ultimately develop new treatments for the disease with these generated models.

7. CONCLUSION

In the scope of this study, we have recapitulated certain pathophysiological features of CMT disease in *Drosophila* by altering the expression levels of *CG4623* and *mtm* genes. The generated CG4623 antibody allowed us to investigate the expression of the protein in Western blot and immunohistochemistry assays. This polyclonal antibody is promising to perform further optimizations for its use in investigating sub-cellular localization and interaction partners of CG4623. Synaptic electrophysiology recordings revealed that altered expression of both *CG4623* and *mtm* had an effect on synaptic transmission and neurotransmitter release. This phenomenon recapitulates the fundamental characteristics of CMT disease as patients are also diagnosed by their electrophysiological abnormalities in their extremities. Progressive pathophysiology of CMT can be taken into account since we did not observe any drastic change in NMJ morphology, bouton structure, or mitochondrial dynamics of the third instar larvae upon *CG4623* up-or-down regulation. Analyses in later developmental stages might reveal the exact starting point of CMT phenotype in terms of morphological change, indicating the progressive characteristics of the disease. As we refine the generated *Drosophila* models of *CG4623* and *mtm* genes, it will be possible to find biomarkers or to perform drug screens for new treatments of inherited peripheral neuropathies.

REFERENCES

Akyüz, K., 2013, *Development of Drosophila CMT4A Model via Overexpression and Knocking-in of GDAP1 Gene*, M.S. Thesis, Boğaziçi University.

Altschul, S.F., T.L. Madden, A.A. Schäffer, J. Zhang, Z. Zhang, W. Miller, and D.J. Lipman, 1997, "Gapped BLAST and PSI-BLAST: a New Generation of Protein Database Search Programs", *Nucleic Acids Research*, Vol. 25, No. 17, pp. 3389-3402.

Altschul S.F., J.C. Wootton, E.M. Gertz, R. Agarwala, A. Morgulis, A.A. Schäffer, and Y. K. Yu, 2005, "Protein Database Searches Using Compositionally Adjusted Substitution Matrices", *FEBS Journal,* Vol. 272, No. 20, pp. 5101-5109.

Ambegaokar, S.S, B. Roy, and G.R. Jackson, 2010, "Neurodegenerative Models in Drosophila: Polyglutamine Disorders, Parkinson Disease, and Amyotrophic Lateral Sclerosis", Neurobiology of Disease, Vol. 40, No. 1, pp. 29-39.

Azzedine H., A. Bolino, T. Taïeb, N. Birouk, M. Di Duca, A. Bouhouche, S. Benamou, A. Mrabet, T. Hammadouche, T. Chkili, R. Gouider, R Ravazzolo, A. Brice, J. Laporte, and E. LeGuern, 2003, "Mutations in MTMR13, a New Pseudophosphatase Homologue of MTMR2 and Sbf1, in Two Families with an Autosomal Recessive Demyelinating Form of Charcot-Marie-Tooth Disease Associated with Early-Onset Glaucoma", *American Journal of Human Genetics*, Vol. 72, No. 5, pp. 1141-1153.

Baxter, R.V., K. Ben Othmane, J.M. Rochelle, J.E. Stajich, C. Hulette, S. Dew-Knight, F. Hentati, M. Ben Hamida, S. Bel, J.E. Stenger, J.R. Gilbert, M.A. Pericak-Vance, J.M. Vance, 2002, "Ganglioside-Induced Differentiation-Associated Protein-1 Is Mutant in Charcot-Marie-Tooth Disease Type 4A/8q21", *Nature Genetics*, Vol. 30, No. 1, pp. 21-22.

Bayat, V., M. Jaiswal, and H.J. Bellen, 2011, "The BMP Signaling Pathway at the Drosophila Neuromuscular Junction and its Links to Neurodegenerative Diseases", *Current Opinion in Neurobiology*, Vol. 21, No.1, pp. 182-188.

Berger, P., C. Schaffitzel, I. Berger, N. Ban, and U. Suter, 2003, "Membrane Association of Myotubularin-Related Protein 2 is Mediated by a Pleckstrin Homology-GRAM Domain and a Coiled-Coil Dimerization Module", *Proceedings of the National Academy of Sciences of the United States of America,* Vol. 100, No. 21, pp. 12177-12182.

Boerkoel, C.F., H. Takashima, M. Nakagawa, S. Izumo, D Armstrong, I. Butler, P. Mancias, S.C. Papasozomenos, L.Z. Stern, and J.R. Lupski, 2003, "CMT4A: Identification of a Hispanic GDAP1 Founder Mutation", *Annals of Neurology,* Vol. 53, No. 3, pp. 400-405.

Bolino, A., M. Muglia, F.L. Conforti, E. LeGuern, M.A. Salih, D.M. Georgiou, K. Christodoulou, I. Hausmanowa-Petrusewicz, P. Mandich, A. Schenone, A. Gambardella, F. Bono, A. Quattrone, M. Devoto, and A.P. Monaco, 2000, "Charcot-Marie-Tooth Type 4B Is Caused by Mutations in the Gene Encoding Myotubularin-Related Protein-2", *Nature Genetics*, Vol. 25, No. 1, pp. 17-19.

Bolino, A., A. Bolis, S.C. Previtali, G. Dina, S. Bussini, G. Dati, S. Amadio, U. Del Carro, D.D. Mruk, M.L. Feltri, C.Y. Cheng, A. Quattrini, and L. Wrabetz, 2004, "Disruption of Mtmr2 Produces CMT4B1-like Neuropathy with Myelin Outfolding and Impaired Spermatogenesis", *The Journal of Cell Biology*, Vol. 167, No. 4, pp. 711-721.

Bolis, A., S. Coviello, I. Visigalli, C. Taveggia, A. Bachi, A.H. Chishti, T. Hanada, A. Quattrini, S.C. Previtali, A. Biffi, and A. Bolino, 2009, "Dlg1, Sec8, and Mtmr2 Regulate Membrane Homeostasis in Schwann Cell Myelination", *The Journal of Neuroscience*, Vol. 29, No. 27, pp. 8858-8870.

Braathen, G.J., J.C. Sand, A. Lobato, H. Høyer H, and M.B. Russell, 2011, "Genetic

epidemiology of Charcot-Marie-Tooth in the general population", *European Journal of Neurology*, Vol. 18, No. 1, pp. 39-48.

Bucci, C., O. Bakke, and C. Progida, 2012, "Charcot–Marie–Tooth disease and intracellular traffic", *Progress in Neurobiology,* Vol. 99, No. 3, pp. 191-225.

Cao, C., J.M. Backer, J. Laporte, E.J. Bedrick, and A. Wandinger-Ness, 2008, "Sequential Actions of Myotubularin Lipid Phosphatases Regulate Endosome PI(3)P and Growth Factor Receptor Trafficking", *Molecular Biology of the Cell*, Vol. 19, No. 8, pp. 3334-3346.

Cassereau, J., A. Chevrollier, N. Gueguen, V. Desquiret, C. Verny, G. Nicolas, F. Dubas, P. Amati-Bonneau, P. Reynier, D. Bonneau, and V. Procaccio, 2011, "Mitochondrial dysfunction and pathophysiology of CMT disease involving GDAP1 mutations", *Experimental Neurology,* Vol. 227, No. 1, pp. 31-41.

Chan, D.C., 2012. "Fusion and Fission: Interlinked Processes Critical for Mitochondrial Health", *Annual Review of Genetics,* Vol. 46, pp. 265-287.

Chen, H. and D. C. Chan, 2009, "Mitochondrial Dynamics--Fusion, Fission, Movement, and Mitophagy--in Neurodegenerative Diseases", *Human Molecular Genetics*, Vol. 18, No. 2, pp. 169-176.

Cherbas, L., A. Willingham, D. Zhang, L. Yang, Y. Zou, B. D. Eads, J. W. Carlson, J. M. Landolin, P. Kapranov, J. Dumais, A. Samsonova, J.H. Choi, J. Roberts, C.A. Davis, H. Tang, M.J. van Baren, S. Ghosh, A. Dobin, K. Bell, W. Lin, L. Langton, M.O. Duff, A.E. Tenney, C. Zaleski, M.R. Brent, R.A. Hoskins, T.C. Kaufman, J. Andrews, B.R. Graveley, N. Perrimon, S.E. Celniker, T.R. Gingeras, P. Cherbas, 2011, "The Transcriptional Diversity of 25 *Drosophila* Cell Lines", *Genome Research*, Vol. 21, No. 2, pp. 301-314.

Cherry, S., E.J. Jin, M.N. Ozel, Z. Lu, E. Agi, D. Wang, W.H. Jung, D. Epstein, I.A. Meinertzhagen, C.C. Chan, and P.R. Hiesinger, 2013, "Charcot-Marie-Tooth 2B

Mutations in Rab7 Cause Dosage-Dependent Neurodegeneration Due to Partial Loss of Function", *Elife*, Vol. 10, No. 2, e01064.

Cuesta, A., L. Pedrola, T. Sevilla, J. García-Planells, M.J. Chumillas, F. Mayordomo, E. LeGuern, I. Marín, J.J. Vílchez, and F. Palau, 2002, "The Gene Encoding Ganglioside-Induced Differentiation-Associated Protein 1 Is Mutated in Axonal Charcot-Marie-Tooth Type 4A Disease", *Nature Genetics*, Vol. 30, No. 1, pp. 22-25.

Detmer, S. A., and D. C. Chan, 2007, "Functions and Dysfunctions of Mitochondrial Dynamics", *Nature Reviews Molecular Cell Biology*, Vol. 8, No. 11, pp. 870-879.

Di Paolo, G. and P. De Camilli, 2006, "Phosphoinositides in Cell Regulation and Membrane Dynamics", *Nature*, Vol. 443, No. 7112, pp. 651-657.

Doerks, T., M. Strauss, M. Brendel, and P. Bork, 2000, "GRAM, a Novel Domain in Glycosyltransfereases, Myotubularins and Other Putative Membrane-Associated Proteins", *Trends in Biochemical Sciences*, Vol. 25, No. 10, pp. 483-485.

Eaton, D.L., and T.K. Bammler, 1999, "Concise Review of the Glutathione S-transferases and Their Significance to Toxicology", *Toxicological Sciences,* Vol. 49, No. 2, pp. 156-164.

Ermanoska, B., W.W. Motley, R. Leitão-Gonçalves, B. Asselbergh, L.H. Lee, P. De Rijk, K. Sleegers, T. Ooms, T.A. Godenschwege, V. Timmerman, K.H. Fischbeck, and A. Jordanova, 2014. "CMT-Associated Mutations in Glycyl- and Tyrosyl-tRNA Synthetases Exhibit Similar Pattern of Toxicity and Share Common Genetic Modifiers in Drosophila", *Neurobiology of Disease*, Vol. 68, pp. 180-189.

Harding, A.E., and P.K. Thomas, 1980, "Genetic Aspects of Hereditary Motor and Sensory Neuropathy (Types I and II)", *Journal of Medical Genetics*, Vol. 17, No. 5, pp. 329-336.

Hirth F., 2010, "*Drosophila melanogaster* in the Study of Human Neurodegeneration",

CNS & Neurological Disorders - Drug Targets, Vol. 9, No. 4, pp. 504-523.

Huber, N., S. Guimaraes, M. Schrader, U. Suter, and A. Niemann, 2013, "Charcot- Marie-Tooth Disease-Associated Mutants of GDAP1 Dissociate Its Roles in Peroxisomal and Mitochondrial Fission". *EMBO Reports*, Vol. 14, pp. 545–552.

Imlach, W., and B.D. McCabe, 2009, "Electrophysiological Methods for Recording Synaptic Potentials from the NMJ of *Drosophila* Larvae", *Journal of visualized experiments,* Vol. 6, No. 24.

Jones, W.D., 2009, "The Expanding Reach of the GAL4/UAS System into the Behavioral Neurobiology of Drosophila*", Biochemistry and Molecular Biology Reports,* Vol. 42, No. 11, pp. 705-712.

Kerk, D. and G.G.B. Moorhead, 2010, "A Phylogenetic Survey of Myotubularin Genes of Eukaryotes: Distribution, Protein Structure, Evolution, and Gene Expression", *BMC Evolutionary Biology*, Vol. 10, No. 196, pp. 1-16.

Kılınç, M., 2013, *Development and Molecular Analysis of CMT4B1 Drosophila Model*, M.S. Thesis, Boğaziçi University.

Küey, C., 2015, *Expression Analysis and Behavioral Assays in Drosophila CMT Models*, M.S. Thesis, Boğaziçi University.

Laborde, E., 2010, "Glutathione Transferases as Mediators of Signaling Pathways Involved in Cell Proliferation and Cell Death", *Cell Death and Differentiation*, Vol. 17, No. 9, pp. 1373-1380.

Laporte, J., L.J. Hu, C. Kretz, J.L. Mandel, P. Kioschis, J.F. Coy, S.M. Klauck, A. Poustka, and N. Dahl, 1996, "A Gene Mutated in X-Linked Myotubular Myopathy Defines a New Putative Tyrosine Phosphatase Family Conserved in Yeast", *Nature Genetics*, Vol. 13, No. 2, pp. 175-182.

Lee H.W., Y. Kim, K. Han, H. Kim, and E. Kim, 2010, "The Phosphoinositide 3-Phosphate MTMR2 Interacts with PSD-95 and Maintains Excitatory Synapsis by Modulating Endosomal Traffic", *The Journal of Neuroscience*, Vol. 30, No. 26, pp. 5508-5518.

Lloyd, T.E., P. Verstreken, E.J. Ostrin, A. Phillippi, O. Lichtarge, H.J. Bellen, 2000, "A Genome-Wide Search for Synaptic Vesicle Cycle Proteins in *Drosophila", Neuron,* Vol. 26, No. 1, pp. 45-50.

Lloyd, T.E., and J.P. Taylor, 2010, "Flightless Flies: *Drosophila* Models of Neuromuscular Disease", *Annals of the New York Academy of Sciences*, Vol. 1184, e1-20.

López Del Amo, V., M. Seco-Cervera, J.L. García-Giménez, A.J. Whitworth, F.V. Pallardó, and M.I. Galindo, 2014, "Mitochondrial Defects and Neuromuscular Degeneration Caused by Altered Expression of *Drosophila* Gdap1: Implications for the Charcot–Marie–Tooth Neuropathy", *Human Molecular Genetics*, Vol. 24, No. 1, pp. 21-36.

Marco, A., A. Cuesta, L. Pedrola, F. Palau, and I. Marin, 2004, "Evolutionary and Structural Analyses of GDAP1, Involved in Charcot-Marie-Tooth Disease, Characterize a Novel Class of Glutathione Transferase-Related Genes", *Molecular Biology and Evolution,* Vol. 21, pp. 176–187.

Mcllwain, C.C., D.M. Townsend, and K.D. Tew, 2006, "Glutathione S-transferase Polymorphisms: Cancer Incidence and Theraphy", *Oncogene*, Vol. 25, No. 11, pp. 1639-1648.

Nakhro, K., J.M. Park, Y.B. Hong, J.H. Park, S.H. Nam, B.R. Yoon, J.H. Yoo, H. Koo, S.C. Jung, H.L. Kim, J.Y. Kim, K.G. Choi, B.O. Choi, and K.W. Chung, 2013, "SET Binding Factor 1 (SBF1) Mutation Causes Charcot-Marie-Tooth Disease Type 4B3", *Neurology*, Vol. 81, No. 2, pp. 165-173.

Niemann, A., M. Ruegg, V. La Padula, A. Schenone, and U. Suter, 2005, "Ganglioside-

Induced Differentiation Associated Protein 1 Is a Regulator of the Mitochondrial Network: New Implications for Charcot-Marie-Tooth Disease", *The Journal of Cell Biology,* Vol. 170, pp. 1067–78.

Niemann, A., K.M. Wagner, M. Ruegg, and U. Suter, 2009, "GDAP1 mutations differ in their effects on mitochondrial dynamics and apoptosis depending on the mode of inheritance", *Neurobiology of Disease*, Vol. 36, No. 3, pp. 509–520.

Niemann, A., N. Huber, K.M. Wagner, C. Somandin, M. Horn, F. Lebrun-Julien, B. Angst, J.A. Pereira, H. Halfter, H. Welzl, M.L. Feltri, L. Wrabetz, P. Young, C. Wessig, K.V. Toyka, and U. Suter, 2014, "The Gdap1 Knockout Mouse Mechanistically Links Redox Control to Charcot–Marie–Tooth Disease", *Brain*, Vol. 137, No. 3, pp. 668-682.

Noack, R., S. Frede, P. Albrecht, N. Henke, A. Pfeiffer, K. Knoll K, T. Dehmel, G. Meyer Zu Hörste, M. Stettner, B.C. Kieseier, H. Summer, S. Golz, A. Kochanski, M. Wiedau-Pazos, S. Arnold, J. Lewerenz, and A. Methner, 2012, "Charcot-Marie-Tooth Disease CMT4A: GDAP1 Increases Cellular Glutathione and the Mitochondrial Membrane Potential", *Human Molecular Genetics*, Vol. 21, No. 1, pp. 150–162.

Pandey, U.B. and C.D. Nichols, 2011, "Human Disease Models in *Drosophila Melanogaster* and the Role of the Fly in Therapeutic Drug Discovery", *Pharmacological Reviews*, Vol. 63, No. 2, pp. 411-436.

Parman, Y., E. Battaloglu, I. Baris, B. Bilir, M. Poyraz, N. Bissar-Tadmouri, A. Williams, N. Ammar, E. Nelis, V. Timmerman, P. De Jonghe, A. Najafov, F. Deymeer, P. Serdaroglu, P.J. Brophy, and G. Said, 2004. "Clinicopathological and genetic study of early-onset demyelinating neuropathy", *Brain*, Vol. 127, No. 11, pp. 2540-2550.

Parman, Y., and E. Battaloglu, 2013, *Handbook of Clinical Neurology,* "Chapter 48-Recessively transmitted predominantly motor neuropathies", Vol. 115, Elsevier B.V., Amsterdam.

Pedrola, L., A. Espert, X. Wu, R. Claramunt, M.E. Shy, and F. Palau, 2005, "GDAP1, the Protein Causing Charcot-Marie-Tooth Disease Type 4A, Is Expressed in Neurons and Is Associated with Mitochondria", *Human Molecular Genetics*, Vol. 14, No. 8, pp. 1087–1094.

Pedrola, L., A. Espert, T. Valdes-Sanchez, M. Sanchez-Piris, E.E. Sirkowski, S.S. Scherer, I. Farinas, and F. Palau, 2008, "Cell Expression of GDAP1 in the Nervous System and Pathogenesis of Charcot-Marie-Tooth Type 4A Disease", *Journal of Cellular and Molecular Medicine,* Vol. 12, No. 2, pp. 679–689.

Pla-Martin, D., C.B. Rueda, A. Estela, M. Sanchez-Piris, P. Gonzalez-Sanchez, J. Traba, S. de la Fuente, L. Scorrano, J. Renau-Piqueras, J. Alvarez, J. Satrústegui, and F. Palau, 2013, "Silencing of the Charcot-Marie-Tooth Disease-Associated Gene GDAP1 Induces Abnormal Mitochondrial Distribution and Affects Ca^{2+} Homeostasis by Reducing Store-Operated Ca^{2+} Entry", Neurobiology of Diseaes, Vol. 55, pp. 140–151.

Previtali S.C., B. Zerega, D.L. Sherman, P.J. Brophy PJ, G. Dina, R.H. King, M.M. Salih, L. Feltri, A. Quattrini, R. Ravazzolo, L. Wrabetz, A.P. Monaco, and A. Bolino, 2003, "Myotubularin-Related 2 Protein Phosphatase and Neurofilament Light Chain Protein, both Mutated in CMT Neuropathies, Interact in Peripheral Nerve", *Human Molecular Genetics*, Vol. 12, No. 14, pp. 1713-1723.

Quattrone, A., A. Gambardella, F. Bono, U. Aguglia, A. Bolino, A.C. Bruni, M.P. Montesi, R.L. Oliveri, M. Sabatelli, O. Tamburrini, P. Valentino, C. Van Broeckhoven, M. Zappia, 1996, "Autosomal Hereditary Motor and Sensory Neuropathy with Focally Folded Myelin Sheaths: Clinical, Electrophysiologic and Genetic Aspects of a Large Family", *Neurology*, Vol. 46, No. 5, pp. 1318-1324.

Reiter, L.T., L. Potocki, S. Chien, M. Gribskov, and E. Bier, 2001, "A Systematic Analysis of Human Disease-Associated Gene Sequences In Drosophila Melanogaster", *Genome Research*, Vol. 11, No. 6, pp. 1114-1125.

Robinson, F.L., and J.E. Dixon, 2006, "Myotubularization Phosphatases: Policing 3-Phosphoinositides", *Trends in Cell Biology,* Vol. 16, No. 8, pp. 403-412.

Siskind C.E., S. Panchal, C.O. Smith, S.M. Feely, J.C. Dalton, A.B. Schindler, K.M. Krajewski, 2013. "A review of Genetic Counseling for Charcot Marie Tooth Disease (CMT)", *Journal of Genetic Counseling,* Vol. 22, No. 4, pp. 422-436.

Shield, A.J., T.P. Murray, and P.G. Board, 2006, "Functional Characterization of Ganglioside-Induced Differentiation-Associated Protein 1 as a Glutathione Transferase", *Biochemical and Biophysical Research Communications*, Vol. 347, No. 4, pp. 859-866.

Storkebaum E, R. Leitão-Gonçalves, T. Godenschwege, L. Nangle, M. Mejia, I. Bosmans, T. Ooms, A. Jacobs, P. Van Dijck, X.L. Yang, P. Schimmel, K. Norga, V. Timmerman, P. Callaerts, and A. Jordanova, 2009, "Dominant Mutations in the Tyrosyl-tRNA Synthetase Gene Recapitulate in Drosophila Features of Human Charcot-Marie-Tooth Neuropathy", *Proceedings of the National Academy of Sciences*, Vol. 106, No. 28, ppi 11782-11787.

Tosch, V., H.M. Rohde, H. Tronchère, E. Zanoteli, N. Monroy, C. Kretz, N. Dondaine, B. Payrastre, J.L. Mandela, and J. Laporte, 2006, "A novel PtdIns3P and PtdIns(3,5)P2 Phosphatase with an Inactivating Variant in Centronuclear Myopathy", *Human Molecular Genetics*, Vol. 15, No. 21, pp. 3098-3106.

Tronchère, H., J. Laporte, C. Pendaries, C. Chaussade, L. Liaubet, L. Pirola, J.L. Mandel, and B. Payrastre, 2004, "Production of Phosphatidylinositol 5-Phosphate by the Phosphoinositide 3-Phosphotase Myotubularin in Mammalian Cells", *Journal of Biological Chemistry*, Vol. 279, No. 8, pp. 7304-7312.

Tsujita, K., T. Itoh, T. Ijuin, A. Yamamoto, A. Shisheva, J. Laporte, and T. Takenava, 2004, "Myotubularin Regulates The Function of the Late Endomose Through the Gram-Domain-Phophatidylinositol 3,5—Bisphosphate Interaction", *Journal of Biological Chemistry*, Vol. 279, No. 14, pp. 13817-13824.

Tyson, J., D. Ellis, U. Fairbrother, R.H. King, F. Muntoni, J. Jacobs, S. Malcolm, A.E. Harding, and P.K. Thomas, 1997, "Hereditary demyelinating neuropathy of infancy. A genetically complex syndrome", *Brain*, Vol. 120, No. 1, pp. 47-63.

Uytterhoeven, V., 2012, *Loss of Skywalker Reveals Synaptic Endosomes as Sorting Stations for Synaptic Vesicle Proteins*, Ph.D. Thesis, Katholieke Universiteit Leuven.

Vaccari, I., G. Dina, H. Tronchère, E. Kaufman, G. Chicanne, F. Cerri, L. Wrabetz, B. Payrastre, A. Quattrini, L.S. Weisman, M.H. Meisler, and A.Bolino, 2011, "Genetic Interaction Between MTMR2 and FIG4 Phospholipid Phosphatases Involved in Charcot-Marie-Tooth Neuropathies", *PLoS Genetics*, Vol. 7, No. 10, e1002319.

Vallat, J.M., S. Mathis, and B. Funolat, 2013, "The Various Charcot-Marie-Tooth Diseases", *Current Opinion in Neurology*, Vol. 26, No. 5, pp. 473-480.

Van Paassen, B.W., A.J. van der Kooi, K.Y. van Spaendonck-Zwarts, C. Verhamme, F. Baas, and M. de Visser, 2014. "PMP22 related neuropathies: Charcot-Marie-Tooth disease type 1A and Hereditary Neuropathy with liability to Pressure Palsies", Orphanet Journal of Rare Diseases, Vol. 9. No. 38.

Velichkova, M., J. Juan, P. Kadandale, S. Jean, I. Ribeiro, V. Raman, C. Stefan, and A.A. Kiger, 2010, "*Drosophila* Mtm and Class II PI3K Coregulate a PI(3)P Pool with Cortical and Endolysosomal Functions", The Journal of Cell Biology, Vol. 190, No. 3, pp. 407-425.

Verny, C., N. Ravisé, A.L. Leutenegger, F. Pouplard, O. Dubourg, S. Tardieu, F. Dubas, A. Brice, E. Genin, and E. LeGuern, 2004, "Coincidence of Two Genetic Forms of CMT Disease in A Single Family", *Neurology*, Vol. 63, No. 8, pp. 1527- 1529.

Vicinanza, M., G. D'Angelo, A. Di Campli and M.A. De Matteis, 2008, "Function and Dysfunction of the PI System in Membrane Trafficking", *EMBO Journal*, Vol. 27, No. 19, pp. 2457-2470.

Wagner, K.M., M. Rüegg, A. Niemann, and U. Suter, 2009, "Targeting and Function of the Mitochondrial Fission Factor GDAP1 Are Dependent on Its Tail-Anchor", Plos One, Vol. 4, No. 4, e5160.

Wishart, M.J. and J.E. Dixon, 2002, "PTEN and Myotubularin Phosphatases: from 3-Phosphoinositide Dephosphorylation to Disease", *Trends in Cell Biology*, Vol. 12, No. 12, pp. 579-585.

Zimon, M., J. Baets, G.M. Fabrizi, E. Jaakkola, D. Kabzinska, J. Pilch A.B. Schindler, D.R. Cornblath, K.H Fischbeck, M. Auer-Grumbach, C. Guelly, N. Huber, E. De Vriendt, V. Timmerman, U. Suter, I. Hausmanowa-Petrusewicz, A. Niemann, A. Kochański, P. De Jonghe, A. Jordanova, 2011, "Dominant GDAP1 Mutations Cause Predominantly Mild CMT Phenotypes", *Neurology*, Vol. 77, No. 6, pp. 540–548.